Julius-Maximilians-Universität Würzburg

Engineered Human Airway Mucosa for Modelling Respiratory Infections: Characterisation and Applications

Gewebemodelle der humanen Atemwegsschleimhaut für Infektionsstudien der Atemwege: Charakterisierung und Anwendungen

Doctoral thesis for a doctoral degree
at the Graduate School of Life Sciences,
Julius-Maximilians-Universität Würzburg

Section: Biomedicine

submitted by

Rinu Sivarajan

from

Kerala, India

Würzburg, 2023

Submitted on: ……..……..

Office stamp

Members of the Thesis Committee

Chairperson: Prof. Dr. David Stegner

Primary Supervisor: Dr. Maria Steinke

Supervisor (Second): Prof. Dr. Jochen Bodem

Supervisor (Third): Prof. Dr. Roy Gross

Supervisor (Fourth): Prof. Dr. Sibylle Schneider-Schaulies

Date of Public Defence: 13.07.2023

Date of Receipt of Certificates: ……

Table of Contents

Abstract

Respiratory infections are a significant health concern worldwide, and the airway epithelium plays a crucial role in regulating airway function and modulating inflammatory processes. However, most studies on respiratory infections have used cell lines or animal models, which may not accurately reflect native physiological conditions, especially regarding human pathogens. We generated human nasal mucosa (hNM) and tracheobronchial mucosa (hTM) models to address this issue using primary human airway epithelial cells and fibroblasts.

We characterised these human airway tissue models (hAM) using high-speed video microscopy, single-cell RNA sequencing (scRNA-seq), immunofluorescence staining, and ultrastructural analyses that revealed their complexity and cellular heterogeneity. We demonstrated that *Bordetella pertussis* virulence factor adenylate cyclase toxin (CyaA) elevated the intracellular production of cyclic adenosine monophosphate (cAMP) and secretion of interleukin (IL)-6, IL-8, and human beta defensin-2 (HBD-2). In addition, we compared the responses of the tissue models from two different anatomical sites (the upper and lower respiratory mucosa) and are the first to report such differential susceptibility towards CyaA using 3D primary airway cell-derived models. The effect of toxin treatment on the epithelial barrier integrity of the tissue models was assessed by measuring the flux of fluorescein isothiocyanate (FITC)-conjugated dextran across the models. Though we observed a cell type-specific response with respect to intracellular cAMP production and IL-6, IL-8, and HBD-2 secretion in the models treated with CyaA on the apical side, the epithelial membrane barrier integrity was not compromised.

In addition to toxin studies, using these characterised models, we established viral infection studies for Influenza A (IAV), Respiratory Syncytial Virus subtype B (RSV), and severe acute respiratory syndrome coronavirus 2 (SARS-CoV-2). We visualised the morphological consequences of the viral infection using ultrastructural analysis and immunofluorescence. We verified the effective infection in hAM by measuring the viral RNA using RT-qPCR and detected elevated IL-6 and IL-8 levels in response to infection using biochemical assays. In contrast to cell lines, studies on viral infection using hAM demonstrated that infected areas were localized to specific regions. This led to the formation of infection hotspots, which were more likely to occur when models

derived from different donors were infected separately with all three viruses. IAV-infected tissue models replicate the clinical findings of H1N1 infection, such as mucus hypersecretion, cytokine release, and infection-associated epithelial cell damage.

Finally, we paved the steps towards understanding the impact of IAV infection on disease models. We generated hTM from biopsies obtained from chronic obstructive pulmonary disease (COPD) patients. As a model to study the impact of COPD on respiratory infections, considering the increase in COPD cases in the past decade and the continued predicted increase in the future. We established the IAV infection protocol to capture the early infection signatures in non-COPD and COPD conditions using scRNA-seq. We investigated the infection kinetics of IAV (H1N1-clinical isolate) in hTM and found that viruses were actively released approximately 24 hours post-infection. The scRNA-seq data from the hTM derived from non-COPD and COPD patients, revealed lower levels of SCGB1A1 (club cell marker) gene expression in the COPD-control group compared to the non-COPD control group, consistent with previous clinical studies. Furthermore, we observed that IAV infection elevated SCGB1A1 gene expression especially in secretory cells of both the COPD and non-COPD groups. This may imply the role of club cells as early responders during IAV infection providing epithelial repair, regeneration, and resistance to spread of infection. This is the first study to address the molecular diversity in COPD and non-COPD disease models infected with IAV investigating the early response (6 h) of specific cell types in the human lower airways towards infection using scRNA-seq. These findings highlight the potential interplay between COPD, IAV infection, and altered vulnerability to other viral infections and respiratory illnesses making the hAM applicable for addressing more specific research questions and validating potential targets, such as SCGB1A1 targeted therapy for chronic lung diseases.

Our findings demonstrate the potential of the hNM and hTM for investigating respiratory infections, innate immune responses, and trained immunity in non-immune cells. Our experiments show that hAM may represent a more accurate representation of the native physiological condition and improve our understanding of the disease mechanisms. Furthermore, these models promote non-animal research as they replicate clinical findings. We can further increase their complexity by incorporating dynamic flow systems and immune cells catered to the research question.

Zusammenfassung

Infektionen der Atemwege stellen weltweit ein erhebliches Gesundheitsproblem dar, und das Epithel der Atemwege spielt eine entscheidende Rolle bei der Regulierung der Atemwegsfunktion und der Steuerung von Entzündungsprozessen. In den meisten Studien zu Atemwegsinfektionen wurden jedoch Zelllinien oder Tiermodelle verwendet, die die natürlichen physiologischen Bedingungen nicht genau widerspiegeln, insbesondere im Hinblick auf menschliche Krankheitserreger. Wir haben Modelle der menschlichen Nasenschleimhaut (hNM) und der Tracheobronchialschleimhaut (hTM) entwickelt, um dieses Problem mit primären menschlichen Epithelzellen und Fibroblasten der Atemwege zu lösen.

Wir charakterisierten diese humanen Atemwegsgewebemodelle (hAM) mithilfe von Hochgeschwindigkeits-Videomikroskopie, Einzelzell-RNA-Sequenzierung (scRNA-seq), Immunfluoreszenzfärbung und ultrastrukturellen Analysen, die ihre Komplexität und zelluläre Heterogenität offenlegten. Wir konnten zeigen, dass der Virulenzfaktor Adenylatzyklasetoxin (CyaA) von *Bordetella pertussis* die intrazelluläre Produktion von zyklischem Adenosinmonophosphat (cAMP) und die Sekretion von Interleukin (IL)-6, IL-8 und humanem Beta-Defensin-2 (HBD-2) erhöht. Darüber hinaus verglichen wir die Reaktionen der Gewebemodelle aus zwei verschiedenen anatomischen Bereichen (obere und untere Atemwegsschleimhaut) und sind die ersten, die eine solche unterschiedliche Empfindlichkeit gegenüber CyaA anhand von 3D-Modellen aus Atemwegsprimärzellen berichten. Die Auswirkung der Toxinbehandlung auf die epitheliale Barriereintegrität der Gewebemodelle wurde durch Messung des Flusses von Fluorescein-Isothiocyanat (FITC)-konjugiertem Dextran durch die Modelle ermittelt. Obwohl wir eine zelltypspezifische Reaktion in Bezug auf die intrazelluläre cAMP-Produktion und die Sekretion von IL-6, IL-8 und HBD-2 in den mit CyaA behandelten Modellen auf der apikalen Seite beobachteten, war die Integrität der Epithelmembranbarriere nicht beeinträchtigt.

Anhand dieser gut charakterisierten Modelle haben wir Virusinfektionsstudien für Influenza A (IAV), das respiratorische Synzytialvirus Subtyp B (RSV) und das schwere akute respiratorische Syndrom Coronavirus 2 (SARS-CoV-2) durchgeführt. Wir haben die morphologischen Folgen der Virusinfektion mithilfe von Ultrastrukturanalysen und Immunfluoreszenz sichtbar gemacht. Wir verifizierten die effektive Infektion in hAM

durch Messung der viralen RNA mittels RT-qPCR und wiesen erhöhte IL-6- und IL-8-Spiegel als Reaktion auf die Infektion mittels biochemischer Assays nach. Im Gegensatz zu Zelllinien zeigten die Virusinfektionsstudien mit hAM, dass die infizierten Bereiche auf bestimmte Regionen beschränkt waren, was zu Infektions-Hotspots führte, die eher bei Modellen auftraten, die von verschiedenen Spendern stammten und mit allen drei Viren separat infiziert waren. IAV-infizierte Gewebemodelle replizieren die klinischen Befunde einer H1N1-Infektion, wie beispielsweise Schleimhypersekretion, Zytokinfreisetzung und infektionsassoziierte Epithelzellschäden.

Schließlich haben wir die Auswirkungen einer IAV-Infektion auf Krankheitsmodelle untersucht. Dazu haben wir hTM aus Biopsien von Patienten mit chronisch obstruktiver Lungenerkrankung (COPD) isoliert. In Anbetracht der Zunahme an COPD-Fällen in den letzten zehn Jahren und der prognostizierten weiteren Zunahme in der Zukunft dient dies als Modell zur Untersuchung der Auswirkungen von COPD auf Atemwegsinfektionen. Wir erstellten ein IAV-Infektionsprotokoll, um die frühen Infektionssignaturen bei nicht-COPD- und COPD-Patienten mit Hilfe von scRNA-seq zu erfassen. Bei der untersuchten der Infektionskinetiken von IAV (klinisches H1N1-Isolat) in hTM stellten wir fest, dass die Viren etwa 24 Stunden nach der Infektion aktiv freigesetzt wurden. Die scRNA-seq-Daten von hTM, zeigten eine geringere Genexpression von SCGB1A1 (Clubzellmarker) in der COPD-Kontrollgruppe verglichen mit der nicht-COPD-Kontrollgruppe, was mit früheren klinischen Studien übereinstimmt. Darüber hinaus stellten wir fest, dass eine IAV-Infektion die SCGB1A1-Genexpression insbesondere in den sekretorischen Zellen beider Gruppen erhöhte. Dies könnte darauf hindeuten, dass Keimzellen während einer IAV-Infektion früh aktiviert werden und damit eventuell für die Reparatur und Regeneration des Epithels sorgen sowie der Ausbreitung der Infektion entgegenwirken. Hierbei handelt es sich um die erste Studie, die sich mit der molekularen Vielfalt in mit IAV infizierten COPD- und nicht-COPD-Modellen befasst und dabei ein besonderes Augenmerk auf die frühe Reaktion (6 Stunden) spezifischer Zelltypen der unteren Atemwege legt und diese mittels scRNA-seq untersucht. Diese Ergebnisse unterstreichen das potenzielle Zusammenspiel zwischen COPD, IAV-Infektion und der Anfälligkeit für andere Virusinfektionen sowie anderer Atemwegserkrankungen. Das zeight, dass die hAM für die Beantwortung spezifischerer Forschungsfragen und die Validierung potenzieller

Zielstrukturen, wie z. B. einer gezielten SCGB1A1-Therapie für chronische Lungenerkrankungen, geeignet sind.

Unsere Ergebnisse zeigen das Potenzial von hNM und hTM für die Untersuchung von Atemwegsinfektionen, angeborenen Immunreaktionen und ausgebildeter Immunität in nicht-immunen Zellen. Mit unseren Experimenten haben wir gezeigt, dass hAM eine genauere Darstellung des natürlichen physiologischen Zustands darstellen und unser Verständnis der Krankheitsmechanismen verbessern kann. Darüber hinaus könnten diese Modelle die Forschung ohne Tierversuche fördern, da sie dazu neigen, klinische Befunde zu replizieren. Wir können ihre Komplexität weiter erhöhen, indem wir dynamische Strömungssysteme und auf die Forschungsfrage abgestimmte Immunzellen einbeziehen.

1. Introduction

1.1. Human airway epithelium

The airway epithelium is a thin continuous layer of epithelial cells that lines a major part of the upper (nasal cavity, pharynx, and larynx) and lower (trachea, bronchi, bronchioles, and alveoli) respiratory tract (Breeze et al., 1977). The airway epithelium differs between regions. The upper respiratory tract comprises mainly of the ciliated columnar epithelial cells, the lower respiratory tract (bronchioles) contains simple cuboidal epithelial cells, and the alveolar region has squamous epithelial cells that are very thin and allow efficient gas exchange (Widdicombe et al., 2019). The epithelial layer forms tight cell-cell networks that help maintain the structural integrity of the epithelial layer and are essential for the normal functioning of the respiratory system (Baldassi et al., 2021).

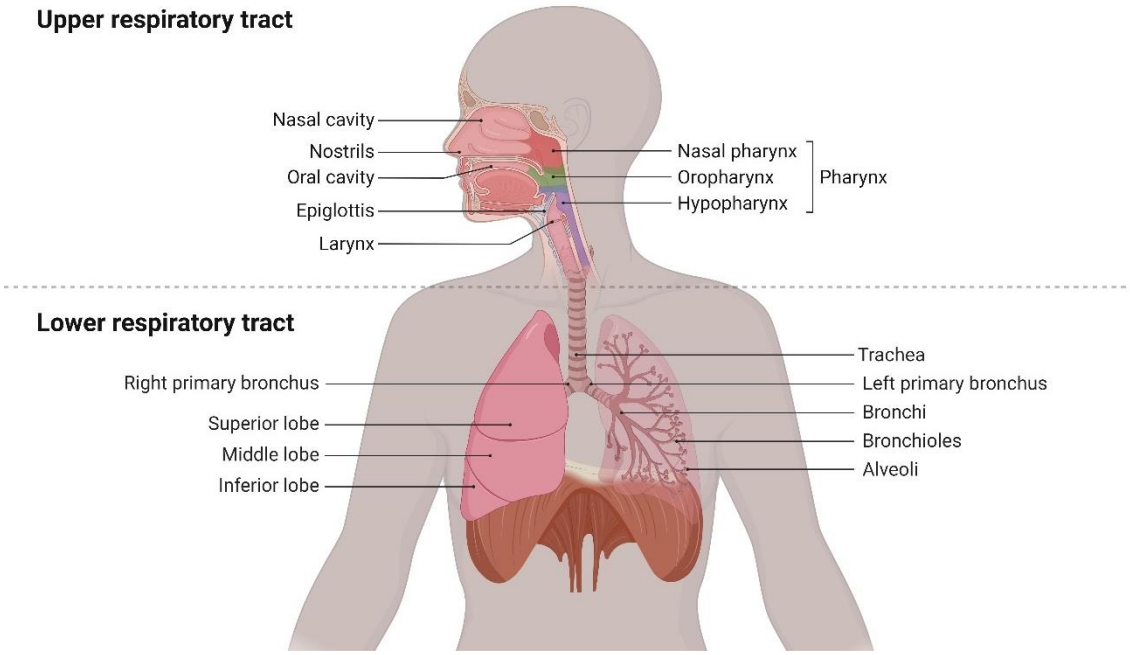

Figure 1. Anatomy of the human respiratory tract: The upper respiratory tract consists of the nasal cavity, pharynx, and larynx. The lower respiratory tract comprises the trachea, left and right bronchus, bronchi, bronchioles, and alveoli (Breeze et al., 1977). The image was adapted from the BioRender template.

The airway epithelium plays several roles in the respiratory system, including providing a physical barrier, producing mucus, and secreting enzymes that degrade harmful substances. We also have advanced in exploring other functional aspects of the airway mucosa besides the physical barrier. They can respond to environmental changes and interact and cooperate with other specialised cellular systems to initiate immune responses (Hewitt et al., 2021; Johnston et al., 2021). The epithelial layer plays a critical role in maintaining the function of the respiratory system and is composed of a complex mixture of cells. The airway epithelium comprises ciliated, mucus-secreting goblet and basal cells. The ciliary action of ciliated cells helps remove particles from the upper and lower respiratory tract to the throat, where they can be swallowed and destroyed in the low pH environment of the stomach. Secretory cells help maintain the humidity of airways by producing and secreting mucus and filtering air by trapping particles such as dust and pollen (Ruysseveldt et al., 2021; Schürch et al., 1990).

Several factors lead to disruption, inflammation, and damage to the airway epithelium including bacterial or viral infections, genetic disorder (primary ciliary dyskinesia), allergies (asthma), autoimmune diseases, physical injury caused by exposure to toxic chemicals or smoke, prolonged exposure may also lead to chronic obstructive pulmonary disease (COPD). Under normal conditions, the airway epithelium acts as a barrier against external agents, but exposure to toxic agents can cause severe changes in its structure and function (Agustí & Vestbo, 2011). For example, the abnormal inflammatory response observed in COPD is associated with increased inflammatory cells in the airways, including neutrophils, macrophages, and CD8+ T cells (Barnes et al., 2014). In addition, they secrete cytokines and chemokines, such as IL-6, IL-8, and TNF-α, which prolong the inflammatory condition (Agustí & Vestbo, 2011; Barnes et al., 2014; Pesci et al., 1998). This may lead to reduced mucociliary clearance and increased permeability to external factors depending on the COPD stage. The Global Initiative for Chronic Obstructive Lung Disease (GOLD) classifies COPD into different stages (1, mild; 2, moderate; 3, severe and 4, very severe) based on the severity of the airflow obstruction (Global Initiative for Chronic Obstructive Lung Disease, https://goldcopd.org/wp-content/uploads/2018/02/WMS-GOLD-2018-Feb-Final-to-print-v2.pdf; accessed in May 2023).

According to the World Health Organization (WHO), in 2000, COPD was assigned as the fifth leading cause of death globally (green, Table 1). By 2019 it became the third leading cause of death worldwide (blue, Table 1). Despite its preventability through measures such as avoiding exposure to irritants, early detection and management, the disease remains a significant public health issue due to its chronic nature and increasing prevalence. The primary cause of COPD is long-term exposure to lung irritants, which leads to difficulty in breathing and lung damage. Therefore, ongoing research and development of new treatments for COPD are essential for the increasing demand. WHO reported lower respiratory infections as the fourth leading cause of morbidity and mortality worldwide and the sixth leading cause was the trachea, bronchus, or lung cancer, which increased from the ninth leading cause in 2000 (Global Health Estimates 2020: Deaths by Cause, Age, Sex, by Country and by region, 2000-2019. Geneva, World Health Organization; 2020 https://www.who.int/data/gho/data/themes/mortality-and-global-health-estimates/ghe-leading-causes-of-death) accessed in March 2023.

Table 1. **Summary of the global health estimates published by WHO in 2000 (green) and 2019 (blue):** COPD is the 3rd leading cause of death globally followed by lower respiratory infections and the trachea, bronchus, and lung cancer. The tables are adapted from the Global Health Estimates 2020: Deaths by Cause, Age, Sex, by Country and by region, 2000-2019. Geneva, World Health Organization; 2020.

Global health estimates: 2000			
Rank	**Cause**	**% of total deaths**	**Crude death rate (per 100,000 population)**
0	**All Causes**	**100,0**	**835,1**
1	Ischaemic heart disease	13,2	110,0
2	Stroke	10,7	89,0
3	Neonatal conditions	6,2	52,1
4	**Lower respiratory infections**	**6,0**	**49,7**
5	**Chronic obstructive pulmonary disease**	**5,8**	**48,6**
6	Diarrhoeal diseases	5,2	43,1
7	Tuberculosis	3,4	28,3
8	HIV/AIDS	2,7	22,5
9	**Trachea, bronchus, lung cancers**	**2,4**	**19,6**
10	Road injury	2,3	19,0

Global health estimates: 2019			
Rank	Cause	% of total deaths	Crude death rate (per 100,000 population)
0	**All Causes**	**100,0**	**719**
1	Ischaemic heart disease	16,0	115
2	Stroke	11,2	80
3	**Chronic obstructive pulmonary disease**	**5,8**	**42**
4	**Lower respiratory infections**	**4,7**	**34**
5	Neonatal conditions	3,7	26
6	**Trachea, bronchus, lung cancers**	**3,2**	**23**
7	Alzheimer disease and other dementias	3,0	21
8	Diarrhoeal diseases	2,7	20
9	Diabetes mellitus	2,7	19
10	Kidney diseases	2,4	17

The increase in respiratory diseases over the past 20 years can be attributed to a complex interplay of factors, like the emergence of antibiotic-resistant strains of bacteria, virus strains that are rapidly mutating, limited access to healthcare in low- and middle-income countries, decrease in air quality, climate change and tobacco use. Effective prevention strategies, including vaccination, promoting good respiratory hygiene, and reducing exposure to risk factors, are crucial for reducing the burden of respiratory diseases. In addition, developing clinically relevant models to study the infection or drug validation may help increase the treatment efficacy.

1.1.1. Composition of human airway epithelium

The airway epithelium comprises mainly ciliated, secretory cells (goblet and mucous) and basal cells (Figure 2). Other recently identified and continuously studied cell types are deuterosomes, rare cells like pulmonary ionocytes, hillock cells, pulmonary neuroendocrine cells (PNEC), and tuft cells (Deprez et al., 2020; Goldfarbmuren et al., 2020; Montoro et al., 2018).

The ciliated cells have tiny hair-like projections called cilia, with a length of about 5-20 µm. Cilia comprise tiny microtubules, rod-like structures that are part of the cell's cytoskeleton. The microtubules are arranged in a 9+2 pattern (Satir et al., 2007). The microtubules in cilia are arranged in a specific way, with nine doublet microtubules arranged in a ring and two central microtubules in the centre. Unlike cilia, the microvilli on the respiratory mucosa are tiny, finger-like protrusions that increase the surface area for absorption or secretion. They are typically about 1-2 µm long and are made of actin filaments.

The goblet and mucous cells in the submucosal glands found throughout the respiratory tract produce and secrete mucus. Mucus is a viscous, gel-like material consisting of various macromolecules, inorganic salts, and water. The gel-like property is due to the glycoprotein mucin present in the mucus. The mucus layer consists of the gel layer and the periciliary liquid layer. The former blocks invading pathogen penetration into the airway epithelium, while the latter contributes to ciliary beating and mucociliary clearance. The mucus contains a high concentration of mucins, which helps keep the airways moist and protects them from irritants and infections. In addition, mucus acts as a barrier to trap and remove any foreign particles or pathogens that may be present in the airway (Lillehoj et al., 2013; Abdul-Haq et al., 1997). MUC5B and MUC5AC are the major gel-forming mucins in the airway mucosa (Thornton et al., 2000; Kirkham et al., 2002). Further research on the species-specific properties of mucus can provide more information on the role of mucus as a virus-host range determinant against the establishment of zoonotic and enzootic infections (Wallace et al., 2021). Together the ciliated and secretory cells are responsible for mucociliary clearance. The mucociliary phenotype refers to the combination of the mucus layer and the ciliated cells that help to move mucus and trapped particles out of the airway. Several respiratory diseases like asthma, chronic bronchitis, primary ciliary dyskinesia (PCD), and cystic fibrosis (CF) lead to disruption or dysfunction in mucociliary clearance. Lifestyle (e.g., smoking) may also contribute to this effect. It was reported that nicotine significantly interferes with the normal function of mucins in the airway. The interaction of nicotine and mucins also allows the airway mucus to serve as a reservoir for prolonged nicotine release (Chen et al., 2014).

The basal cells are the stem cell progenitors of the airway that can divide and differentiate into different types of cells, such as goblet and ciliated cells. They help to repair and maintain the integrity of the mucosa (Rock et al., 2009; Hong et al., 2004). Naik et al. (2017) demonstrated that skin epithelial stem cells could retain a memory of previous inflammation exposure, which sensitises them to subsequent tissue damage (Naik et al., 2017). Recent studies suggest that tissue-specific stem cells and other non-immune cells (fibroblasts) can have trained immunity based on their previous exposure to the stimulus and in detail discussed in these reviews (Hamada et al., 2019; Novakovic & Stunnenberg, 2017; Ruysseveldt et al., 2021).

Studies have shown that Notch signalling plays a crucial role in regulating the differentiation of basal cells towards a secretory cell fate. Loss of Notch signalling leads to basal cells differentiating into ciliated cells (Carraro et al., 2020; Gomi et al., 2015; Jason et al., 2011). Ciliated cells differentiate from basal cells and go through different stages of maturation. During this process, the cells go through deuterosomes, characterised by centrioles and basal bodies that eventually form cilia. The formation of ciliary basal bodies indicates this stage. They were recently described as a precursor subgroup of ciliated cells, characterised by high gene expression associated with cilia development and cell proliferation (Ruiz García et al., 2019). They also reported that deuterosomes could be a source of growth factors and signalling molecules that promote ciliary development and proliferation.

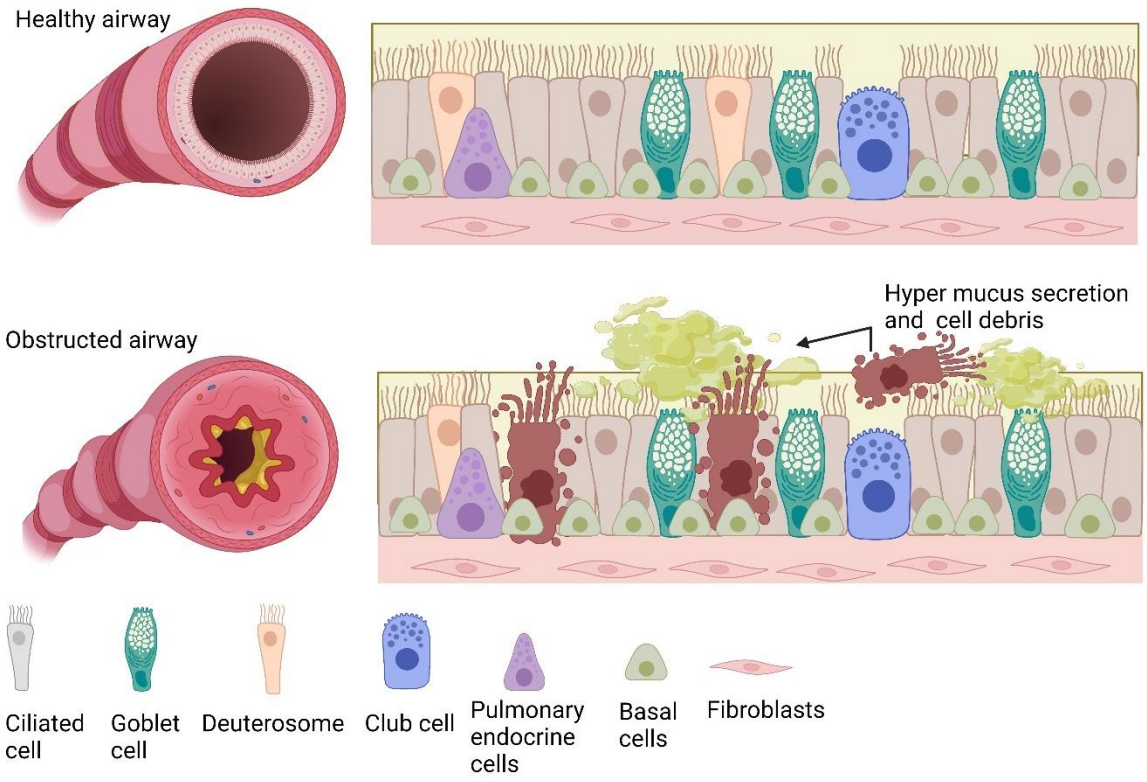

Figure 2. The healthy human airway mucosa vs. inflammatory condition: The upper panel shows the healthy airway mucosa with different cell types (ciliated cells, goblet cells, club cells, basal cells, deuterosome, pulmonary endocrine cells, and the fibroblasts embedded in the connective tissue) and their orientation in the respiratory tract. The bottom panel shows the airways under inflammatory conditions (allergy or chronic obstructive pulmonary disease), where the airways are constricted, and the lumen has excess mucus secretion and cell debris. The image was created using BioRender.

Tuft or brush cells are characterised by their unique bottle-shaped morphology and apical microvilli. They are described as chemosensory epithelial cells that can sense and respond to chemical stimuli and share similarities with the tongue's Type II taste bud cells. They have been shown to play an essential role in the innate immune response to pathogens and are thought to regulate the airways' inflammatory response (O'Leary et al., 2019). PNECs are specialised cells in the airway epithelium responsible for sensing changes in the environment, such as changes in oxygen levels or chemical stimuli, and respond by releasing neuropeptides and neurotransmitters that can affect immune and physiological processes in the lungs (Branchfield et al., 2016). Hillock cells, a type of neuroendocrine cell, have been identified as a transitional cell type that links tracheal basal cells and secretory club cells in the developmental pathway. They are found in stratified, non-ciliated structures and are described to play a role in maintaining the squamous barrier function and modulating the immune response in the airways (Montoro et al., 2018).

The airways are complex structures connected through various cell-cell contact networks, including tight junctions, adherens junctions, and desmosomes. These junctions provide mechanical strength to the airway wall, allow for selective permeability of ions and molecules, and facilitate communication between different cell types. The tight junctions, also known as occluding junctions, are cell-cell junctions found in and between the cells to make a tight epithelial layer. They are composed of proteins called occludins and claudins. Tight junctions maintain tissue integrity by preventing membrane protein mixing between the apical and basolateral membranes. They also regulate the paracellular passage of ions and small molecules across the epithelial or endothelial cell layers. This is important for many physiological processes, including maintaining electrolyte balance, absorbing nutrients, and secretion of hormones and other signalling molecules. They can be identified by the electron-dense cell-cell contacts located at the apical layer of epithelial cells (Van Itallie et al., 2006; Chang et al., 2011).

Adherens junctions are a type of cell-cell adhesion complex that helps to hold cells together in tissues. They are located below tight junctions and are identified by the characteristic electron-dense areas on both sides of the visible intercellular space. They comprise transmembrane proteins called cadherins, which bind to each other through their extracellular domains, forming a strong adhesive bond. The intracellular

domains of cadherins are anchored to the cytoskeleton, which helps maintain the tissue's structural integrity. Adherens junctions are essential for maintaining tissue architecture and transmitting mechanical forces between cells. They also play a role in cell communication and differentiation during development (Niessen et al., 2007; Chang et al., 2011).

Desmosomes are major intercellular adhesive junctions at basolateral membranes of epithelial cells and other cell types. Desmosomes are more resistant to mechanical stress and are essential for maintaining the structural integrity of tissues. They are also involved in cell communication and differentiation during development. These proteins play a critical role in maintaining the structural integrity of the airway and regulating the movement of ions, fluids, and other molecules across the cell barrier (Chang et al., 2011; Green et al., 1996).

1.2. Current challenges in the disease modelling of airways

Animal models are generally used to study viral pathogenesis. They can provide crucial information on host-pathogen interaction. However, species-specific differences can be a limiting factor for applying these findings to humans. The most significant differences between the mouse and human lungs are related to the organisms' size, as airway diameter and alveolar size are naturally much smaller in mice, and their respiratory rate is much higher than in humans (Rydell-Törmänen et al., 2019). This lack of functional homology highlights the need for caution when interpreting and applying research findings from animal models to human health. A most recent study showed that even the gender of the experimenter modulates the experimental outcome in mice/rat studies (Georgiou et al., 2022).

Primary airway epithelial cells in 2D conditions (cells grown as a monolayer on cell culture plates or dishes) are also used for respiratory research. They can provide specific information on the impact of infection or pathogen-associated toxin effect (Bianchi et al., 2021; Elbert et al., 1999). Using 2D cell line-based approaches can be an important tool for infection research e.g., tracking life cycle of viruses, calculation

of multiplicity of infection, virus propagation, target identification and assay development (Carius et al., 2023; Hillyer et al., 2018; Dou, D et al., 2017). As the 2D cell line models are submerged cultures mainly containing single cell type, limits their application for understanding the host-pathogen interaction in a complex in vivo environment. For example, immortalised human cell lines, such as Calu-3, can help evaluate virus replication cycles in lung epithelial cells. However, the natural target cells of viruses in the respiratory tract are differentiated cells, which may have different characteristics than immortalised cells. As a result, the analysis of virus infections in continuous cell lines may only partially capture essential aspects of viral pathogenesis. The cell lines often used in research, for example, MDCK (Madin-Darby Canine Kidney) cells and CHO- cell lines, are not of human origin and are derived from a single cell type and hence may not fully capture the human-specific responses.

Furthermore, the cell lines with higher passage numbers may have undergone genetic and phenotypic changes, making their characteristics different from the original cells. These changes may affect the accuracy of the results obtained from one lab to another, affecting their reproducibility (Mohammadi Farsani et al., 2018). Additionally, maintaining the authenticity and integrity of cell lines can be challenging, mainly when cell lines are distributed to different laboratories for research purposes. This may lead to cross-contamination, variations in growth conditions, handling, and loss of identity over time. These issues can lead to inconsistencies in results and make it challenging to replicate findings.

As the support for the 3R principle (reduce, refine, replace) in animal testing grows, the development of alternative in vitro cell culture methods that mimic the respiratory tract is improving faster. These methods aim to reduce the number of animals used in testing, refine the conditions under which they are used, and replace animal testing with non-animal alternatives where possible. This shift in research focus is driven by recognising the limitations and ethical concerns associated with animal testing and the need for more accurate and reliable methods to predict human responses to respiratory viruses.

1.3. Engineered human airway models

Researchers aim to bridge the gap between cell lines/undifferentiated cell cultures and animal studies to better understand the complex interactions in the human body. This is typically done by culturing cells on a scaffold or matrix that mimics the physical properties of the airway tissue, allowing the cells to differentiate and function as they would in vivo. These models are used to study the effects of infection, toxins, or toxicology, on the airway epithelium in a physiological setting. Primary cultures of airway cells cultivated at ALI offer a valuable opportunity to investigate the innate immune responses triggered by respiratory infections and disease pathology (Zarkoob et al., 2022; Sivarajan et al., 2021; Kessie et al., 2021; Min et al., 2016; Qian et al., 2013). Infection and toxicology studies are also performed using cell lines such as Calu-3, A549 and immortalised primary airway cell lines grown under 3D ALI culture conditions (Grainger et al., 2006).

Organoids derived from tissue samples or stem cells is another alternative that are used for respiratory research. Organoid could generate continuous cultures for long term use and help with the current limitation in the availability of human tissue samples. Organoids are extensively used for infection research and as a model to study distal lung in vitro (Ekanger et al., 2022; Tran et al., 2022; Porotto et al., 2019). The use of precision cut lung section (PCLS) makes it possible to better understand the cell types that are infected in the intact lung. Studies have used PCLS for drug studies, infection research and disease modelling (Zimniak et al., 2021; Liu et al., 2019; Lauenstein et al., 2014; Wu et al., 2010). Organ-on-a-chip or lung-on-a-chip models are used for the in vitro replication of viral infection and the assessment of antiviral medications at a faster pace (Tan et al., 2023; Ruft et al., 2022; Sengupta 2022). They are also used to study smoking/air quality effects on the airway mucosa (Yang et al., 2020). There is a variety of different 3D airway models available today, using more complex systems that include immune cells, vascularisation, and induced breathing simulation of the airways (Chandra et al., 2023; Luengen et al., 2022; Costa et al., 2019; Blom et al., 2016).

There are also challenges to using 3D airway mucosa models. As they are more complex than traditional 2D cell culture models, they require specialised techniques, media and equipment for maintenance and study, leading to a more expensive

experimental setup. It can be challenging to scale up 3D airway epithelial models from different donors for high throughput for the drug discovery and development studies. The restricted access and legal procedures to acquire donor materials may impact the time and cost of the experiments.

1.3.1. Scaffolds for 3D airway engineering

Scaffolds are materials used to support the growth of cells into functional tissue in a 3D environment. This is important because it allows the cells to form a tissue that more closely mimics the structure and function of native airway epithelial tissue. The scaffolds can be of biological or synthetic origin. Examples of biological scaffolds are collagen found in the extracellular matrix (ECM), gelatine, a denatured form of collagen that can be derived from the bovine and porcine origin, decellularized tissues with intact extracellular matrix and seaweed cellulose scaffold (Bar-Shai et al., 2021). Two materials mainly used as scaffolds for commercial airway epithelial models are PDMS (polydimethylsiloxane) and PET (polyethylene terephthalate) membranes. PDMS is a polymer commonly used because of its biocompatibility and flexibility. PET membrane is a biocompatible synthetic polymer, which is easy to sterilise, and provides mechanical support for the cells to grow.

One of the main disadvantages of using PDMS as a scaffold is its hydrophobicity. Hence, the cells may not be able to adhere to the surface or require more nutrients. This also limits its application in high throughput assays during drug screening. Another limitation is its relatively brittle nature, making it challenging to handle without causing damage (Ariati et al., 2021; Miranda et al., 2021). While PET (polyethylene terephthalate) membrane is widely used in tissue engineering due to its biocompatibility, ease of sterilisation and proper mechanical support, there are also limitations. PET membranes have low permeability, which can limit their use for understanding epithelial membrane permeability and transmigration. Therefore, evaluating the suitability of scaffold material is essential based on the specific goals and requirements of the study.

Based on a previously established protocol, this study used a biological scaffold derived from the decellularized porcine small intestine (Sivarajan et al., 2021; Steinke et al., 2014).

Biological scaffolds are biocompatible and adding fibroblast provides the additional ECM layer, that mimics the native microenvironment, and supports epithelial cell attachment, proliferation, and differentiation. This is absent in PET-based airway epithelial models. However, like other scaffolds, these are also associated with limitations as they contain components from porcine origin, difficult to standardise for large-scale use, sourcing, processing, and sterilisation can be difficult and expensive (Berger et al., 2020).

1.4. Respiratory pathogens

1.4.1. Bordetella pertussis

A Gram-negative obligate human pathogen that causes pertussis, a highly contagious respiratory tract disease. The condition is most dangerous in unvaccinated or partially vaccinated infants and spreads quickly from person to person, mainly through droplets produced by coughing or sneezing. There are three stages during the infection cycle. The initial stage is called the catarrhal stage; symptoms include mild fever, runny nose, and cough, mostly undiagnosed; hence, the bacteria is circulated in the population and mainly transmitted to infants. The next paroxysmal stage is characterised by paroxysmal cough followed by whooping, mucus production, and vomiting. This may continue for 2 – 8 weeks. The final stage is convalescent, where the symptoms gradually fade, and the patient recovers (Cherry, 1984, 1996). There were 35,627 pertussis cases reported by the European Union/European Economic Area countries in 2018, and 72% of the cases accounted for Germany, Netherlands, Norway, Spain, and the United Kingdom. Of this, 62% were reported from the age group ≥15 (https://www.ecdc.europa.eu/en/publications-data/pertussis-annual-epidemiological-report-2018; accessed on 22/04/2023). Pertussis can be prevented by immunisation. Nevertheless, the current acellular pertussis vaccine provides less efficacy than the previously used whole-cell pertussis vaccine and may contribute to the present waning immunity (Bouchez et al., 2015; Gambhir et al., 2015; Sheridan et al., 2012)

The main target for *B. pertussis* attachment is the kinocilia of the airways with the help of adhesins like filamentous haemagglutinin, pertactin, and fimbriae (Weiss & Hewlett, 1986). After attachment, it releases various virulence factors to evade the host's immune response. The major toxins are the adenylate cyclase toxin, pertussis toxin, and tracheal cytotoxin. The bvgAS locus co-ordinately regulates the expression of these virulence factors. Except for tracheal cytotoxin, the others are controlled by the *B. pertussis* virulence genes (Bvg). Bacteria expressing all virulence factors are called Bvg wild-type bacteria. Mutants at the Bvg locus are called Bvg mutants. BvgA and BvgS belong to the family of two-component signal transduction proteins found in prokaryotes and lower eukaryotes. They are responsible for sensing external stimuli and coordinating the transcription of genes and operons that function during the

infectious cycle (Stibitz & Yang, 1991). The expression of virulence factors characterises the Bvg+ phase, which is necessary and sufficient for colonising rabbits and rats (Akerley et al., 1995; Cotter & Miller, 1994). The Bvg⁻ phase is avirulent and characterised by the loss of virulence gene expression and the induction of repressed genes in the Bvg+ phase.

1.4.1.1. Major toxins

1.4.1.1.1. Pertussis toxin (PT)

It is a 106 kDa, ADP-ribosylating AB-type toxin produced exclusively by *B. pertussis.* PT comprises one catalytic subunit (A subunit) and five membrane-binding subunits (B subunit) (Stein et al., 1994). They are assembled in the periplasm and exported by the type IV secretion system (Kotob et al., 1995). It is also known as a lymphocytosis-promoting factor as it induces lymphocytosis in mammals (Morse & Morse, 1976). After binding, PT enters the host cell via receptor-mediated endocytosis. In the cytoplasm, the A subunit catalyses the transfer of ADP-ribose from NAD+ to a cysteine residue near the C-terminus of the α-subunit of heterotrimeric G proteins. This modification eliminates the ability of inhibitory G proteins to inhibit adenylate cyclase activity and blocks other G protein-regulated enzymes and pathways, leading to dysregulation of the immune response. Animal studies suggest that the production of PT by *B. pertussis* suppresses early pro-inflammatory chemokine, cytokine production, decreased recruitment of neutrophils to the lungs, and the microbicidal action of inflammatory cells (Andreasen & Carbonetti, 2008; Kirimanjeswara et al., 2005). However, whether the toxin also induces these effects in humans is unknown.

1.4.1.1.2. Tracheal cytotoxin (TCT)

It is a 0.921 kDa disaccharide tetrapeptide monomer of peptidoglycan released from the colonising *B. pertussis* (Goldman et al., 1982). It induces the uncontrolled release of reactive oxygen species (ROS) via Interleukin -1 mediated Type-II nitric oxide synthases. It damages the ciliated airway epithelium, induces excess mucus production by goblet cells, and inhibits vital cellular processes (Heiss et al., 1994). In

hamster models, TCT synergises with LOS to induce NO production and pro-inflammatory cytokines. Though NO primarily affects ciliated epithelial cells, the source of NO is not just the ciliated epithelium but also the goblet cells. The goblet cells remain undamaged during this process, NO may be released through diffusion, contributing to remote cytopathologic effects on the ciliated epithelium (Flak & Goldman, 1999). TCT also disrupted tight junctions and extrusion of ciliated cells in engineered human tracheobronchial models (Kessie et al., 2021), as seen in the hamster tracheal models (Goldman et al., 1982). It has been postulated that TCT-mediated cytopathology contributes to the characteristic cough in pertussis.

1.4.1.1.3. Adenylate cyclase toxin (CyaA)

CyaA is a multifunctional, 1706 AA (~177kDa) long protein secreted by *B. pertussis* via Type I secretion system (T1SS) where the toxin is transferred directly via a channel tunnel created between the inner membrane and the bacterial outer membrane without a periplasmic intermediate (Bumba et al., 2016; Sakamoto et al., 1992). CyaA has an N-terminal catalytic domain/adenylate cyclase (AC) domain and a C- terminal repeats in the toxin (RTX)/hemolysin domain. It mainly targets cells expressing complementary receptor 3 (CR3, or CD11b/CD18 or Mac-1 or αMβ2 integrin) present in immune cells (El-Azami-El-Idrissi et al., 2003; Guermonprez et al., 2001). More recent studies show that CyaA can also interact with cells that are $CR3^-$ (Angely et al., 2020; Bassinet et al., 2004; Bianchi et al., 2021; Eby et al., 2010; Hasan et al., 2018). In the absence of CD11b/ CD18, the toxin might bind to surface-expressed glycosylated structures, such as gangliosides clustered in the membrane microdomains (Hasan et al., 2015; Morova et al., 2008) and the cholesterol-rich lipid microdomains favour the translocation of the AC domain into the cell cytosol to catalyse the formation of cAMP (Bumba et al., 2010). After binding to the host cell, the AC domain is inserted into the host membrane by an uncharacterised mechanism and activated by the cytosolic calmodulin (Glaser et al., 1988; Wolff et al., 1980). This creates an uncontrolled and rapid conversion of cellular adenosine triphosphate (ATP) to cyclic adenosine monophosphate (cAMP) (Confer & Eaton et al., 1982; Hanski et al., 1989). The RTX domain can permeabilise the host cell membrane and promote K^+ efflux, disturbing ion homeostasis (Gray et al., 1998).

The cAMP signalling, ATP depletion, and pore formation may lead to cell intoxication, impairment of anti-microbial functions, and apoptosis. The rapid increase in cAMP concentration triggers and deregulates signalling pathways downstream to protein kinase A (PKA) and Epac (exchange protein directly activated by cAMP). cAMP activated Epac signalling leads to inhibition of Phospholipase C (PLC), preventing activation of PKC, which usually contributes to the assembly and activation of NADPH oxidase and, consequently, ROS production, which is required to kill invading pathogens. The activation of PKA by cAMP activates the tyrosine phosphatase SHP-1. This controls numerous fundamental mechanisms in Toll-like receptor ligand-induced expression of inducible nitric oxide synthase and bactericidal NO production in macrophages (Cerny et al., 2017; Cerny et al., 2015; Confer & Eaton, 1982; Pearson et al., 1987). Several studies were performed to assess the susceptibility of hAM to CyaA in a 3D environment (Bassinet et al., 2004; Bianchi et al., 2020). Hasan et al., showed that CyaA induced IL-6 secretion but neither IL-8 nor HBD-2 secretion in airlifted VA10 cells, a human bronchial epithelial cell line (Hasan et al., 2018). We reported for the first time a differential susceptibility of human nasal and tracheobronchial engineered airway mucosa to CyaA in terms of cAMP production and innate immune response (Sivarajan et al., 2021). A study on A549 cell line (2D) showed that CyaA treatment altered the cell morphology, adhesion, and cytoskeleton remodelling, which could directly impact or compromise the airway epithelial barrier integrity (Angely et al., 2020). CyaA treatment on VA10 cell line-based models showed for 24 h also caused a significant drop in the transepithelial electrical resistance, suggestive of the compromised membrane integrity (Hasan et al., 2018). CyaA treatment on human primary cell derived 3D hAM for 1 h or 24 h showed no significant disruptions in the cell-cell contact or the tight junctions (Sivarajan et al., 2021) a similar effect is yet to be validated at higher toxin concentration or prolonged exposure in a complex 3D environment using primary human airway cells.

1.4.2. Influenza Virus A (IAV)

IAV belongs to the negative sense, single-stranded RNA viruses of the family *Orthomyxoviridae* family. It can be transmitted by zoonoses and caused pandemics in 1918 and the most recent H1N1 pandemic in 2009. The Centers for Disease Control

and Prevention estimated that 151,700-575,400 people worldwide died from H1N1 infection during the first year of the pandemic (https://www.cdc.gov/flu/pandemic-resources/2009-h1n1-pandemic.html; assessed on 28/02/2023). Globally, 80% of virus-related deaths were estimated to have occurred in people younger than 65. This differs significantly from seasonal influenza epidemics, which mainly target people in the age group 65 years and older. Seasonal outbreaks typically occur during the winter months in temperate regions and throughout the year in tropical areas (Tamerius et al., 2011). The symptoms of IAV infection range from a mild respiratory disease affecting the upper respiratory tract, including fever, sore throat, runny nose, cough, headache, muscle pain, and fatigue, to severe and potentially deadly pneumonia caused by the virus or secondary bacterial infection in the lower respiratory tract. In some cases, influenza virus infection can result in various non-respiratory complications (Kwong et al., 2018; Sellers et al., 2017).

The differentiated human airway epithelial cultures when infected by aerosol or liquid inoculums of influenza showed tropism towards ciliated cells followed by significant decrease in the number of ciliated cells over the first 24 hours (Smith et al., 2019). The IAV infection have also shown to increase the expression of the SARS-Co-2 entry receptor ACE2, and essential TMPRSS2 protease necessary for infection of the distal airways which may increase the disease severity during COVID (Schweitzer et al., 2021). But this increased susceptibility to other viral infections is also dependent on the individual viruses. As co-infection studies with rhinovirus on ALI cultures, showed that rhinovirus can block IAV infection through stimulation of antiviral defences in the airway mucosa (Wu et al., 2020).

The correlations between phenotypic observations, physiological measures and virogenomic signatures in well differentiated HAE models infected with different viruses demonstrated that the viral peak was correlated with a decrease in the trans-epithelial electrical resistance (TEER) values and these changes on the epithelial surface were visualised using microscopy in the case of influenza viruses (Nicolas de Lamballerie et al., 2019). During the initial stages of infection on ALI cultures, the respiratory epithelium induces a highly specific innate immune response (IL-6/IL-8) to viral infection, mainly directed towards the basolateral side which play a role in attracting and activating immune cells from the lung interstitium or the circulation towards the area of infection (Ioannidis et al., 2012). Studies conducted on primary cultures of human bronchial epithelial from different donors also showed inter-

individual variations in the IAV-induced innate immune response. They observed a significantly higher type III interferons (IFNs) and IFN stimulated gene (ISG) expression in one of the donors compared to the other though there were no significant differences in the IAV replication kinetics (Ilyushina et al., 2019).

Seasonal influenza epidemics can be controlled by annual vaccination and Influenza vaccines are formulated each year to match the evolving antigenic strains circulating at the time due to antigenic drift and shift. Despite these efforts, the vaccine's efficacy is often suboptimal and can be significantly reduced when an antigenic mismatch exists between the vaccine and the circulating virus strain (Krammer et al., 2018). Hence, there is urgent need to investigate more on the early events during IAV infection and spread in appropriate engineered human airway models for better disease prevention and control strategies (Zhou et al., 2018; Tan et al., 2018; Essaidi-Laziosi et al., 2018).

1.4.2.1. Structure of IAV

It consists of several components, including hemagglutinin (HA), neuraminidase (NA), and the M2 ion channel, located on the virus's envelope derived from the host's lipid membrane. The virus also contains a matrix protein (M1) located beneath the envelope and a ribonucleoprotein complex (RNP) in the core, consisting of eight viral RNA segments, polymerases, and nucleoprotein (NP). The morphology of the IAV is characterised by spikes (~10-14 nm), which correspond to HA and NA in a ratio of 4 trimers of HA to 1 tetramer of NA. IAVs are named based on their HA (H1-H16 and hemagglutinin-like proteins H17 and H18), and NA (N1-N9 and neuraminidase-like proteins N10-N11). NA cleaves the sialic acid in mucus, enabling virus entry through the thick mucus layer (Cohen et al., 2013; Kaler et al., 2022). IAV is pleomorphic and appears in two forms, the spherical form with a diameter of 100 nm and the filamentous form with a diameter of >300 nm (Howley & Knipe, 2020).

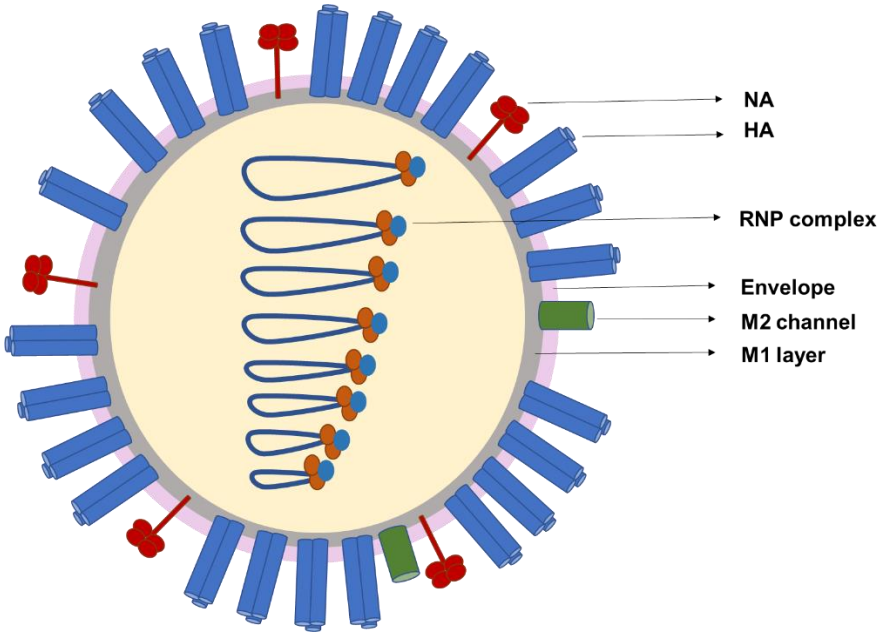

Figure 3. The structure of IAV: IAV harbours hemagglutinin (HA), neuraminidase (NA), and the M2 ion channel on its envelope. The matrix protein (M1) lies beneath the envelope, and the core of the virus particle has a ribonucleoprotein complex (RNP) composed of eight viral RNA segments, polymerases, and nucleoprotein. The diagram is adapted from Fields Virology: Emerging viruses part 1, Seventh Edition.

1.4.2.2. Stages of the IAV replication cycle

IAV binds to Sialic acids (Sas) present on the cell surface. Sas are a family of sugar units with a nine-carbon backbone and are typically found attached to the terminal positions of N- and O- linked glycans (Kuchipudi et al., 2021; Varki et al., 2008). SA α 2,6 – Gal receptors are mainly distributed in the ciliated and non-ciliated epithelium of the human respiratory tract (Yao et al., 2008). The human IAVs have a high affinity towards SA linked to galactose via α 2,6 linkage. SA α 2,3-Gal receptors are found in the ciliated epithelium lining the bronchioles and alveoli (Walther et al., 2013). The distribution of influenza virus sialic acid receptors in human airway epithelial cells cultured under air-liquid interface (ALI) have been previously reported to correlate with that in human airway tissue (Thompson et al., 2006). Slepushkin et al., showed that influenza viruses with SA α 2,3-Gal binding specificity, productively infect differentiated human airway epithelia cultures from the apical surface (Slepushkin et al., 2001). While the HA of avian IAVs preferentially binds to SA linked to galactose via α 2,3 linkage (Connor et al., 1994). IAV can use various mechanisms for entry, including

receptor-mediated, clathrin-mediated endocytosis, and micropinocytosis (Edinger et al., 2014).

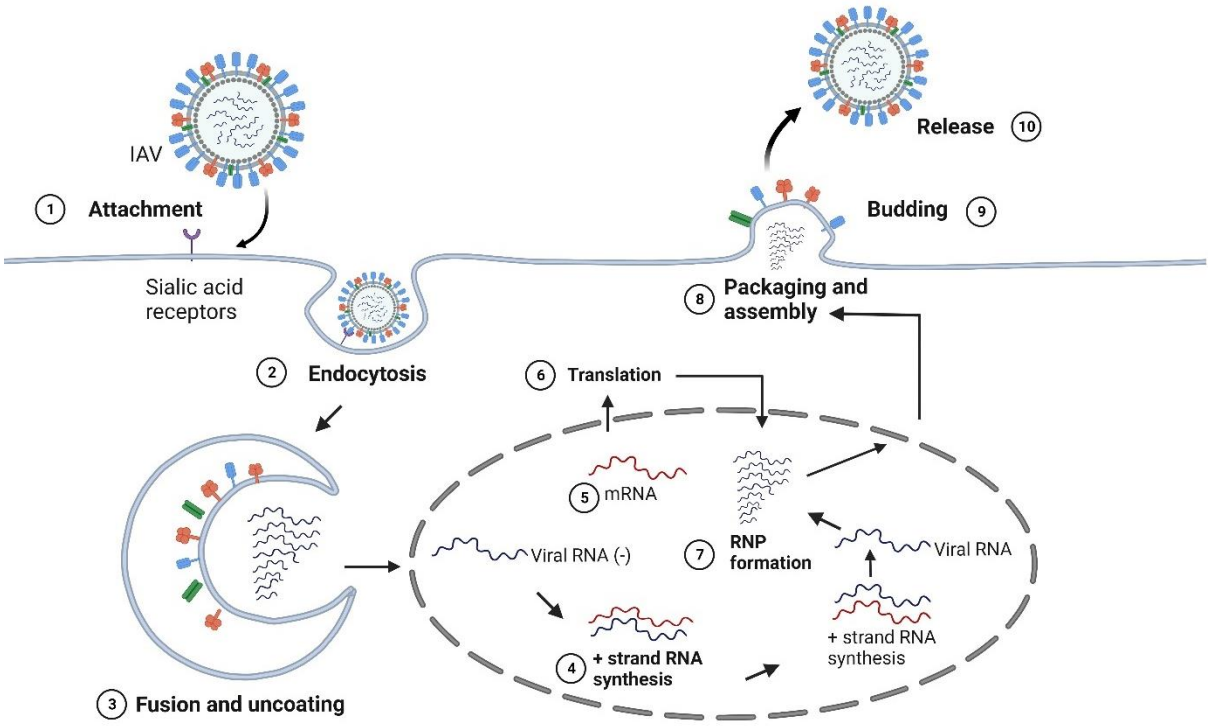

Figure 4. Stages of IAV replication: IAV has a strong affinity for sialic acid (SA) linked to galactose via α 2,6 linkage on the cell surface. When IAV binds to the target cell, it undergoes endocytosis. The low pH in the endosome triggers a conformational change in the IAV's hemagglutinin (HA) protein, forming a pore. The viral ribonucleoproteins (RNPs) are released into the cytoplasm through these pores, which are mediated by the M1 protein, and after uncoating, they are transported to the nucleus. The replication process involves two steps, with the viral RNA (vRNA) being transcribed into a complementary RNA (cRNA), which is then used to produce more vRNA. In addition, the incoming vRNA is transcribed into capped and polyadenylated mRNA, which is translated to produce new viral proteins. Following assembly, the IAV buds from the apical plasma membrane of polarised cells are released after the viral envelope completely separates from the cell membrane. The image was adapted from BioRender template.

On binding to the target cell followed by receptor-mediated endocytosis, the fusion of the viral membrane to the endosome is activated by the low pH in the endosome, which induces a conformational change in the HA of IAV, and the change in several HA creates a pore. The M2 protein mediates the release of the viral RNPs into the cytoplasm through these pores (Galloway et al., 2013). After the uncoating, the RNPs

are transported into the nucleus. The replication consists of two steps, where the viral RNA (vRNA) is transcribed into a complementary (cRNA) and is used as a template to produce further vRNA. The incoming vRNA is also transcribed into capped and polyadenylated mRNA, which is translated to produce new viral proteins. Correct assembly and packaging of the RNA genome are critical for fully infectious virions. However, the exact mechanism for packaging has yet to be fully understood (Le Sage et al., 2018). After the assembly, the IAV buds out from the apical plasma membrane of the polarised cells and is released after the viral envelope completely separates from the cell membrane. The virus particles can remain localised or spread to neighbouring cells based on the viral dose, the presence of viral entry receptors, the innate immune response, and the release of infectious virus particles.

1.4.3. Respiratory Syncytial Virus - subtype B (RSV)

RSV is a negative sense, single-stranded RNA virus belonging to the family *Paramyxoviridae* family. It is a common respiratory virus that can cause mild to severe respiratory illness in people of all ages. It targets infants and young children but can also affect older adults and immunocompromised individuals (Shi et al., 2017; Falsey et al., 1992). Symptoms of RSV infection are like other respiratory infections, including fever, runny nose, cough, and difficulty breathing caused due to the inflammation of the airways. In severe cases, RSV can lead to pneumonia or bronchiolitis and can be dangerous for people with weakened immune systems or underlying lung conditions (Larrañaga et al., 2009)

The RSV virion is composed of several structural components. The envelope comprises the lipid bilayer with the glycoproteins F, G and SH proteins. The G protein helps in cell attachment and binding to the host cell receptors, initiating the first step of the viral life cycle. The main difference in the RSV subtypes A and B are their differences in the genetic makeup of their G protein (McConnochie et al., 1990; Taylor et al., 1989; Johnson et al., 1987). The fusion (F) protein helps mediate the fusion of the viral and host cell membranes. The Small hydrophobic (SH) protein is a pentameric ion channel thought to be involved in delaying apoptosis in infected cells. The matrix (M) protein lines the inner layer of the viral envelope. The M2-1 protein mediates the association between M and the enclosed ribonucleoprotein complexes (RNPs),

consisting of the viral RNA, the nucleoprotein (N) and the non-structural proteins (NS-1 and NS-2) (Howley & Knipe, 2020; Collins, P. L., et al. 1996).

The recombinant RSV (rRSV) infection on well differentiated HAE showed that the rRSV primarily, targeted the ciliated columnar airway epithelial cells. They also reported that the virus spread in the human airway epithelium appeared to be affected by the directionality of the cilial beat (Zhang et al., 2002). In addition to ciliated cells being the primary target of RSV, studies also report that basal cells were also infected by RSV in both ALI cultures and monolayer (Persson et al., 2014). Another study reported that though the ciliated cells were infected by RSV, they were less susceptible to infection than the human epithelial cell-lines. In vitro models of human nasopharyngeal mucosa, infected with RSV grows to moderate titers in HAE, though they are significantly lower than those in a continuous epithelial cell line, HEp-2. (Wright et al., 2005). This could be due to the more complex structure or the protective mucus layer. Human ALI cultures and hamster model infected with rRSV reported NS-2 protein as a viral genetic determinant for initiating RSV-induced distal airway obstruction by promoting shedding of infected epithelial cells (Liesman et al., 2014). Glaser et al., addresses in detail the airway epithelium derived cytokines and chemokines and their role in the immune response to RSV infection in their recent review (Glaser et al., 2019).

1.4.3.1. Stages of the RSV replication cycle

There are various cell surface receptors studied for RSV attachment. Studies on differentiated ciliated ALI cultures showed that the CX3 chemokine receptor 1 (CX3CR1) binding to G protein (Johnson et al., 2015), the insulin-like growth factor 1 receptor (IGF1R) binding to F protein (Griffiths et al., 2020), epidermal growth factor binding to F protein (EGFR) (Currier et al., 2016) as cell surface receptors for RSV. It has been previously in cell lines that the heparan sulphate proteoglycans bind to the G protein of RSV (Krusat & Streckert, 1997), nucleolin bind to F protein (Mastrangelo et al., 2021; Tayyari et al., 2011). The list of RSV host receptors and the host factors regulating its life cycle are in detailed addressed in a recent review (Feng et al., 2022). After binding, the current evidence based on primary human bronchial epithelial cells and cell line studies suggests that RSV utilises a two-step entry mechanism, which

involves the utilisation of macropinocytosis, followed by the fusion in endosomes (Krzyzaniak et al., 2013) or that RSV can enter host cells through plasma membrane fusion and endocytic vesicle fusion (San-Juan-Vergara et al., 2012).

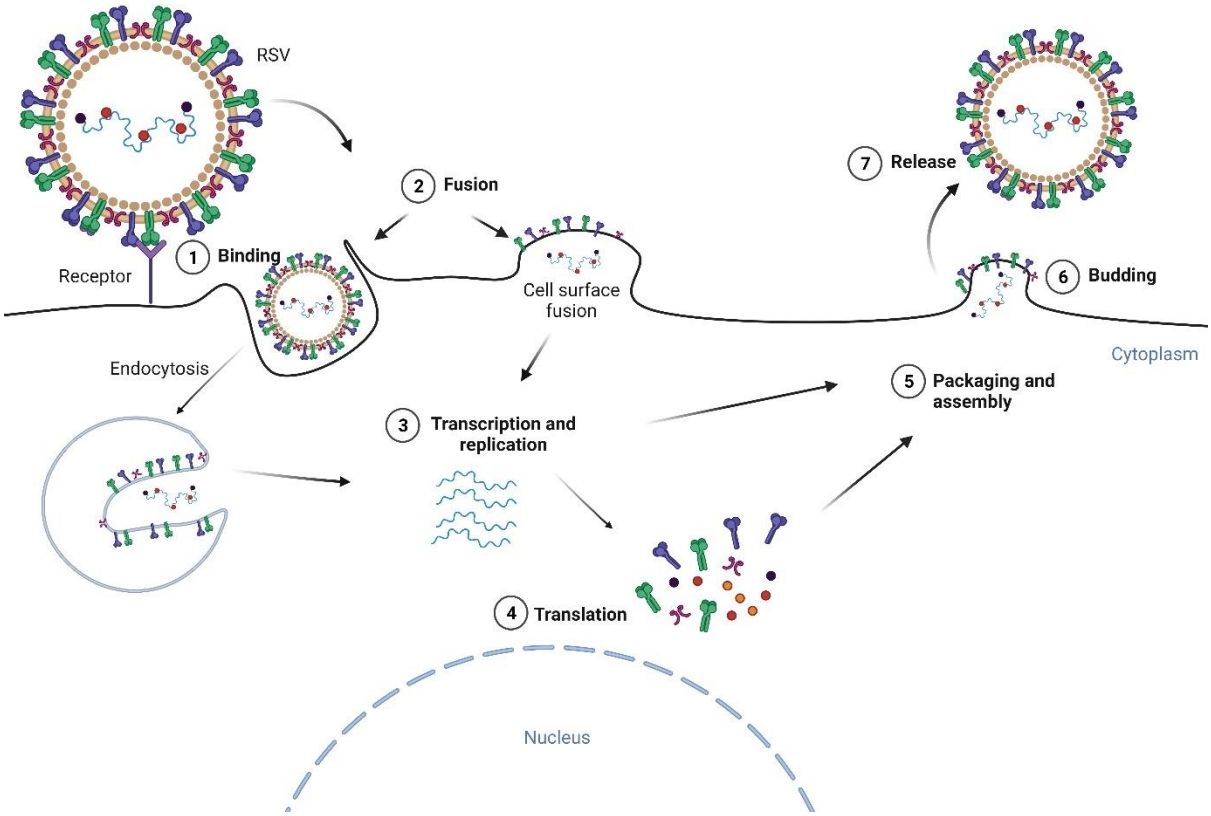

Figure 5. Stages of RSV replication: On binding to the specific cell surface receptor, current evidence suggests RSV utilises a two-step entry mechanism, which involves the utilisation of macropinocytosis, followed by the fusion in endosomes or that RSV can enter host cells through plasma membrane fusion and endocytic vesicle fusion. Once fusion is complete, the ribonucleoprotein complex (RNP) is released into the host cell cytoplasm. Transcription and replication of the virus occur in the cytoplasm within viral inclusion bodies. The negative-sense viral RNA serves as a template for synthesising positive-sense RNA by the viral RNA-dependent RNA polymerase (RdRp). The positive-sense RNA acts as mRNA and a template for synthesising new viral RNA. The RdRp complex also caps and polyadenylates viral mRNAs. It is then translated into viral proteins by the host cell's machinery. The viral proteins and RNAs then assemble to form new virions and are released through budding or cell lysis. The image was adapted from BioRender template.

After fusion, the RNPs are released into the host cell cytoplasm. Transcription and replication of the virus occur in the cytoplasm within viral inclusion bodies. The

negative-sense viral RNA serves as a template for synthesising positive-sense RNA by the viral RNA-dependent RNA polymerase (RdRp). The positive-sense RNA acts as mRNA and a template for synthesising new viral RNA. The RdRp complex also caps and polyadenylates viral mRNAs. It is then translated into viral proteins by the host cell's machinery. The viral proteins and RNAs then assemble to form new virions and are released through budding or cell lysis (El Najjar et al., 2014; Utley et al., 2008). RSV studies on HAE showed that the new viruses are shed exclusively from the apical surface (luminal side) as seen in the hospitalized infants (Villenave et al., 2012).

1.4.4. Severe acute respiratory syndrome coronavirus 2 (SARS-CoV-2)

SARS-CoV-2 is a positive, single-stranded RNA virus that belongs to the family *Coronaviridae*, the causative agent of the coronavirus disease 2019 (COVID-19) pandemic. According to WHO, there have been 757,264,511 confirmed cases of COVID-19, including 6,850,594 deaths (https://covid19.who.int/; accessed on 28/02/2023). Though 13,223,135,400 vaccinations have been administered globally until February 2023, the emergence of new viral variants of concern poses a considerable challenge (Chen et al., 2021; Planas et al., 2021; Wibmer et al., 2021). Patients with SARS-CoV-2 infection show symptoms ranging from mild to severe, with many asymptomatic carriers. The most reported symptoms include fever (83%), cough (82%), and shortness of breath (31%). In addition, gastrointestinal symptoms such as vomiting, diarrhoea, and abdominal pain are described in 2–10%, and in 10% of patients, diarrhoea and nausea were reported (Chen et al., 2020; Wang et al., 2020).

SARS-CoV-2 contains four major structural proteins: spike (S), membrane (M), envelope (E) proteins, and nucleocapsid (N). The spikes of coronaviruses are glycoproteins composed of trimers of S proteins (Delmas & Laude, 1990) that bind to the host cell receptor and mediate the early steps of infection (Cai et al., 2020; Li, 2016; Mariano et al., 2020). Early studies on ex-vivo cultures of bronchus showed that SARS-CoV-2 infected both ciliated and secretory cells. They reported that the viral titres of SARS-CoV-2 at 24 h p.i and 48 h p.i were significantly lower than that of H1N1 which suggests the longer incubation time for SARS-CoV-2 (Hui et al., 2020). Fully

differentiated HAE cultures from different donors infected with SARS-CoV-2 also showed similar tropism also reporting the susceptibility of basal cells to SARS-CoV-2 (Ravindra et al., 2021). SARS-CoV-2 infected ciliated, goblet and club cells and the viral release was reported to be at its peak between 48 – 72 h p.i in the apical washes. Furthermore, they also reported that at 96 h p.i the TEER reduced which directly co-relates to the compromised epithelial barrier integrity post infection (Zhu et al., 2020). In SARS-CoV-2, the viruses are released from both the apical and basolateral sides of the differentiated HAE layer. Hence leading to systematic infection (Zhu et al., 2020). Human bronchial epithelial cells cultured under ALI conditions infected with SARS-CoV-2 showed, up-regulation of genes involved in inflammation (type I IFN, type III IFNs, IL-6 and ISG), apoptosis, and viral gene expression. Furthermore, the genes involved in cilium function, calcium signalling, and iron homeostasis were downregulated (Ravindra et al., 2021). Which could explain the adverse outcome followed by infection in patients.

1.4.4.1. Stages of SARS-CoV-2 replication cycle

The S protein of the SARS-CoV-2 is a homotrimer consisting of two functionally distinct domains, S1 and S2. The S1 contains the receptor binding domain, which binds to the host cell receptor. The S2 domain mediates the viral fusion with the cell membrane triggered by the priming of the S protein, mainly by TMPRSS2 (transmembrane protease serine 2). Angiotensin-converting enzyme 2 (ACE2) has been identified as the critical functional receptor for SARS-CoV-2 (Beyerstedt et al., 2021; Li et al., 2003). ACE2 is especially expressed in the ciliated and goblet cells in the human airways, but not limited to these cell types. The wide distribution of ACE2 receptors in organs may be the reason for cardiovascular, gastrointestinal, kidney, liver, central nervous system, and ocular damage (Hamming et al., 2004). It binds to the receptor-binding domain (RBD) of the spike protein (S protein), which is responsible for the entry of the SARS-CoV-2. The binding affinities between the S protein and ACE2 may also determine the different host cell tropisms of SARS-CoV-2, which leads to the severity of infection (Li et al., 2005).

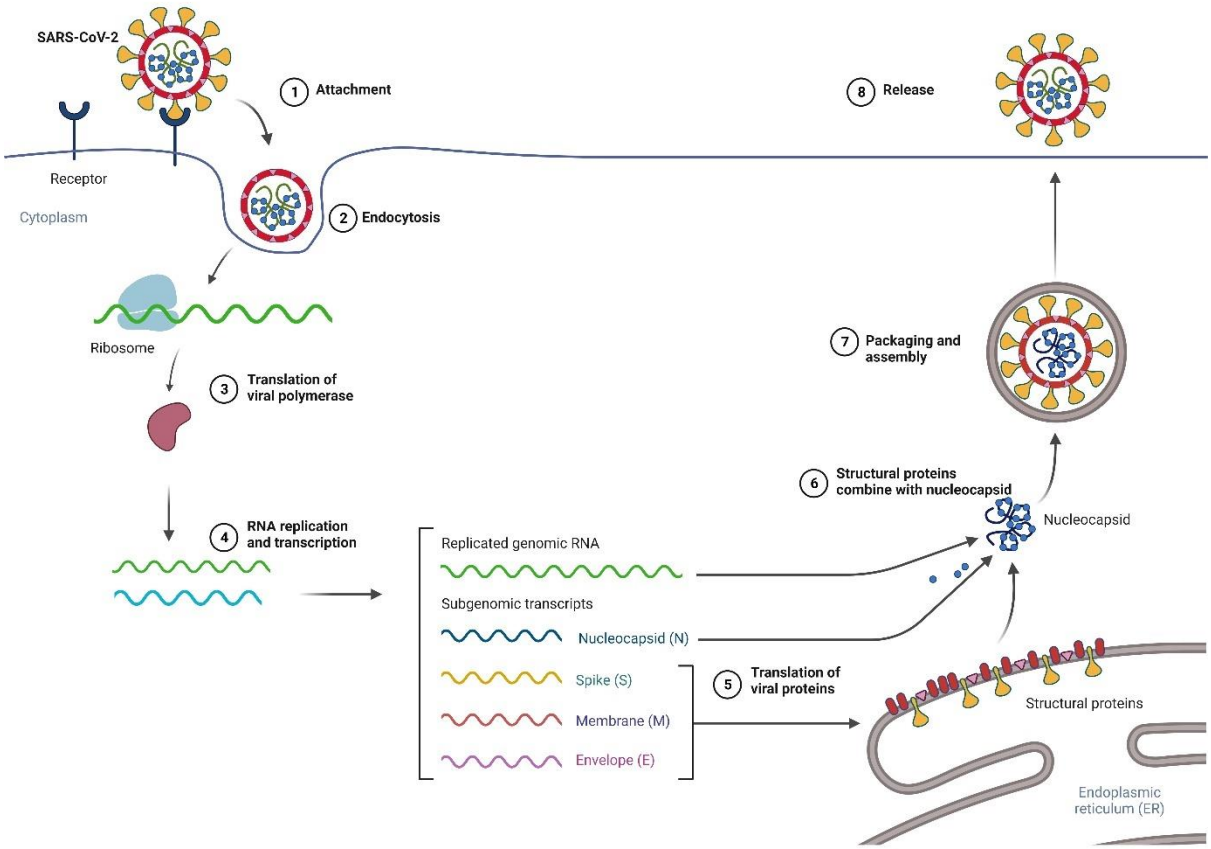

Figure 6. Stages of SARS-CoV-2 replication: SARS-CoV-2 enters the host-cell via ACE2-mediated endocytosis or fusion with the plasma membrane. TMPRSS2 determines the entry pathway. The viral RNA is then immediately translated, using host cell machinery. The newly synthesised RNA and structural proteins then assemble to form viral particles, which bud into secretory vesicles. Finally, the vesicles are secreted from the cell through exocytosis or fusion with the cell membrane. The image was adapted from BioRender template.

The TMPRSS2 plays a significant role in the entry of SARS-CoV-2 by cleaving the S protein, which causes a conformational change that enhances its attachment to the ACE2 receptor following fusion with the cell membrane (Gierer et al., 2013), or the virus can be directly endocytosed followed by the release of viral RNA. Thus, the concentration of TMPRSS2 determines the viral entry pathway (Avota et al., 2021). Using host cell machinery, the viral RNA is then translated to two large polypeptide chains which undergo proteolytic cleavage to form non-structural proteins (nsps). The nsps are suggested to be responsible for the membrane remodelling to form organelles like double-membrane vesicles (DMVs), convoluted membranes (CMs), and small open double-membrane spherules (DMSs), which appear to be the sites of active viral replication (Knoops et al., 2008; Neuman et al., 2016). The newly

synthesised RNA and structural proteins assemble to form viral particles (Khan et al., 2020; Poduri et al., 2020). The particles bud into secretory vesicles, which are then secreted from the cell via exocytosis or fusion with the cell membrane (Pizzato et al., 2022; V'kovski et al., 2021).

2. Aim

The rise in airway-associated diseases, the recent COVID-19 pandemic and the fast-mutating pathogens have raised awareness for the development of more physiologically relevant human disease models for both infection research and drug discovery. The use of animals and cell lines in infection research fail to simulate or replicate the species-specific host-pathogen interactions. Hence, there is a growing need to develop better disease models specific to human pathogens. The advances in the single-cell genomics approaches have now made it possible to identify the cellular heterogeneity in the human airway mucosa and decipher its complex functions (Deprez et al., 2020). Based on the reference data we aim to characterise the in vitro airway tissue models at gene and protein level which helps the researcher to adopt the best model system catered to their study and further expand the diversity of the model's application.

The first aim of this study hence was to characterise the already established hNM and hTM using scRNA-seq to reveal their cell composition and heterogeneity compared to the data from the healthy human airways and further confirm the major cell types at protein level. For this, we combined single-cell technology along with in-detail morphological characterisation using immunohistochemistry, fluorescence, and ultrastructural analyses. The second aim was to use these well-characterised models for infection research. Initially we started with the investigation of the susceptibility of hNM and hTM to *B. pertussis*, virulence factor CyaA. Here, we focussed on determining the innate immune response, intracellular cAMP production, and the impact of toxin treatment on short-term and long-term exposure to the cells in the models. Previous toxin studies were performed on cell lines under 2D or 3D growth conditions or in primary cells in 2D conditions. Thus, this study aimed to answer the impact of the toxins on the primary human airway mucosa models from two different anatomical sites, the upper and lower airway mucosa.

We further aimed to increase the complexity of the study by establishing human respiratory viral infection studies. We aimed to establish physiologically relevant infection studies of IAV, RSV and SARS-CoV-2 in these models. Here, we strived for understanding the early innate immune response of the airway mucosa against the viruses, infection patterns and the morphological changes that occur in the early

events of viral infection. The final aim of this study was to investigate the early infection events of the lower airway mucosa models derived from the non-COPD and COPD patients (GOLD stage 2 and 4) infected with IAV using scRNA-seq. Here, the focus was to generate disease models that capture patient's characteristics/molecular identity without genetic manipulation followed by IAV infection that best capture the native physiological early infection patterns in the human lower airway mucosa.

3. Materials and Methods

3.1. Donor information

The human primary cells used to generate human nasal mucosa models (hNM) were obtained from three different sources. The patients who underwent functional sinus surgery (two female and twelve male donors; 18-72 years old), brush biopsies taken from healthy volunteers (two female donors; 27 and 38 yrs. old) at the Department of Otorhinolaryngology, Plastic, Aesthetic, and Reconstructive Head and Neck Surgery of the University Hospital Würzburg. Additionally, one female and two male nasal epithelial cells (41-63 yrs. old) were purchased from Epithelix Sarl (Geneva, Switzerland). Similarly, the biopsies to build human tracheobronchial mucosa models (hTM) were obtained from five different sources. The patients who underwent elective pulmonary resection at the University Hospital Magdeburg (six male and five female donors; 51 - 79 yrs. old); four male donors (66 - 75 yrs. old) who underwent elective pulmonary resection at the Department of Thoracic Surgery and Lung Support, Ibbenbueren General Hospital, Ibbenbueren, Germany and one male donor (84 yrs) who underwent elective pulmonary resection from KWM Missioklinik, Würzburg, Germany. Additionally, tracheobronchial epithelial cells from three female and one male donor (59-71 yrs) were purchased from Epithelix Sarl (Geneva, Switzerland) and Mattek (Massachusetts, US). Informed consents was obtained from the donors, and trained doctors handled all the surgical procedures. The institutional ethics committees approved the studies on human research of the Julius-Maximilians-University Würzburg (votes 182/10, 179/17 and 116/17) and Otto-von Guericke University Magdeburg (votes 163/17), respectively. Table 2 summarises anonymised donor information used for this study. Both nasal and tracheobronchial epithelial cells were used at passage two to build the tissue models.

3.2. Primary cell isolation from biopsies

Biopsies were given DPBS wash to remove blood clots and debris. Then placed on a 10 cm cell culture dish and sliced into smaller pieces using a surgical blade and sterile forceps, and 3 mL airway epithelial cell growth medium (AECGM) was added to allow the biopsies to adhere to the culture dish but not float and incubated overnight in a humidified incubator with 5% CO_2 at 37 °C. The following day 5 mL fresh media was added and cultured until confluent (Figure 7). The nasal brush biopsies were collected by brushing the gentle touch tip cell collector (Cytobrush Plus GT, C0112, Netherlands) against the superior turbinate of the nose and were immediately placed onto a 15 mL reaction tube containing media with antibiotics. The brush was mixed vigorously to disperse the cells attached to the brush's bristles and carefully removed. The samples were centrifuged at 1000 rpm for 5 min, the supernatant was discarded, and the pellet was slowly resuspended and added to a collagen type-I-coated plate (Greiner bio-one, 690950, USA). Media change was given three times per week. On days 7-12, we observed that the epithelial cells migrated out of the biopsy. After days 12-14 of culture, the biopsy pieces are gently removed from the cell culture plate using sterile forceps for fibroblast isolation. The collected biopsy sections were added in a 15 mL reaction tube and added 5 mL collagenase, 500 U/mL (Collagenase NB 4 Standard Grade from *Clostridium histolyticum*, S1745401, Nordmark Biochemicals, Germany) for 30 min at 37 °C in the incubator. The enzyme was aspirated and washed with fibroblast growth medium (DMEM containing 10% foetal calf serum) and centrifuged at 1000 rpm for 3 min to remove excess enzyme. The biopsy pieces were then added to a 10 cm dish in a 3 mL fibroblast growth medium. The next day 5 mL media was added and cultured for three more days. Media exchange was given a week thrice. On days 7-10, we observed that the fibroblasts grew out of the tissue sections and could be harvested after 10-15 days of cell culture (Lodes et al., 2020; Schweinlin et al., 2017). Isolated epithelial and fibroblast cells were expanded to develop the 3D airway mucosa models or cryopreserved until usage. Airway epithelial cells were grown in Airway Epithelial Cell Growth Medium (PB-C-MH350-0099, PeloBiotech, Germany) and the fibroblasts were grown in DMEM (61965-026, Thermo Fisher Scientific, USA) supplemented with 10% foetal calf serum (P150508, PAN Biotech, Germany). The media used for cell isolation contained 100 units/mL of Penicillin and 0.1 mg/mL Streptomycin (P/S) (P4333, Sigma, Israel). All cells were

cultured under standard conditions (37 °C, 5% CO_2), and fresh media was given thrice weekly.

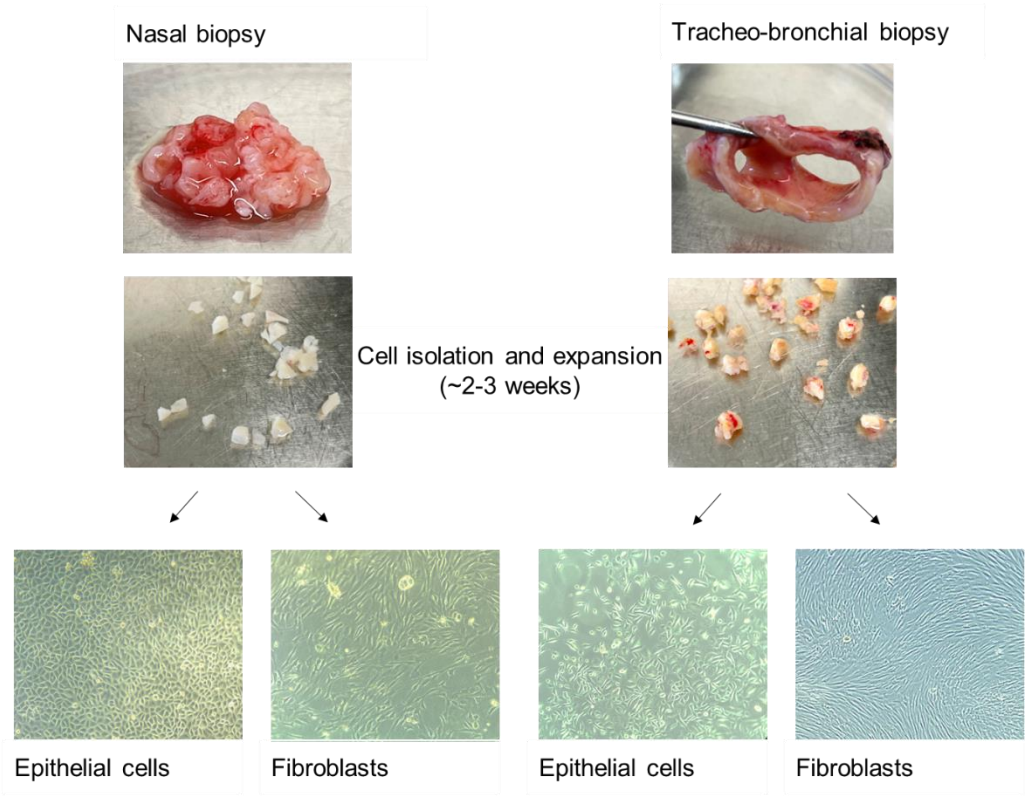

Figure 7. Isolation of primary airway epithelial cells from patient biopsies: The biopsies samples were sliced into small pieces using sterile scalpel blades and cultured with AECGM in a cell culture dish. Media exchange was given a week thrice. When the epithelial cells started to sprout from the biopsies, the biopsy sections were carefully collected and treated with collagenase for fibroblast isolation.

Table 2. List of donors used for the experiments: Details the information regarding the gender and the age of all the human nasal and tracheobronchial biopsy donors used to generate hNM and the hTM sourced ethically from hospitals or purchased commercially.

hNM_Donors	Gender	Age	hTM_Donors	Gender	Age
1	Female	27	1	Female	51
2	Female	38	2	Female	56
3	Female	41	3	Female	59
4	Female	43	4	Female	59
5	Female	45	5	Female	66
6	Male	18	6	Female	68
7	Male	22	7	Female	70
8	Male	26	8	Female	71
9	Male	33	9	Male	52
10	Male	44	10	Male	55
11	Male	45	11	Male	62
12	Male	49	12	Male	64
13	Male	50	13	Male	66
14	Male	53	14	Male	67
15	Male	54	15	Male	69
16	Male	56	16	Male	74
17	Male	57	17	Male	75
18	Male	63	18	Male	82
19	Male	68	19	Male	79
20	Male	71	20	Male	54
21	Male	72			

3.3. Cell culture

The epithelial cells isolated from biopsies cultured in AECGM, were expanded to make models at passage two or cryopreserved at passage one and used when required. When the primary airway epithelial cells were 80% confluent (passage 0) in the 10 cm dish, we expanded the cells to 2-3 x collagen coated T75 flasks. The cell culture media was aspirated and washed with 5 mL DPBS to remove dead cells, debris, and spent media. 5 mL of Trypsin-EDTA was used to detach the cells (5% CO_2 at 37 °C) for 5 min. The flasks were observed under a microscope and given a gentle tap on the sides of the flask to dissociate tightly bound cells. The trypsin-EDTA was inactivated by adding 5 mL of media containing foetal calf serum (P30-3306, PAN-Biotech, Germany). The cells were pipetted into 15 mL reaction tubes and centrifuged at 1000

rpm for 5 min at room temperature (RT). The supernatant was aspirated, and the cell pellet was resuspended in AECGM and reseeded in new flasks at a density of 1:2. The fibroblasts isolated from the biopsy were cultured in FGM and followed a similar procedure for cell expansion but reseeded at a smaller cell density (0.5 x 10^6/mL) in a T-75 flask as the fibroblasts are fast-growing compared to epithelial cells. For making the 3D airway mucosa models, the primary airway epithelial cells were used up to passage two. The cells lose their ability to differentiate at higher passages, and the fibroblasts were used up to passage 7. The immortalised human bronchial epithelial cell line HBEC3-KT (ATCCVR CRL4051TM; LGC Standards GmbH, Wesel, Germany) was cultured in Defined Keratinocyte-SFM (10744019, Thermo Fisher Scientific, Germany). HBEC3-KT were also expanded and cultured as primary airway epithelial cells and were used up to passage 16.

3.4. Cryopreservation and cell revival

Cells were frozen in a mix containing 90% foetal calf serum (FCS) and 10% DMSO. DMSO acts as a cryoprotectant. A prechilled freezing mix was used to reduce the toxic effect of DMSO on the cells. The vials containing cells (10^6 cells/mL) were immediately transferred to cryo boxes and placed at -80 °C. The frozen cells were transferred from freezing containers into cryo boxes at a gas phase of liquid nitrogen. During cell revival, the vials were placed in a water bath set to 37 °C for 1-2 min, and then transferred into a 15 mL reaction tubes containing 5 mL of the appropriate media and centrifuged at 1000 rpm for 5 min at RT. The supernatant was aspirated, the cell pellet was resuspended in 5 mL of the appropriate medium and transferred into cell culture flasks, and 5 mL of fresh media was added the following day.

3.5. Generation of human airway tissue models

Porcine small intestinal submucosa (SIS) was decellularized and used as a biological scaffold for seeding the cells (Sivarajan et al., 2021; Lodes et al., 2020). Animal research was performed according to German law and institutional guidelines and approved by the Ethics Committee of the District of Unterfranken, Würzburg, Germany

(approval number 55.2- 2532-2-256). The method for 3D airway mucosa models was adapted from the protocol of Steinke et al., 2014.

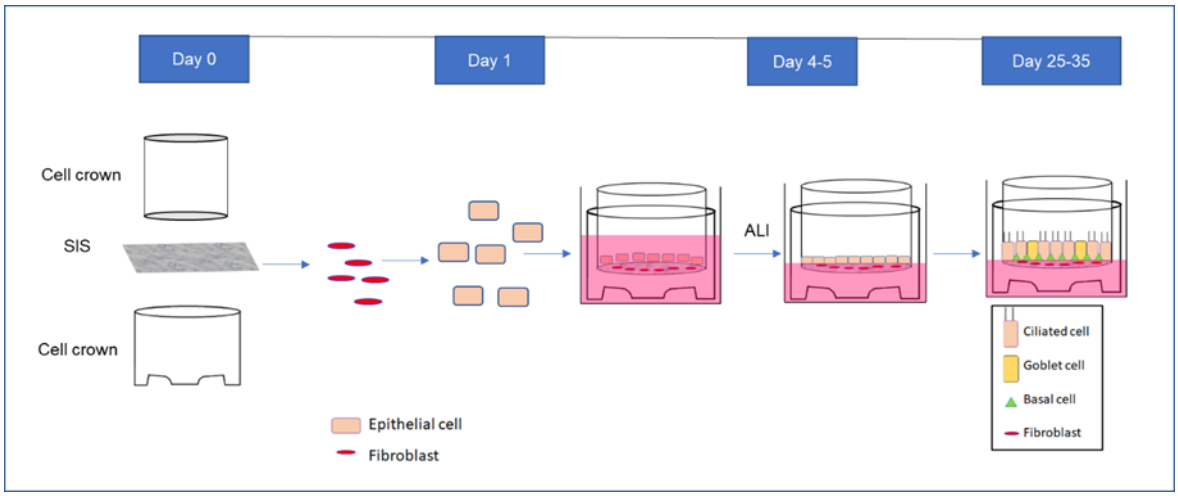

Figure 8. Generation of 3D airway models: The SIS was cut into small sections to fit between the cell crowns and incubated for 2 h with FGM of 500 µL at the apical and 2 mL on the basal compartments. On the same day (day 0), 50,000 nasal or tracheobronchial fibroblasts were seeded on the SIS on the apical side and cultured under submerged conditions. On day 1, 250,000 human nasal epithelial cells or tracheobronchial epithelial cells or HBEC3-KT were added from the apical side and cultured under submerged conditions until the cells were confluent on days 4-5. Then, the media from the apical compartment was removed and further cultured under airlift conditions for 21–31 days until they were fully differentiated and produced mucus (observed visually) and possessed beating kinocilia, observed using high-speed video microscopy.

The SIS was placed on a cell culture dish and cut on one side for the model generation and using sterile forceps, the serous membrane was removed from the SIS. The SIS was then cut into small sections to fit between the two cylinders (cell crowns) and incubated for 2 h with FGM of 500 µL and 2 mL on the apical and basal compartments, respectively (Figure 8). On the same day (day 0), we seeded 50,000 nasal or tracheobronchial fibroblasts on the SIS from the apical side and cultured them under submerged conditions (FGM). On day 1, 250,000 human nasal epithelial cells or human tracheobronchial epithelial cells (co-culture medium - 50% of AECGM and 50% FGM) or HBEC3-KT (co-culture medium - 50% of K-SD and 50% FGM) were added from the apical side and cultured under submerged conditions until the cells were confluent on days 4-5. Then, the media from the apical compartment was removed and further cultured under airlift conditions for 21–31 days. During culture, the apical side was washed once a week with warm DPBS. A fully differentiated model has mucus production (visually) and beating kinocilia which can be, observed using high-

speed video microscopy. The cell culture medium was changed three times per week. The apical side of the 3D tissue models was washed with DPBS to remove excess mucus and cell debris before the experiments were performed and given fresh media. The same protocol was also followed for the COPD disease models.

3.6. Cell dissociation for single-cell RNA sequencing (scRNA-seq)

One of the most critical steps during scRNA-seq is cell dissociation, where the cells are dissociated from the tissue in a single-cell suspension. Therefore, the choice of method is crucial as it should not induce cell stress, damage, or cytotoxicity. The protocol that yielded the best outcome are explained in detail, and the other six tried protocols are briefly described in Figure 9. The same protocol was also used for the infected samples.

The cell culture media from the 3D models was aspirated and washed with 3 x DPBS. 1 mL accutase (A6964, Sigma, USA) was added to the apical side and placed on a shaking incubator (200 rpm) at 37 °C for 30 min (mixed every 10 min with 1 mL pipette); accutase from the apical side was collected into a reaction tube containing 200 µL FCS. 500 µL of 10 mg/mL protease (*Bacillus licheniformis,* subtilisin A, P5380-100MG, Sigma, Germany) diluted in DPBS from a stock solution of 100 mg/mL was added to the apical compartment and incubated for 10 min at RT and mixed 3-4 times using a 1 mL pipette. After 5 min of continued incubation, protease from the apical side was collected in the collection tube, followed by 1 mL PBS addition to the scaffolds to collect remaining cells and added to the collection tube to collect maximum cells from the models. The final volume was adjusted to 5 mL using DPBS and centrifuged at 1200 rpm for 5 min. The supernatant was removed, and 5 mL fresh DPBS was added, mixed gently, and centrifuged for 6 min at 1000 rpm. The pellet was resuspended in 3 mL DPBS.

3.7. Sample preparation for scRNA-seq

The cell suspensions were then transported to the sequencing facility on ice. The cell count and viability were rechecked and transferred to 1 mL microcentrifuge tubes and centrifuged at 300 g for 5 min at RT. The supernatant was carefully removed, and then 100 µL of CMO (10x Genomics multiplexing oligos) were added to each tube, mixed gently, and incubated at RT for 5 min. 1900 µL of ice-cold DPBS was then added, and centrifuged at 300 g for 5 min at 4 °C. The wash step was repeated two more times. 50% cell recovery was expected, and the cells were diluted (~1000 cells/µL) accordingly and checked for viability and cell count. The viability remained > 85% for all samples. The control and infected groups were taken and mixed in a ratio to represent an equal percentage of donors in the final mix. The remaining steps of RNA processing for sequencing for nasal models were done according to the in-house protocol by Dr. Fabian Imdahl (AG Dr. Saliba, Helmholtz institute of RNA - based infection research, Würzburg). The tracheal samples were processed from the Single-Cell seed grant (AG Vogel, Institute for Molecular Infection Biology) by Mélanie Villard (AG Gräfenhan, Single-Cell Center, Würzburg) and the initial data processing by Panagiota Arampatzi, Mugdha Srivastava. Prof. Florian Erhard and Kevin Berg, MSc did the final bioinformatical data processing and analyses (Institute of Virology and Immunobiology, Würzburg).

3.8. cAMP Assay

CyaA or CyaA-AC $^-$ was thawed and immediately diluted to 1.0 µg/mL from stock solutions in 50 mM Tris pH 8.0, 8 M Urea, and 2 mM $CaCl_2$ (TUC). The 3D models were incubated with 1.0 µg/mL of CyaA, CyaA-AC $^-$ or TUC on the apical side. TUC-treated samples served as controls as the working solutions of toxin and toxoids were prepared using TUC. The CyaA activity depends on the binding of free Ca^{2+}, which induces a conformational change that triggers the folding of the RTX domain and penetration of the AC domain into the cell membrane. Hence 2 mM $CaCl_2$ was incorporated into the buffer. After 1 h of incubation, the apical surface was washed with PBS to stop the reaction, followed by cell lysis with 0.1 M HCl at 95 °C for 20 min. The samples were centrifuged at 3000 rpm for 5 min, and a direct competitive ELISA,

quantified cAMP, in the supernatant according to the manufacturer's instructions (ADI-901-066, Enzo life sciences, Germany). The samples were run following the acetylated protocol, and five dilutions in duplicates were performed to ensure that the values were within the detection limit of the kit. The amount of cAMP-HRP bound to the plate was determined by reading the colorimetric HRP activity at OD 405 nm. The measured cAMP values were normalised to the total protein content using the DC™ protein assay (5000113 BioRad, Germany). We performed independent experiments (N=7 for hNM, N=6 for hTM, N= 7 for HBEC3-KT in duplicates. All the CyaA and CyaA-AC⁻ aliquots for the experiments on IL-6, IL-8, HBD-2 secretion, epithelial barrier properties, and histology were also used for cAMP assay to make sure that the toxin was active.

3.9. Histological Analyses

3.9.1. Fixation, paraffin embedding, and microtome sectioning

The models were given PBS wash, then 500 µL and 2 mL of 4% PFA were added to the apical and basal compartments and incubated for 2 h at RT or overnight at 4 °C. Then the models were detached from the cell crowns, the excess scaffolds were removed using a surgical blade, and transferred into embedding cassettes lined with filter paper. The embedding cassettes were then placed in the water compartment of the automated spin tissue processor. The embedding process was as follows:

Table 3. Steps during the paraffin embedding of fixed samples.

No	Solution	Time [h]	Step/ Remarks
1	Distilled water	2	Wash
2	50% EtOH	1	Dehydration
3	70% EtOH	1	
4	90% EtOH	1	
5	96% EtOH	1	
6	Isopropanol	1	
7	Isopropanol	1	
8	Isopropanol/Xylene (1:2)	1	RT, alcohol removal

9	Xylene	1	
10	Xylene	1	
11	Paraffin	1.5	60 °C, Paraffin infiltration
12	Paraffin	1.5	

After embedding, paraffin-infiltrated models were removed from the cassettes, and paraffin blocks were made using metal moulds. The blocks were cooled on a cooling plate at 4 °C and 5 µm thin sections were made using a microtome for histology and immunostaining. The slides were heat-fixed overnight at 37 °C followed by 30 min at 60 °C to melt the wax before placing it in xylene.

3.9.2. Deparaffination and rehydration of the tissue sections

The paraffin-embedded sections were deparaffinised and rehydrated according to the following protocol.

Table 4. Steps during deparaffination and rehydration of the tissue sections

Solution	Time [min]
Xylene	10
Xylene	10
96% Ethanol	1
96 % Ethanol	1
70% Ethanol	1
50% Ethanol	1
Distilled water	1

3.9.3. Hematoxylin and Eosin (H & E) staining

Table 5. Represents the steps during H & E staining

Solution	Time [min]	Step/Remarks
Hematoxylin	6	Stains the cell nucleus
Deionised water	-	Rinsing until no colour washes out
Eosin	3	Stains the cytoplasm
Deionised water	-	Rinsing until no colour washes out

Ethanol 70 %	1	Dehydration
Ethanol 96 %	2	Clearing
Isopropyl alcohol	5	Dehydration
Isopropyl alcohol	5	Clearing
Xylene	5	
Xylene	5	

3.9.4. Alcian blue staining

Table 6. Represents the steps during Alcian blue staining

Solution	**Time [min]**	**Step/Remarks**
3% glacial acetic acid	3	
1% Alcian blue	30	Stains the negatively charged proteoglycans
Deionised water	-	Rinses
Nuclear fast red solution	5	Stains the cell nucleus
70% Ethanol	2x short dip	
96% Ethanol	2	
Isopropyl alcohol	5	
Isopropyl alcohol	5	
Xylene	5	
Xylene	5	

3.9.5. Transmission Electron Microscopy (TEM)

After an hour of incubation with TUC, CyaA, or its toxoid, hAM was washed and fixed in 2.5% glutaraldehyde, then fixed in 2% OsO_4, washed with H_2O, and incubated in 0.5% uranyl acetate. Then, the samples were processed at the Imaging Core Facility of the Biocenter - Prof. Dr. Christian Stigloher's lab, University of Würzburg, by Daniela Bunsen and Claudia Gehrig-Höhn were they dehydrated and embedded the samples in Epon812 (Prüfert et al., 2004). Methylene blue staining was carried out on semi-thin sections for quality control. The same protocol was followed for all the samples used for TEM in this study. Ultrathin sections were then imaged at a JEOL JEM-2100 transmission electron microscope equipped with a TVIPS F416 camera or a JEOL

JEM-1400 Flash transmission electron microscope equipped with a Matataki Flash camera.

3.9.6. Immunofluorescence staining

The thin paraffin sections were unmasked to expose the epitopes, which may be masked during the embedding process. The slides were immersed in the buffer (Sodium-citrate buffer (pH 6) or Tris-EDTA buffer (pH 9), depending on the antibody as recommended by the manufacturer, or optimised for each antibody and placed in a steam chamber for 10-12 min. The slides were retrieved and placed in distilled water for 3 min to cool before immunostaining. The sections were permeabilised with 0.2% TritonX-100 in PBS for 5 min and washed with wash buffer (PBS containing 0.05% Tween-20) for 5 min. Samples were covered with a blocking solution (5% BSA in PBS) for 1 h at RT to reduce the non-specific binding of the antibodies. The primary antibodies were diluted in the antibody diluent, pipetted over the sections, and incubated overnight at 4 °C in a dark, humidified chamber. The slides were recovered the next day and washed three times in wash buffer, followed by secondary antibody incubation for 1 h at RT. The slides were rewashed three times, added Fluoromount® G+ DAPI, and covered with coverslips to prevent drying. Negative controls (slides without primary antibodies) were also prepared to monitor non-specific binding. The samples were imaged using Keyence/Leica microscope.

3.10. Epithelial barrier integrity assay

The epithelial barrier integrity of the tissue models was determined using fluorescein isothiocyanate (FITC) conjugated dextran (4 kDa; 46944-100MG-F, Sigma, Germany). Pre- and post-treatment with 1.0 µg/mL CyaA, CyaA-AC– or TUC buffer for 24 h, the apical surface was washed with PBS, and 1 mL of fresh co-culture medium was added to the basal compartment. Next, 500 µL of 0.25 mg/mL of FITC-dextran dissolved in DMEM (61965-026, Thermo Fisher Scientific, USA) was incubated in the apical compartment for 30 min protected from light in the incubator. 100 µL of the medium was collected from the basal compartment into a microplate (PS, 96 well, black, F-

bottom; 655076, Greiner bio one, Germany) in duplicates and analysed in a TECAN reader (absorbance: 490 nm, emission: 525 nm). The mean absorbance measured in four independent experiments (N=4, in duplicates) was normalised to a cell-free SIS scaffold mounted on a cell crown. The permeability of the hAM to FITC-dextran was displayed as percentage values.

3.11. Human inflammatory cytokine cytometric bead array

hAM was washed in PBS to remove debris and excess mucus secretion and then treated from the apical side with 1.0 µg/mL CyaA, CyaA-AC^{-} or TUC buffer for 24 h. The supernatants were collected from the apical compartment and analysed for secreted IL-6 and IL-8 using the human inflammatory cytokine cytometric bead array (CBA) kit (551811, BD Biosciences, USA). The CBA kit simultaneously quantifies 6 inflammatory cytokines (IL-1b, IL-6, IL-8, IL-10, TNF, IL-12p70). Cell culture supernatants were collected from the apical compartments after 24 h toxin treatment. The supernatants were centrifuged at 3000 rpm at 4 ℃ for 3 min to remove the cell debris. The supernatant was frozen at -80 ℃ until they were analysed. IL-6 and IL-8 in the cell culture supernatants were quantified for this study as they were actively secreted in response to the toxin treatment. Each bead was vortexed, and 2.5 µL of the cytokine beads, 12.5 µL of each sample, and 2.5 µL of the human inflammatory cytokine PE detection reagent were added to the 96 well conical bottom plates. The plate was placed on a shaker and mixed at 1100 rpm for 5 min and followed by incubation for 3 h in the dark at RT. Then, 200 µL of wash buffer was added to each well and centrifuged for 5 min at 800 rpm. The supernatant was removed, and the beads were resuspended in 200 µL wash buffer. BD Accuri™ C6 Plus flow cytometer was used to assess the cytokine level. The cytokines were quantified using the FCAP Array™ software version 3.0. Appropriate dilution was done for each sample to have the values within the detection limit of the kit. The treatment groups inflammatory cytokine concentrations were normalised to the control group and expressed as relative concentrations to eliminate the basal difference in individual cytokine release within individual donors.

3.12. Enzyme-linked immunosorbent assay (ELISA)

The supernatants were analysed for secreted HBD-2 by ELISA (ARG80903, Arigo Biolaboratories, Taiwan). ELISA was also used for interleukin (IL-6, IL-8, TNF-α) analyses for viral infection study (ab178013, ab214030, ab181421, Abcam, UK) following the manufacturer's instructions. The assays were performed in independent experiments, each in duplicates (IL-6 and IL-8: N=6 for hNM, N= 5 for hTM, and N = 6 for HBEC3-KT). For the basal cytokine release analyses, the fully differentiated models were given mucus wash, and the following day 500 µL of DPBS was added to the apical side of the model. The supernatant was analysed for IL-6 and IL-8 secretion.

3.13. Propagation of viruses

The patient-derived SARS-CoV-2, IAV and RSV were isolated and characterised at the Institute of Virology and Immunobiology, Würzburg, Germany (Zimniak et al., 2020). For the propagation of IAV, the MDCK cell lines were used. Hep G2 cell lines were used for RSV, Heike Oberwinkler prepared the viral stocks, and Nina Geiger prepared SARS-CoV-2 working stocks in Vero cells. The cell lines were cultured in DMEM with 10% foetal calf serum (FCS), 1% penicillin/streptomycin(P/S), and 1% L-Glutamine. For the experiments, we have used Influenza A subtype H1N1. The characterisation was performed at Virus diagnostics – Institute of Virology and Immunobiology, Würzburg, Germany.

3.14. Determination of the viral titer

On day 0, the respective cell lines were seeded (5000 cells per well) on a 96-well plate, MDCK for IAV and Hep G2 for RSV. On Day 2, when the cells were 80% confluent, serially diluted virus was added and incubated for 24 h. The supernatant was removed and was given 3 x DPBS wash to remove unbound virus and cell debris. Histofix was used to fix the sample for 15 min at RT. Given a PBS wash, the sections were permeabilised with 0.2% TritonX-100 in PBS for 1 min and washed with wash buffer

(PBS containing 0.05% Tween-20) for 5 min. Samples were covered with the blocking solution of 100 µL per well (5% BSA in PBS) for 1 h at RT to reduce the non-specific binding of the antibodies. The primary antibodies were diluted in the antibody dilution solution, pipetted over the sections, and incubated overnight at 4 ℃. The samples were recovered the next day and was washed with wash buffer (3 times), followed by secondary antibodies incubation for 1 h at RT. The samples were further washed three times and covered with Fluoromount® G+ DAPI. The samples were imaged using Keyence, and the cell count was done using ImageJ.

3.15. RNA extraction

3.15.1. Intracellular RNA extraction

The cell culture media was removed, and the apical surface was washed with 3x DPBS to remove unbound virus particles. The total RNA was isolated following a kit-based protocol (SKU: R6934-02, omega BIO-TEK, USA), starting with 500 µL of RNA-Solv® Reagent containing 2-mercaptoethanol on the apical compartment and pipetting up and down 5-6 times to dissociate the cells from the model. The remaining steps were followed as per the manufacturer's instructions. The suspension was collected in a 1.5 mL microcentrifuge tube and incubated at RT for 3 min, and 100 µL (for < 5 x 10^6 cells) of chloroform was added and vortexed for 20 s to mix thoroughly, and incubated at room temperature for 2-3 min. Then centrifuged at maximum speed (13,000 x g) at 4°C for 15 min to separate the aqueous and organic phases (the sample separates into 3 phases: an upper colourless aqueous phase, which contains RNA, white interphase, and a lower blue organic phase). The upper aqueous phase (~350 µL) was transferred into a new 1.5 mL microcentrifuge tube, and an equal volume of 70% ethanol was added and vortexed to mix thoroughly. A HiBind® RNA Mini Column was inserted into a 2 mL Collection tube, transferred 700 µL sample (including any precipitate that may have formed) to the HiBind® RNA Mini Column and was centrifuged at 10,000 x g for 1 min. The filtrate was discarded, and the collection tube was reused. Then, 500 µL RNA Wash Buffer I were added to the HiBind® RNA Mini Column. The columns were centrifuged at 10,000 x g for 30 s the filtrate was discarded, and the collection tube was reused. Added 500 µL RNA Wash Buffer II to

the HiBind® RNA Mini Column and centrifuged at 10,000 x g for 1 min. The filtrate was discarded, and the collection tube was reused. A second was performed with RNA Wash Buffer II and centrifuged at maximum speed for 2 min to completely dry the HiBind® RNA Mini Column. The HiBind® RNA Mini Column was transferred to a clean 1.5 mL microcentrifuge tube and 50 µL Nuclease-free Water was added and centrifuged at maximum speed for 2 min, eluted RNA was stored at -80°C.

3.15.2. Viral RNA extraction from cell culture supernatant

After the infection, 500 µL of DPBS was added to the control and non-infected model's apical compartments. The supernatant was collected in a nuclease-free 1.5 mL microcentrifuge tube. 200 µL from this was used for the RNA isolation. (11858874001, Roche, Germany). 200 µL of the supernatant was added to a microcentrifuge tube. To this was added 200 µL of freshly prepared working solution (200 µL Binding buffer + 4 µL poly A per 200 µL sample: carrier RNA- supplemented Binding buffer). Proteinase K solution was added, immediately mixed, and incubated for 10 min at 72°C. 100 µL Binding buffer was added and mixed. A high Pure filter tube was inserted into a collection tube, and the entire sample was pipetted into the upper reservoir of the filter tube and centrifuged at 8,000 x g for 1 min. After the centrifugation, the filter tube was removed, and the flow through with the collection tube was discarded. The filter tube was inserted into a new collection tube, and 500 µL Inhibitor Removal Buffer was added to the upper reservoir and centrifuged at 8,000 x g for 1 min. After the centrifugation, the filter tube was placed on a fresh collection tube, and the others were discarded. 450 µL of Wash Buffer was added to the upper reservoir of the filter tube and centrifuged at 8,000 x g for 1 min, and the flow through was discarded again. The filter tube was inserted into a new collection tube, and 450 µL of Wash Buffer was added, then centrifuged at 8,000 x g for 1 min, and the flow through was discarded. The filter–collection tube assembly was again centrifuged at 13,000 x g for 10 s to remove residual Wash Buffer. The filter tube was inserted into a nuclease-free, sterile 1.5 mL microcentrifuge tube. 50 µL of Elution buffer was added to elute the viral nucleic acids and centrifuged at 8,000 x g for 1 min. The eluted RNA was stored at -80°C.

3.16. RT-qPCR

The LightCycler®Multiplex RNA Virus Master was used to amplify the gene of interest (SARS-CoV-2, IAV, and RSV-B) described by the manufacturer (LightCycler® Multiplex RNA Virus Master Version 09 07083173001, Roche, Germany). RT-qPCR was performed and quantified with the LightMix® Modular (Influenza A (InfA M2), 53-0101-96; Respiratory Syncytial Virus (RSV) 61-0110-96; Sarbecovirus SARS-CoV-2, 50-0776-96; RT-qPCR assay kit, TIB MOLBIOL, Germany). All PCRs were performed in duplicates using the LightCycler® 480 II (Roche). Quantifications were performed with the respective cycler software (LightCycler®480SW 1.5.1).

Table 7. List of primers and probes

GAPDH_forward primer	ACAACGAATTTGGCTACAGC
GAPDH reverse primer	AGTGAGGGTCTCTCTCTTCC
GAPDH hydrolysation probe	[HEX]ACCACCAGCCCCAGCAAGAGCACAA[BHQ1]

Table 8. Information on the reaction mix

Reagent	**Volume [µL]**
Water, PCR Grade	10.4
Virus-specific probes	0.5
Roche Master	4
RT Enzyme Solution, 200X conc.	0.1
Total Volume	15

3.17. Determination of IAV release

The models were infected with 200,000 ifu (infectious units). 500 µL of mixed media was added to the apical side to collect the viral particles at 6 h, 12 h, and 24 h, respectively. The RNA was isolated from the supernatant, and RT-qPCR was done to estimate new viral releases. The models were fixed and stained to monitor the progress of infection over time.

Table 9. List of cell culture media and reagents

Name	Catalogue number	Company
DMEM	61965-026	Thermo Fisher Scientific, USA
AECGM (Airway epithelial cell growth medium)	PB-C-MH350-0099	Pelo Biotech, Germany
Defined Keratinocyte-SFM	10744019	Thermo Fisher Scientific, Germany
DPBS	D8537	Sigma-Aldrich, Germany
Collagenase	S1745401	Nordmark Biochemicals, Germany
Penicillin and streptomycin (P/S)	P4333	Sigma, Israel
Trypsin-EDTA	15400-054	Thermo Fisher Scientific, UK
Foetal calf serum (FCS)	P150508	PAN Biotech
Bovine serum albumin (BSA)	0219989925	MP Biomedicals
Protease	P5380-100MG	Sigma-Aldrich, Germany
Accutase	A6964	Sigma-Aldrich, USA

Table 10. List of cells and their culture media

Cells	Media
HBEC3-KT American Type Culture Collection (ATCC)	Defined Keratinocyte-SFM
Hep G2 (ATCC)	DMEM + 10% FCS + P/S
Human primary-nasal and tracheobronchial epithelial cells	AECGM
MDCK (ATCC)	DMEM + 10% FCS + P/S
Nasal and Tracheal fibroblasts	FGM (DMEM + 10% FCS)

Table 11. List of primary antibodies

Target	Host	Dilution	Catalogue number	Company
Acetylated tubulin	Mouse	1:1000	T8328	Sigma-Aldrich, Germany
CK 18	Mouse	1:100	M7010	Agilent, USA
CK 5/6	Mouse	1:200	M7237	Agilent, USA
Influenza A nucleoprotein	Rabbit	1:200	GTEX125989	GeneTex, USA
MUC5AC	Mouse	1:100	HPA008246	Sigma-Aldrich, Germany
MUC5B	Rabbit	1:100	MA1-38223	Thermo Scientific, Germany

RSV Polyclonal	Goat	1:200	PA1-73017	Thermo Scientific, Germany
RSV- Subgroup B	Mouse	1:200	NBP2-50311	Novus Biologicals, Germany
Vimentin	Rabbit	1:1000	Ab92547	Abcam, UK
SARS-CoV-2	Rabbit	1:1000	GTX135357	GeneTex

Table 12. List of secondary antibodies

Name	Host	Dye	Dilution	Catalogue number	Company
Anti-mouse	Donkey	488	1:400	A21202	Invitrogen
Anti-rabbit	Donkey	488	1:400	A21206	Invitrogen
Anti-rabbit	Donkey	555	1:400	A31572	Invitrogen

Table 13. List of chemicals

Name	Details	Company
Antibody diluent	ALI20R500	Labline, Germany
DAPI FluoromountG™	SBA010020	Invitrogen
Descocept	00-311-050	Dr. Schumacher GmbH, Germany
Dimethyl sulfoxide (DMSO)	D2438	Sigma-Aldrich, Germany
Entellan®	1079600500	Merck, Germany
Eosin 1 % aqueous solution	10177.01000	Morphisto GmbH, Germany
Ethanol absolute	9065.2	Carl Roth, Germany
Haematoxylin Solution acidic	10231.01000	Morphisto GmbH, Germany
Hydrochloric acid	K025.1	Carl Roth, Germany
Isopropyl alcohol	2316.5	Carl Roth, Germany
Nuclear fast red 0.1 %	10264.00500	Morphisto
Paraffin	6642.6	Carl Roth, Germany
Roticlear Histofix®	P087	Carl Roth, Germany
Super pap pen	N71310-N	Science services, Japan
Triton X 100	3051.2	Carl Roth, Germany
Trypan Blue, 0.4 %	T8154100	Sigma-Aldrich, Germany
Tween20	8.22184.0500	VWR, Germany
Xylene	9713.3	Carl Roth, Germany

Table 14. List of buffers

Name	Details
Blocking buffer	5% (w/v) BSA in 1x PBS
Permeabilization buffer	0.01% (v/v) TritonX-100 in PBS
Tris-EDTA (pH 9)	10 mM Tris base and 1 mM EDTA
TUC buffer	50 mM Tris pH 8.0, 8 M Urea, 2 mM $CaCl_2$
Wash buffer	PBS in 0.5 % (v/v) Tween-20

Table 15. List of instruments

Name	Details
- 20 ℃ freezer	Liebherr, Germany
- 80 ℃ freezer	Thermo Scientific, Germany
4 ℃ Cold room	Genheimer, Germany
Accu-Jet Pro Pipettor	Brand, Germany
Aspiration Device - VacuBoy	Integra Biosciences, Germany
Bright field (Axio Lab.A1)	Carl Zeiss Microscopy GmbH, Germany
Centrifuge 5417R	Eppendorf, Germany
Confocal microscope TCS SP8	Leica, Germany
Drying oven	Memmert, Germany
Embedding cassette printer VCP-5001	Vogel Medizintechnik, Germany
Embedding center Microm STP 120	Thermo Scientific, Germany
Flow Cytometer BD Accuri C6 Plus	BD Biosciences, USA
Freezing container: Mr. FrostyTM	VWR, Germany
Fume hood	Prutscher Laboratory Systems, Austria
Genie 2 Vortex	Carl Roth, Germany
Ice machine AF-80	Scotsman, Italy
Infinite 200 PRO NanoQuant Microplate Reader	Tecan, Germany
Liquid Nitrogen Storage Tank MVE 815 P190	German cryo, Germany
Microscope BZ9000 E BIOREVO System	KEYENCE, Germany
Microscope BZ-X810	KEYENCE, Germany
NanoDrop 1000	Thermo Scientific, USA
Neubauer cell counting chamber	Marienfeld GmbH & Co. KG, Germany
Nikon 80i	Nikon GmbH, Germany
Refrigerator (MedLine)	Liebherr, Germany
Rocking platform shaker	VWR, Germany
Sliding Microtome RM 2255	Leica, Germany
Transmission Electron Microscope JEM-2100	JOEL, Japan

Table 16. List of commercial kits

Name	Details
Bradford assay	Sigma-Aldrich, Germany
cAMP kit	Enzo life sciences, Germany
Cellular RNA isolation kit	omega BIO-TEK, USA
Cytokine cytometric bead array kit	BD Biosciences, Germany
Human B defensin ELISA kit	Arigo Biolaboratories, Taiwan
IL-6 kit	Abcam, UK
IL-8 kit	Abcam, UK
RT-qPCR assay kit	TIB MOLBIOL, Germany
Supernatant RNA isolation kit	Roche, Germany
TNF-α kit	Abcam, UK

Table 17. List of consumables

Name	Details
Cell culture plates: 6 well, 12 well, 24 well, 96 well	TPP, Germany
Cell culture flasks: 25 cm^2, 75 cm^2, 150 cm^2	TPP, Germany
Collagen type -I coated flask: 25 cm^2, 75 cm^2, 150 cm^2	Greiner bio-one, USA
Centrifuge tubes:15 mL, 50 mL	Greiner Bio-One, Germany
Cover Slips for Object Slides: 24 x 60 mm	Menzel-Gläser, Germany
Cryo tubes: 1.8 mL	Nunc, Germany
Disposable microtome blades (type S35)	pfm medical, GER
Cell strainer: 40 µm, 70 µm	Greiner Bio-One, Germany
Disposable Pipettes: 5 mL, 10 mL, 25 mL, 50 mL	Greiner Bio-One, Germany
Embedding cassettes	Klinipath, Germany
Embedding filter paper	Labonord, Germany
Medical gloves, nitrile	Medline, Germany
Object Slides: Polysine™ (25 x75 x1 mm)	Thermo Fisher Scientific, Germany
Parafilm®	Carl Roth, Germany
Petri Dishes: 145 x 20 mm	Greiner Bio-One, Germany
Pipette tips: 0.5-10 µL, 10-100 µL, 100-1000 µL	Eppendorf, Germany

Table 18. List of software

Name	Details
EndNote 20.2.1	Clarivate™, Australia
FCAP array™ version 3.0	BD Biosciences, USA
GraphPad™ Prism version 9	GraphPad Software, USA
Motion Traveller ®	Imaging Solutions GmbH, Germany
ImageJ (Fiji)	NIH, USA
LightCycler®480SW 1.5.1	Roche, Germany
Biorender	USA

Table 19. List of donors used for COPD vs. non-COPD scRNA-seq

hTM	Sex	Age	COPD	Smoker
#1	male	55	yes	yes
#2	male	69	yes	yes
#3	female	51	no	no
#4	male	75	no	yes
#5	male	74	no	yes

4. Results

4.1. Characterisation of human primary cell-derived airway mucosa tissue models

In this study, we conducted a comprehensive characterisation of the cellular composition of the human airway mucosa tissue models used for respiratory infection studies. To achieve this, we started with scRNA-seq to identify distinct cell populations, determine their frequency, and identify specific markers. The scRNA-seq data was further confirmed at the protein level, and a detailed morphological characterisation was performed, including ultrastructural analyses. In this results section, we present our findings on the cellular heterogeneity of the human airway models and describe the distinct cell populations identified through scRNA-seq. We also discuss the specific markers identified for each cell type and the confirmation of cell types at the protein level. Additionally, we present our ultrastructural analyses, which provide detailed insights into the cellular organisation and structure of the airway models. Our results provide a comprehensive characterisation of the cellular composition of human airway models and lay the foundation for subsequent studies on respiratory infections using these models.

4.1.1. General model characterisation

4.1.1.1. Hematoxylin and Eosin (H & E) and Alcian blue staining

The H & E staining and alcian blue staining provide a quick and general overview of the model morphology regarding the distribution of ciliated cells, mucus secreting cells, shape, structure, and its differentiation status. H & E staining is the gold standard used in histological analyses, which provides an overview of cell morphology and tissue architecture. Hematoxylin, a basic dye that stains the nucleus blue colour, and the acidic dye eosin help us to identify the cellular components – the cytoplasm, kinocilia, and connective tissue, which are stained pink (Figure 9 A and C). Alcian blue is a basic dye that binds to acidic mucins and stains them blue. This allows for the visualisation and differentiation of different tissue components (Figure 9 B and D).

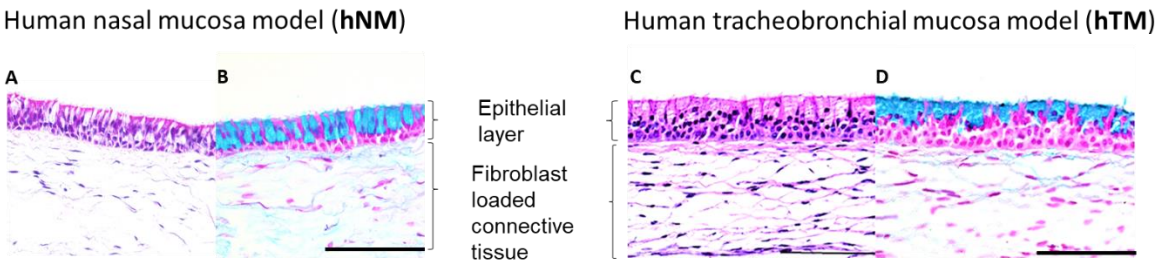

Figure 9. The mucociliary phenotype of the human airway mucosa model: H & E staining shows the differentiated airway epithelium of the human nasal (A and B) and tracheobronchial (C and D) tissue model, and the scaffold containing the fibroblast-loaded connective tissue at the bottom and the Alcian blue staining helps to visualise the mucus-filled vesicles of the secretory cells. Scale bar = 100 µm

4.1.2. Single-cell RNA sequencing (scRNA-seq)

4.1.2.1. Cell dissociation for scRNA-seq

To ensure the success of our experiments, the cell viability post-cell dissociation must be above 80%. However, achieving a single cell suspension with high viability can be challenging due to fibroblasts in the scaffold, which provide extra stability to the epithelial layer. This makes the dissociation process difficult compared to tissue models based on transwell inserts. Therefore, extra care was taken during the dissociation procedure to ensure good cell viability. This may include using gentle enzymatic treatment, optimising the dissociation time, and carefully monitoring the cells during the dissociation process to avoid over-digestion. By doing so, we can ensure that the cells remain viable and functional throughout the experimental procedure, which are essential for obtaining accurate and reliable results.

For this, we compared six different methods (Figure 10). First the models were treated with accutase on the apical side for 30 min at 37 °C. The cell recovery was poor (<20,000 cells per model) after collecting the cells by repeated pipetting to create a cell suspension. In a second approach, the models were treated with accutase on the apical side for 1 h at 34 °C to prevent the inactivation of accutase, but the cell recovery was still poor (<30,000 cells per model). Then, I removed the media, and the cell crowns were flipped, and 100 µL of collagenase was added to the scaffold for 30 min, followed by 30 min of accutase treatment. Due to the significant amount of cell death associated with this approach, it was unsuitable for the purpose and therefore

not utilized. The next approach was a cold dissociation using protease. Here, the models were dismantled from the cell crowns, cut into small sections, and treated with pre-chilled protease for 30 min with repeated pipetting and vortexing every 10 min. The method also yielded fewer cells (<20,000 cells per model). The fifth method was adding 500 µL of protease on the apical compartment followed by 37 °C incubation for 30 min. This method was also associated with high cell stress and death. The final method, the combined use of accutase and protease, are explained in detail in the materials and method section. This method was reproducible across four donors with high cell recovery and cell viability (Figure 10).

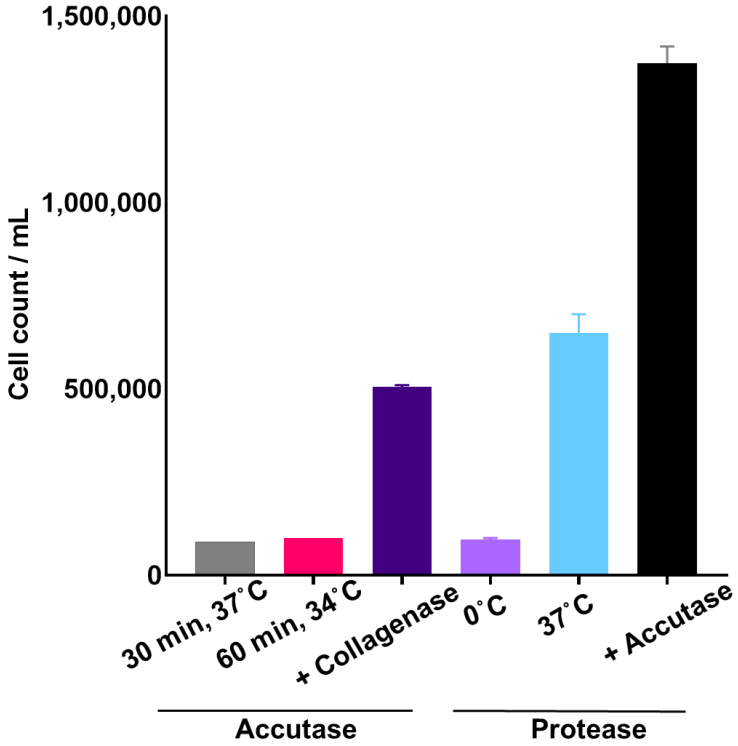

Figure 10. Representative image of cell dissociation from nasal tissue models: Comparison of the methods used for cell dissociation. Harsh dissociation protocols (collagenase) caused cell stress, and death, while the milder methods (accutase) yielded fewer cells. With accutase and protease combination treatment, a cell viability of >90% was obtained (black); N = 4.

4.1.2.2. Cell clustering and frequency distribution of hAM

To understand the correlation of hAM to the native airways we used scRNA-seq to effectively characterise both hNM and hTM and mapped it to the human cell atlas of healthy airways (Deprez et al., 2020) before we used them for infection studies.

Through this method, we could cluster the hAM cell populations into the major cell types found in the native human airways such as the basal cells (suprabasal, and cycling), ciliated cells (indicated as multiciliated and muticiliated N; Figure 11) goblet cells, secretory, serous, fibroblasts (indicated as endothelial cells in Figure 11 A, B) and deuterosomes (Figure 11). The clustering and UMAP assignment were done by Prof. Florian Erhard and Kevin Berg (Institute of Virology and Immunobiology, Würzburg) from this information the specific cell types were then annotated. Our scRNA-seq data of the hAM matched to healthy human airways (Deprez et al., 2020) provided a detailed overview of the molecular heterogeneity of the engineered models including the presence of major and minor cell populations present in the native human airways which recommends their application for host-pathogen interaction studies.

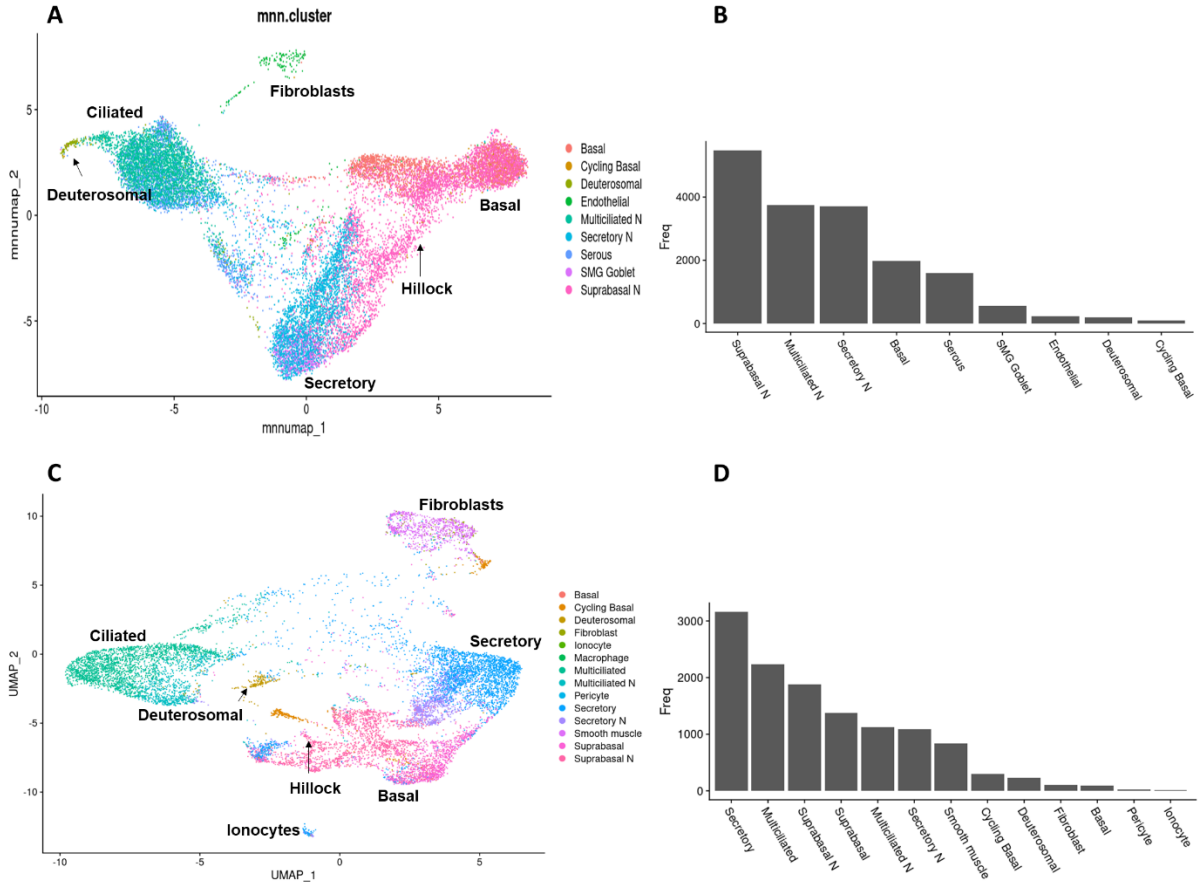

Figure 11. scRNA-seq cluster for hNM and hTM: Characterisation of the tissue models at the single-cell level shows the major cell types like the ciliated cells, secretory cells, basal cells, deuterosomal cells, fibroblasts, hillock cells and minor population of ionocyte in the hTM (A and C). The frequency distribution of the different cell types in the hNM and hTM (B and D) were matched to the human cell atlas of healthy airways (Deprez et al. 2020). Bioinformatics analyses post scRNA-seq was done by Prof. Florian Erhard and Kevin Berg (Institute of Virology and Immunobiology, Würzburg).

4.1.2.3. RNA signature of major cell types in hAM

The single-cell RNA signature of the hNM and hTM (Figure 12 and 13), helps to identify different cell type cluster in the tissue models based on cell markers. FOXJ1 (Figure 12A, 13B), a gene associated with the development and function of cilia, was localised to the upper left corner (ciliated cell cluster). Additionally, the expression of CK5 (Figure 12B, 13A), a marker for basal cells. Basal cells are the stem cell progenitors of the airway epithelium. The expression of MUC5AC (Figure 12C, 13C), a marker for goblet cells, which are cells that produce and secrete mucus, along with MUC5B (Figure 12D, 13D) which is a marker for secretory cells, SCGB1A1 (Figure 12E, 13E) was used in this study to identify the club cell population, The presence of the deuterosome population was checked using the marker, CDC20B (Figure 12F, 13F) which are suggested to be the precursors of ciliated cells. The expression of vimentin (Figure 12G, 13G) was used as a marker to distinguish fibroblast cells, and CK13 was used as a marker to identify Hillock cell population (Figure 12H, 13H). Furthermore, in the hTM models we could find additional ionocytes cell population (Figure 13I). These findings provide valuable insights into the specific cell types present in the engineered hAM comparable to the human airway mucosa and their molecular complexity.

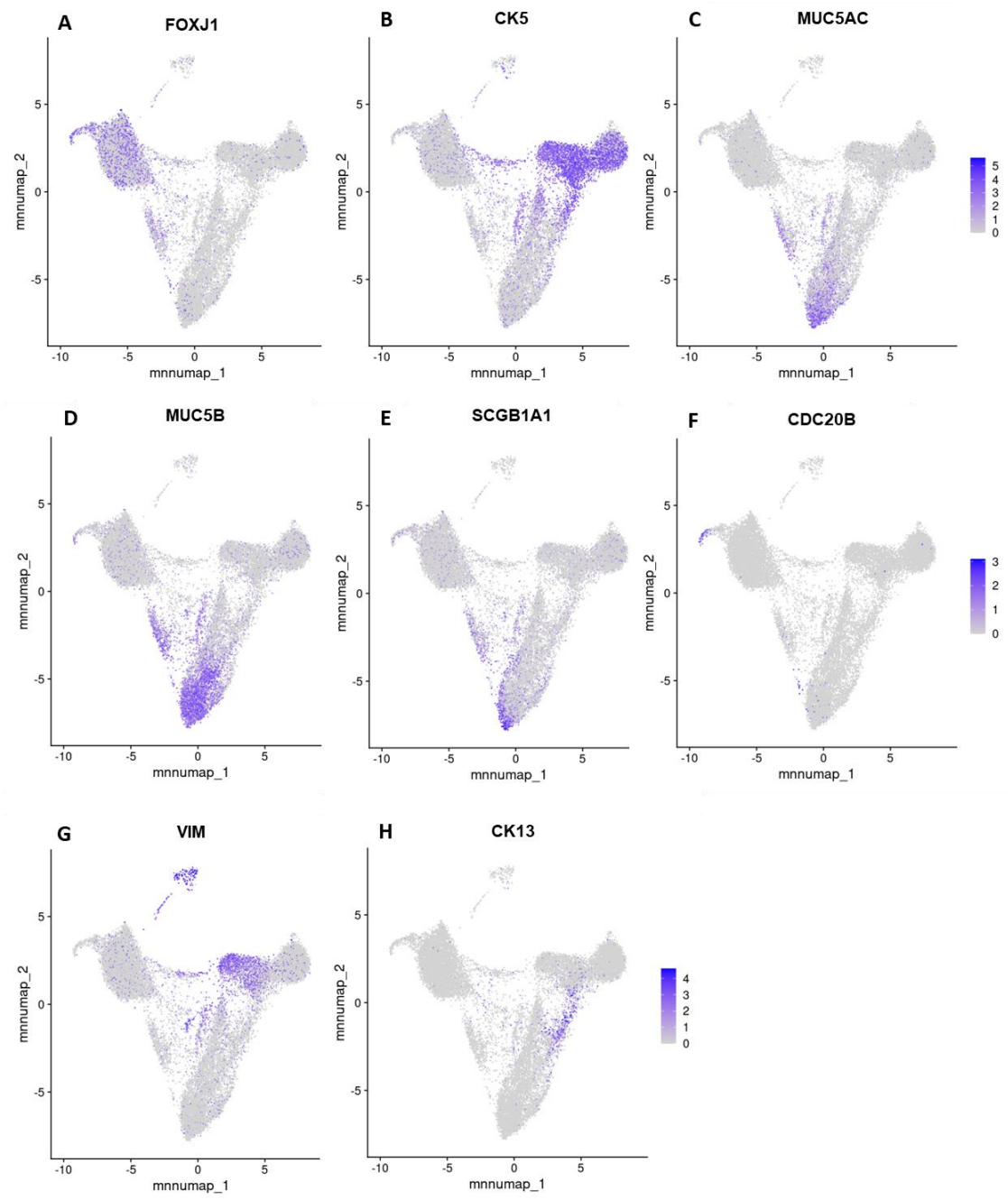

Figure 12. Distribution of specific cell markers at the single-cell RNA level for hNM: (A) The FOXJ1 gene expression polarised to the ciliated cell region, (B) CK5 gene expressing cells that represent the basal cell cluster, (C) MUC5AC gene expressing cells which represents the goblet cell population, (D) MUC5AB gene expressing secretory cells, (E) Club cell marker SCGB1A1, (F) CDC20B cell-specific markers for the deuterosomal population, (G) Vimentin RNA level in the cell population, used as a marker in this study to distinguish the fibroblast population and finally (H) CK13 cell-specific marker for hillock cells. Data extracted from the bioinformatic analyses performed by Prof. Florian Erhard and Kevin Berg (Institute of Virology and Immunobiology, Würzburg)

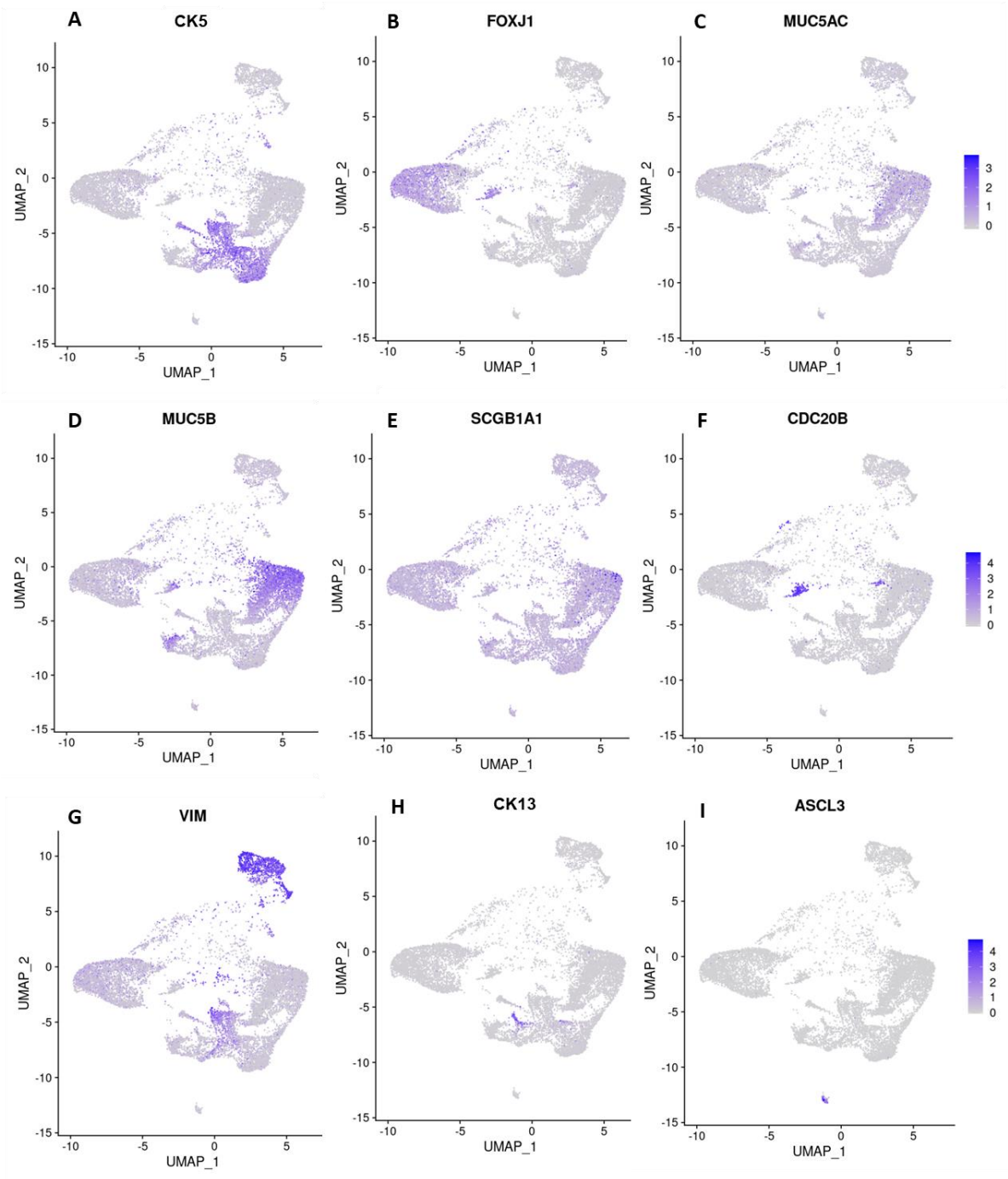

Figure 13. Distribution of specific cell markers at the single-cell RNA level for hTM: (A) CK5-expressing cells that represent the basal cell cluster, (B) FOXJ1 expression, used here as a marker for ciliated cells, (C) MUC5AC expressing cells which represents the goblet cell population, (D) MUC5AB expressing secretory cells, (E) Club cell marker SCGB1A1, (F) CDC20B cell-specific markers for the deuterosomal population, (G) Vimentin RNA level in the cell population, used as a marker in this study to distinguish the fibroblast population, (H) CK13 cell-specific marker for hillock cells and finally (I) ASCL3, used a marker to identify ionocytes. Data extracted from the bioinformatic analyses performed by Prof. Florian Erhard and Kevin Berg (Institute of Virology and Immunobiology, Würzburg).

4.1.3. Morphological characterisation of the hAM

4.1.3.1. Immunofluorescence staining of cell-specific markers

Cell-specific markers for major cell population, displayed and clustered by scRNA-seq (Figure 12, and 13), were visualised at the protein level using the immunofluorescence staining to confirm the results. Ciliated cells, goblet cells, secretory cells, basal cells, and fibroblasts were identified in their spatial orientation using cell-specific markers (Figure 14). The anti-acetylated tubulin antibody used here, at a concentration as low as 1:1000, stains the kinocilia, which was used as the marker for ciliated cells (Figure 14A and E; green). CK18 was used as a marker to identify ciliated and secretory cells, which consist of the goblet cells and mucous secreting cells (Figure 14B and F; green), CK5/6, was used as a marker for basal cells (Figure 14C and G; green), the stem cell progenitor that can differentiate into all other cell types. MUC5AC was used as a marker for goblet cells (Figure 14D and H; green), and vimentin was used to identify the fibroblasts embedded in the connective tissue (Figure 14D and H; magenta).

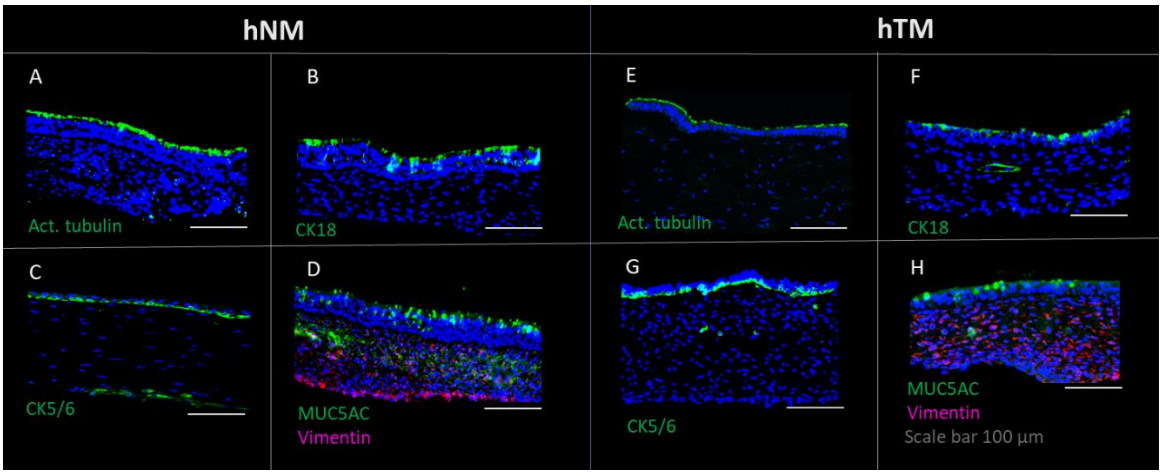

Figure 14. Immunofluorescence images of major cell population in the hAM: Kinocilia in ciliated cells were detected with an anti-acetylated tubulin antibody (A and E, green). The ciliated and secretory cells were characterised using CK18 (B and F, green), CK5/6, was used as a marker for basal cells (C and G, green), the stem cell progenitor that can differentiate into all other cell types. MUC5AC was used as a marker for goblet cells (D and H; green), and vimentin staining was used to identify the fibroblasts embedded in the connective tissue (D and H; magenta) and the scale bar = 100 µm.

4.1.3.2. Ultrastructural analyses

We performed the ultrastructural analyses to investigate the structural characterisation of the cellular components in the hAM in detail, including identification of cell types – the mucus-filled vesicles found in the secretory cells (SC), ciliated cells (CC), basal cells (BC), and fibroblasts (Fb) embedded in the connective tissue (Figure 15 A). In addition, we could identify the ciliated cell with kinocilia (K), microvilli (MV), and high distribution of mitochondria (M) which are indicated by the white arrows close to the apical side, mitochondria provide energy for the beating kinocilia (Figure 15 B). The cross-section of kinocilia (K) showing the 9+2 arrangement of tubulin filaments as in the native tissue was recapitulated also in the hNM (Figure 15 C). (D) The cell-cell contact in the nasal epithelial layer, tight junctions (TJ), adherens junctions (AJ), desmosomes (DE), and microvilli (MV) were also identified (Figure 15 D). The ciliated cells are constantly undergoing renewal and turnover to maintain the mucosal barrier, interestingly we could identify vesicles containing kinocilia (Figure 15 E and F; indicated by red arrows) may suggest the replacement of old cells by new ciliated cells. It could be the normal physiological process that is contributing to the maintenance of the airway epithelium. Another justification for this observation could be that the cells are undergoing micropinocytosis as a normal physiological process for maintaining the integrity and function of the ciliated cells. Hence, by additionally investing the hNM at ultrastructural level we could reveal the more complex cell-cell connections and cellular structures which make the hAM more suitable for investigating human-host pathogen interaction at the airway mucosal interface.

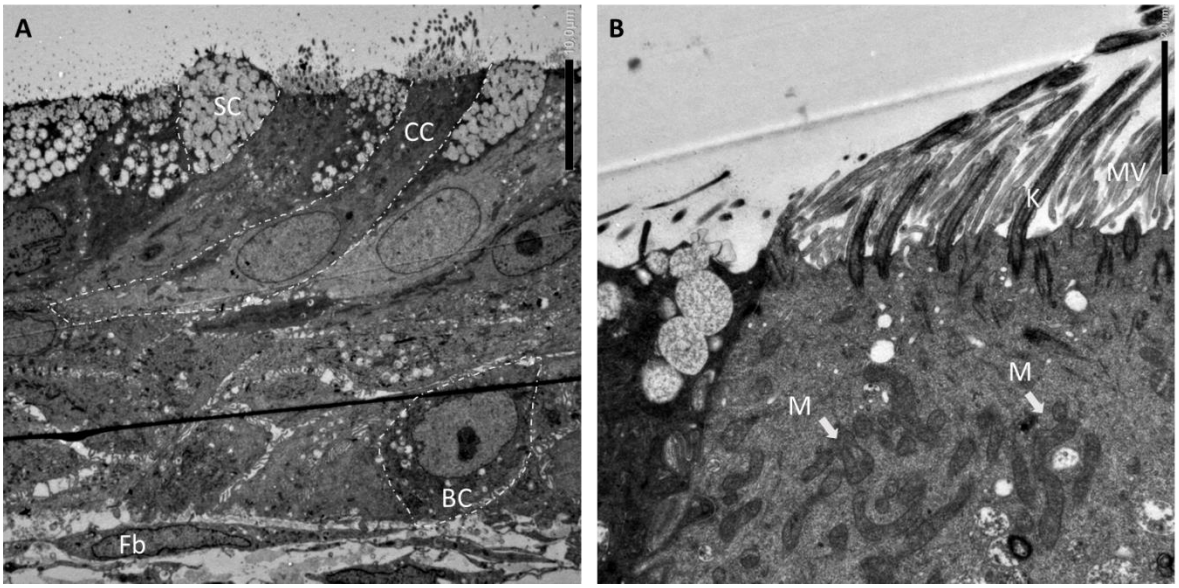

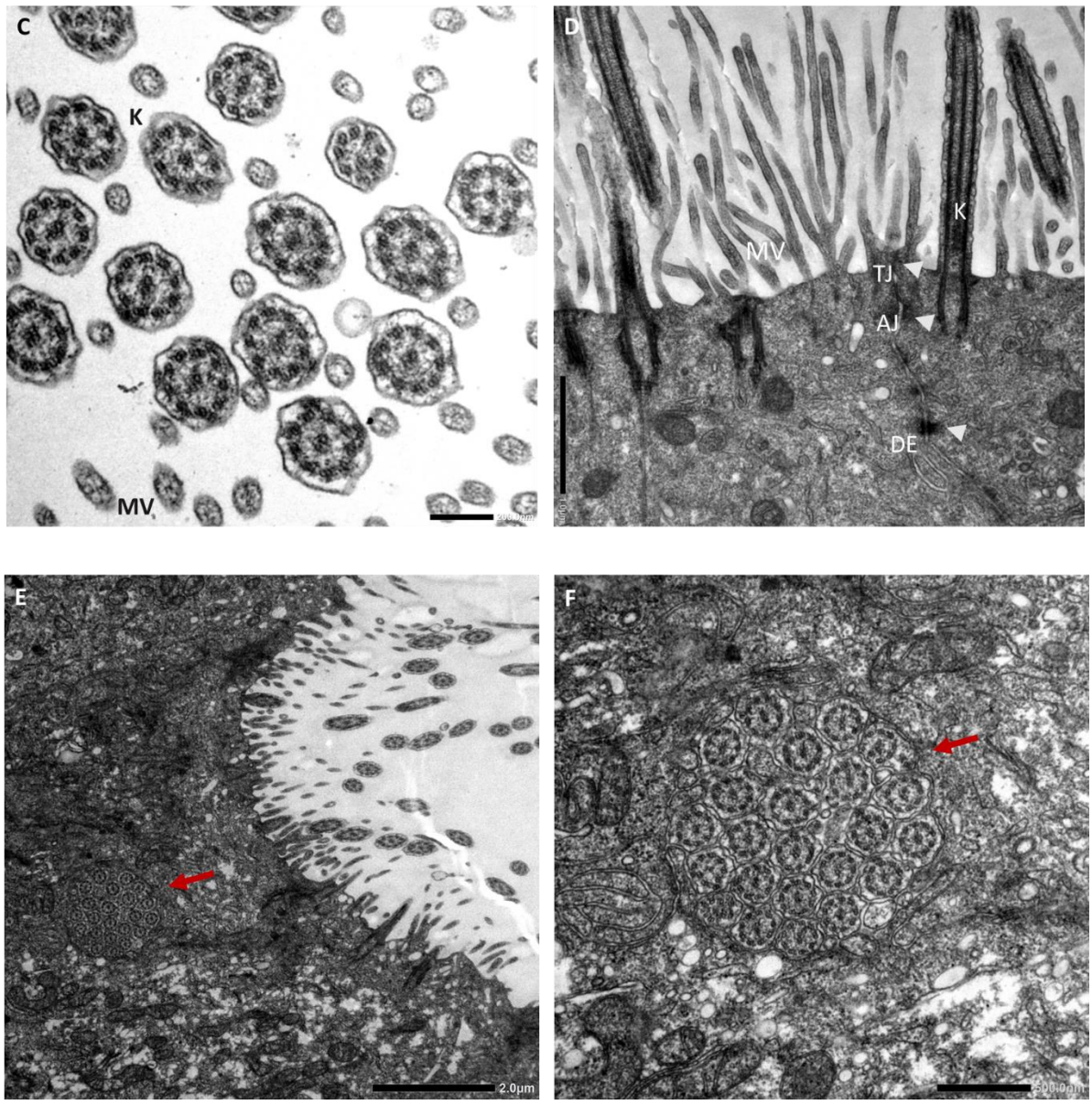

Figure 15. Representative transmission electron microscopy images of the hNM: (A) Mucus-filled vesicles found in the secretory cells (SC), ciliated cells (CC), Basal cells (BC), and Fibroblasts (Fb) embedded in the connective tissue. (B) Ciliated cell possessing kinocilia (K), microvilli, and high distribution of mitochondria (M) are indicated by the white arrows close to the apical side, facilitating energy for the beating kinocilia. (C) Cross-section of kinocilia (K) showing the 9+2 arrangement of tubulin filaments. (D) Cell-cell contacts in the nasal epithelial layer, tight junctions (TJ), adherens junctions (AJ), desmosomes (DE), and microvilli (MV). (E, F) Images depict suggestive micropinocytosis – kinocilia inside the vesicle (red arrow), indicating the dynamic nature of airway epithelium continuously regenerated and repaired to maintain the intact physical barrier integrity. Scale bar = 10 µm, A, E; 2 µm and B; C = 200 nm; D = 1 µm; F = 500 nm.

4.1.3.3. Morphological differences within hNM generated from different donors

We investigated further on the morphological difference within the fully differentiated hNM generated from different donors. To obtain an overview on these differences at a morphological point of view we performed H & E staining of hAM generated from five donors (Figure 16). We could identify differences in the distribution of major cell types, degree of differentiation and thickness of the models and differences in the overall architecture of the airway epithelium.

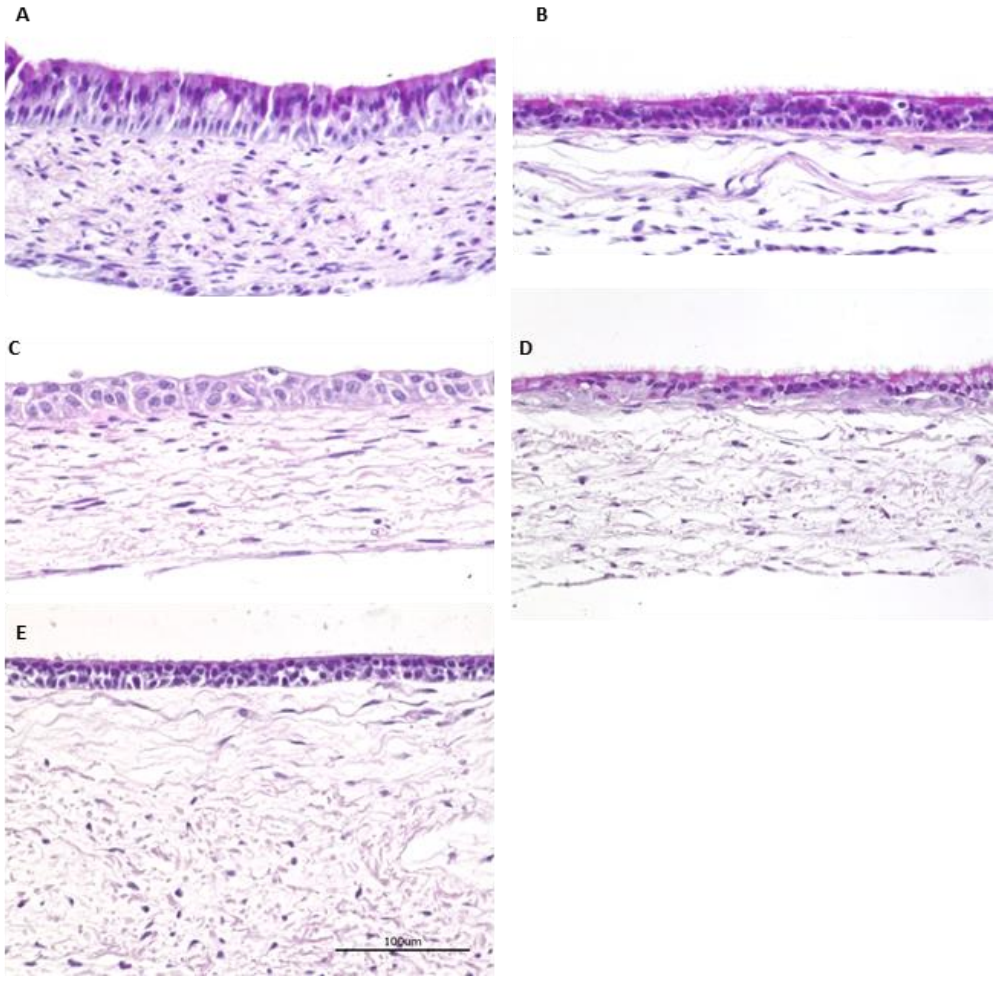

Figure 16. Variation in general morphology of hNM generated from different donors: Represents the morphological features observed in hNM from different donors showing varied thickness (A vs. B), distribution of ciliated cells (B vs. C). We also observed differences in different batches of SIS scaffold used in terms of properties and thickness (D vs. E). N = 6; Scale bar = 100 µm (A-E)

This observation indicates the models represented the different donor-induced variations and not all the models had morphological similarity. We also observed similar observation in the hTM models generated from different donors showing morphological variation. Interestingly we could also observe the difference in the thickness and properties of the SIS scaffold. Together these differences may also influence the variability in results among experimental replicates.

4.1.4. Basal level IL-6 vs. IL-8 secretion in hAM

Basal IL-6/IL-8 refers to the normal, resting levels of the cytokines in the airways without any external stimuli or inflammatory conditions. We measured the basal cytokine levels in the hAM after complete differentiation to investigate further on the differences between hNM and hTM derived from different donors cultured under similar conditions. The cytokine secretion in the supernatant collected from the hNM showed huge variation in IL-6/IL-8 levels among the three donors (Figure 17). The basal IL-8 secretion in hNM ranged between 18,958.13 - 117,669.39 pg/mL; for hTM, it was between 6052.87 - 6470.84 pg/mL.

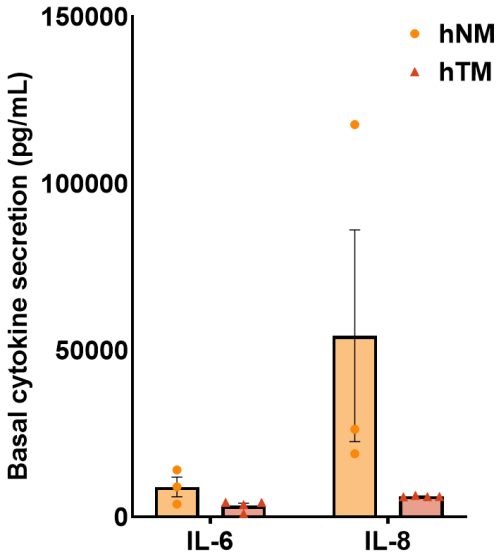

Figure 17. Basal IL-6 and IL-8 secretion in hNM and hTM: IL-6 and IL-8 secretion present in the apical washes of the hNM and hTM under normal cell physiology show that there are differences in the basal cytokine secretion within donors especially for the hNM. The basal IL-8 secretion in hNM ranged between 18,958.13 - 117,669.39 pg/mL; and for hTM, it was between 6052.87 - 6470.84 pg/mL. The data are presented as means ± SEM of independent experiments performed in duplicates, N=3 for hNM, N=4 for hTM.

We used three donors for hNM and four donors from hTM for this experiment. Differences in the IL-8 secretion by the hNM compared to the hTM, was calculated using the Mann-Whitney test ($p = 0.0571$), however the values were not statistically significant due to huge donor variation within the samples. Nevertheless, this data shows the donor associated variation present in individual models derived from human primary epithelial cells which maybe suggestive of a pre-activated/disrupted inflammatory pathway in patient derived samples.

4.2. Applications of human airway mucosa models

4.2.1. Studies on *B. pertussis* virulence factor Adenylate cyclase toxin (CyaA) and its toxoid (CyaA-AC$^-$)

4.2.1.1. CyaA treatment induces cAMP production

To investigate the impact of CyaA on the hAM we collected the supernatant from the cellular lysate of samples treated apically with 1.0 µg/mL of CyaA or CyaA-AC$^-$ or TUC buffer treated control group for 1 h. The samples were diluted and performed ELISA to evaluate the intracellular cAMP production (Figure 18). The 1.0 µg/mL toxin concentration used in this study was discussed earlier in our previous publications and other groups working on this toxin (Bianchi et al., 2021; Sivarajan et al., 2021; Hasan et al., 2018; Eby et al., 2010; Bassinet et al., 2004). The cAMP production in hNM ranged between 3.61 - 122.28 pmol cAMP/mg of total protein; for hTM, it was 18.86 - 88.14 pmol cAMP/mg of total protein, and for HBEC3-KT, it was 0.79 - 4.29 pmol cAMP/mg of total protein. The susceptibility of models derived from primary epithelial cells derived from different donors are also incorporated into the graph to show the individual donor response to the toxin treatment. Data are presented as means ± SEM of independent experiments performed in duplicates, N=7 for hNM and HBEC3-KT models and N=6 for hTM.

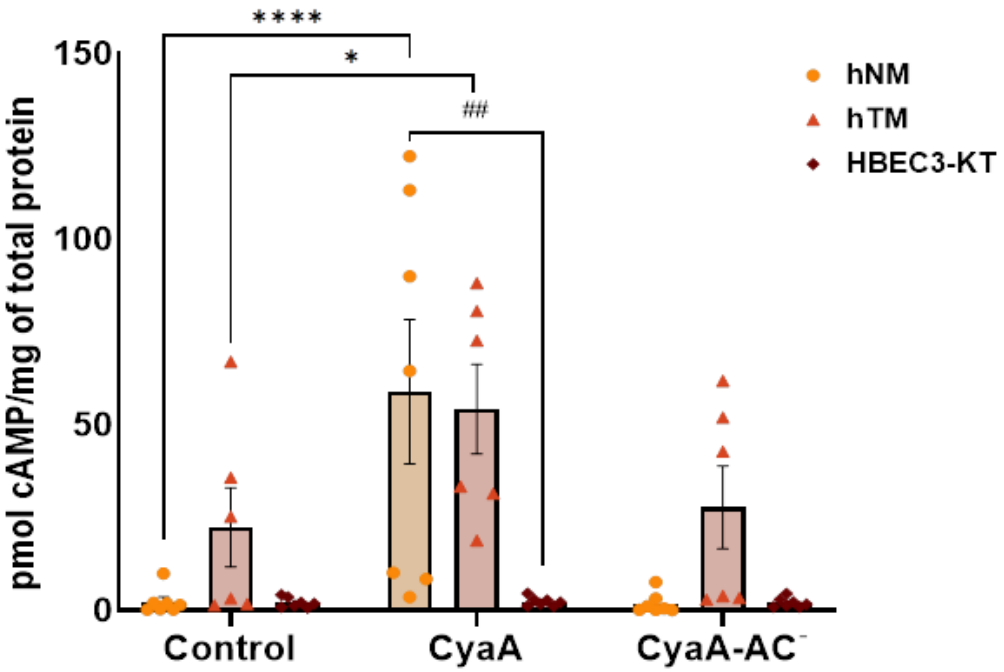

Figure 18. Effect of CyaA on intracellular cAMP production: The models treated apically with CyaA or its toxoid for 1 h showed significant increase in cAMP production in the CyaA-treated hNM and hTM compared to the control. However, the cell line HBEC3-KT had no response to the treatment. The data are represented as means ± SEM of independent experiments performed in duplicates, N=6, hTM and N=7, hNM and HBEC3-KT models. Dunnett's multiple comparison tests were performed on the samples, **** p value (hNM - control vs CyaA) was <0.0001, *p value (hTM - control vs CyaA) was < 0.05. In addition, we compared the response of the three cell types towards CyaA using Tukey's multiple comparison tests, ## p value (hNM- CyaA vs HBEC3-KT-CyaA) = 0.0011.

We observed that the CyaA treatment significantly increased the cAMP level in both hNM and hTM but not the cell line-derived models HBEC3-KT. The toxoid showed no significant increase in cAMP response, as expected. In addition to this we could also observe differences in susceptibility towards the toxin by the individual cell types (represented as ##).

4.2.1.2. CyaA treatment does not influence the epithelial membrane integrity

As we observed previously in the TEM analyses performed by Niklas Pallmann there were no obvious impact when the models were treated with the toxin for 1 h (Sivarajan et al., 2021). CyaA was previously known to disrupt the integrity of the cells by pore

formation in the membrane that allows the leakage of ions and other small molecules. This can lead to the destabilisation of the membrane and the loss of structural integrity and function. This can have several negative consequences triggering an immune response and leading to inflammation in the airways, resulting in tissue damage. Hence, we investigated the effect of prolonged CyaA treatment (24 h) on the epithelial barrier integrity check using 4 KDa FITC-dextran transport across the membrane (Figure 19).

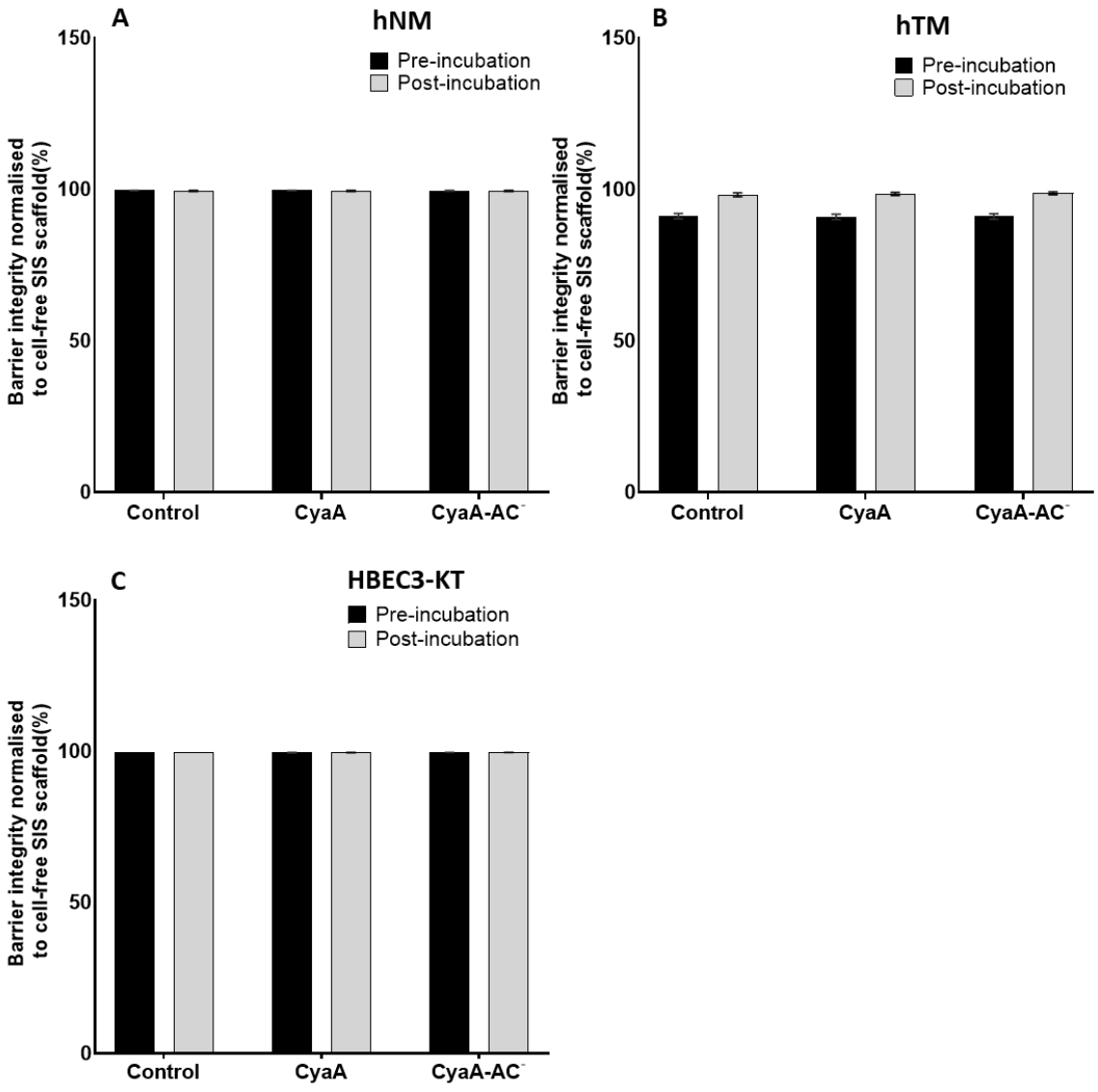

Figure 19. Effect of CyaA on epithelial membrane barrier integrity: The hNM (A), hTM (B), and HBEC3-KT (C) were treated apically with CyaA or its toxoid for 24 h and investigated the impact of the treatment on the epithelial membrane barrier integrity using 4 KDa FITC dextran transport assay. No significant impact was observed, and the integrity of the membrane was intact post-incubation. Data are presented as means ± SEM (N = 4 for hNM, hTM, and HBEC3-KT) in duplicates.

The apical treatment with toxin for 24 h had showed no observable impact on the barrier integrity (Figure 19) in all three cell types, Dunnett's multiple comparison tests were performed, and there was no statistical significance between the respective control vs. CyaA or the toxoid treatment. This suggests that the 1 µg/mL of prolonged CyaA treatment (24 h) had no impact on the epithelial barrier integrity in human primary airway derived hAM.

4.2.1.3. CyaA enhances cytokine release and anti-microbial peptide in hNM

We then investigated other aspects of hAM influenced by the toxin treatment, though CyaA did not impact the epithelial barrier integrity in hAM. To assess if CyaA activates the innate immune response of hAM we treated the models with CyaA/CyaA-AC^{-}/TUC and incubated for 24 h. The supernatant from the apical side were collected and analysed for IL-6, IL-8, and HBD-2. In the hNM, toxin treatment induced a significantly high secretion of IL-6, IL-8, and HBD-2, whereas hTM were not significantly affected by CyaA. The relative IL-6 release in hNM was ~2.1 times higher than hTM and ~8.7 times higher than HBEC3-KT models. The relative IL-8 release in hNM was ~2.6 times higher than hTM and ~4.2 times higher than HBEC3-KT models, and the relative HBD-2 secretion in hNM was ~1.7 times higher than hTM and ~2.2 times higher than HBEC3-KT models. CyaA treatment significantly impacted the cytokines and HBD-2 production in hNM, and it also had the highest inter-donor variation towards the treatment. There was also a significant difference in the response of hNM compared to hTM and cell line-based HBEC3-KT models, indicating the differential susceptibility of the individual models towards toxin treatment (Figure 20 indicated by ###, ## or #).

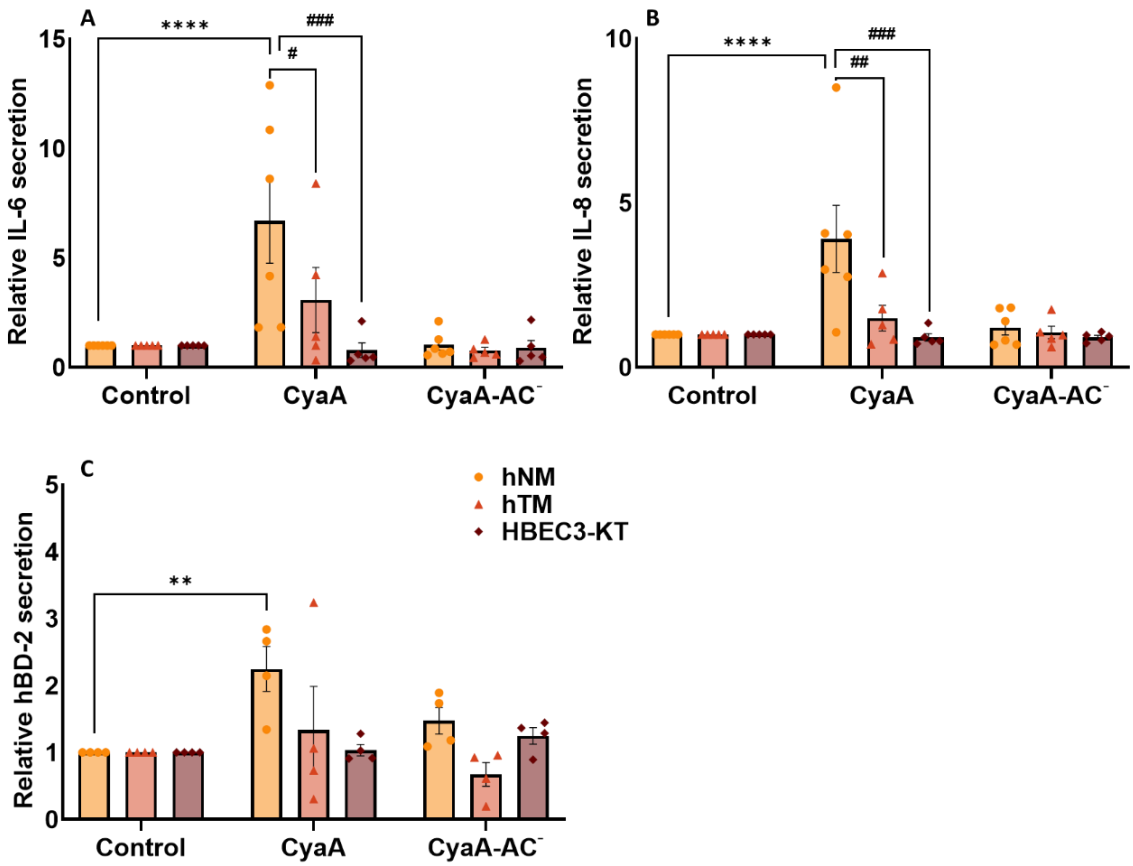

Figure 20. Relative IL-6, IL-8, and HBD-2 secretion of hAM after CyaA treatment: CyaA significantly altered IL-6 (A), IL-8 (B) and HBD-2 secretion (C) in hNM, whereas hTM and HBEC3-KT were not significantly affected. The relative IL-6 release in hNM was ~2.1 times higher than hTM and ~8.7 times higher than HBEC3-KT models (A). The relative IL-8 release in hNM was ~2.6 times higher than hTM and ~4.2 times higher than HBEC3-KT models (B), and the relative HBD-2 secretion in hNM was ~1.7 times higher than hTM and ~2.2 times higher than HBEC3-KT models (C). For IL-6 and IL-8 analyses, N = 6, hNM; N = 5, hTM and HBEC3-KT were used, and for HBD-2 analyses, N = 4 from all cell types were used. Data are presented as means ± SEM of independent experiments performed in duplicates. **** p value for Dunnett's multiple comparison test (hNM - Control vs CyaA) was ≤0.0001, and the ** p value (hNM - Control vs CyaA) was ≤0.005. We further compared the different cell types of response to the treatment using Tukey's multiple comparison tests (A) $^{###}$ p value (hNM- CyaA vs HBEC3-KT-CyaA) = 0.0008 and $^{#}$ p value (hNM- CyaA vs hTM-CyaA) = 0.1159. (B) $^{##}$ p value (hNM-CyaA vs. hTM-CyaA) = 0.0060 and $^{###}$ p value (hNM- CyaA vs. HBEC3-KT-CyaA) = 0.0003.

We observed that CyaA, but not CyaA-AC⁻, had differential effects on cytokine and antimicrobial peptide secretion in the hAM. Regarding relative IL-6/IL-8 secretion, we observed inter-donor variance in both nasal and tracheobronchial tissue models towards the treatment (Figure 21, represented by individual data points).

4.2.2. Viral infection studies

4.2.2.1. Determination of IAV and RSV titers on 2D cell lines

MDCK and Hep G2 were used to optimise the infection conditions. They were infected in a viral concentration-dependent manner in all experimental replicates when infected with IAV and RSV, respectively (Figure 21). The multiplicity of infection was determined in these cell lines, and the concentration of the virus, with minimum cell cytotoxicity, was used to infect the hNM and hTM.

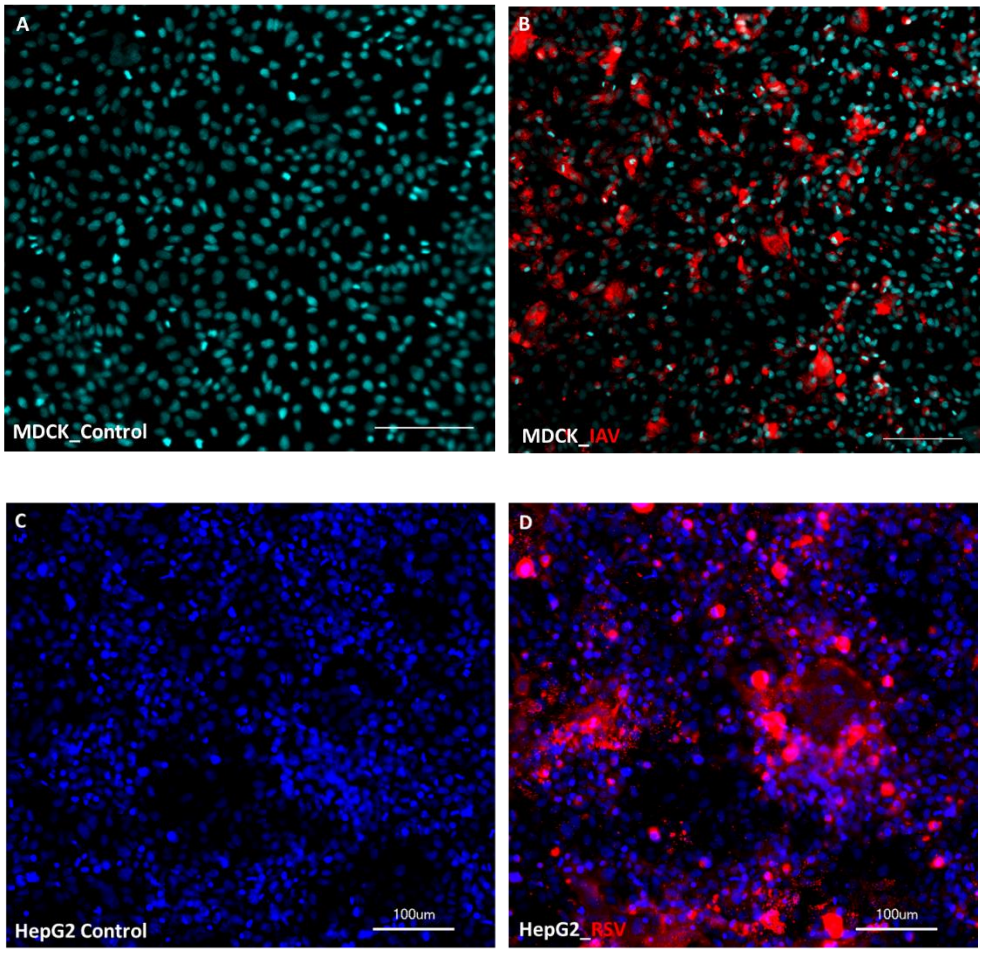

Figure 21. Viral infection checks in cell lines: The top panel shows the (A) control and the IAV-infected (B) MDCK cell lines (MOI = 10) cyan = DAPI and red = IAV nucleoprotein. The bottom panel shows the control and RSV-infected Hep G2 cell line (MOI = 10); Blue = DAPI and red = RSV phosphoprotein. Both cell lines were infected with respective viruses for 24 h. The data are representative of three independent experiments performed in duplicates. Scale bars = 100 µm (A-D)

4.2.2.2. hTM are more sensitive to IAV mediated cytopathic effects

The concentration (10^7 ifu/mL) optimised in MDCK resulted in strong cytopathic effects in the hTM. Within 6 h of infection, the entire epithelial layer of hTM was damaged and largely destroyed (N = 3), (Figure 22) thus, the viral titers were adjusted, and experiments were repeated in hTM with additional concentration and time points to establish a physiologically relevant infection. The calculated concentration (0.2 x 10^6 ifu/mL) was confirmed with two more donors before using this data for further experiments. The models were infected in a donor-dependent manner. Hence entire infection condition had to be repeated with the models to develop an optimised protocol for viral infection in these physiologically relevant models.

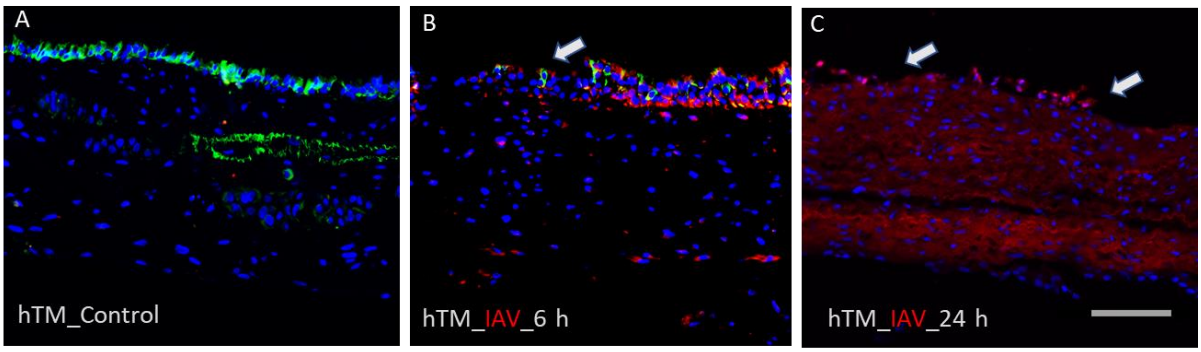

Figure 22. The response of hTM to the concentration of IAV used in MDCK: The concentration that showed maximum cell infection within 24 h in MDCK was used to infect the models and within the initial 6 h of infection there were signs of excessive cytotoxicity and damage, as indicated by white arrows in (B). Continuing the infection for 24 h destroyed the entire epithelial layer of the models, indicated by white arrows (C). The representative images from N = 3 independent experiments in duplicates are shown. Green, CK18; red, IAV nucleoprotein; blue, DAPI. Scale bar = 100 µm (A-C)

4.2.2.3. Susceptibility of human airway mucosa models to different respiratory viruses

To monitor cytopathic effects and viral replication kinetics in the airway mucosa, the models were infected with IAV, RSV, or SARS-CoV-2 for 24 h. The models after the infection were washed and lysed. The cellular RNA was isolated and viral RNAs of IAV, RSV, and SARS-CoV-2 were quantified by RT-qPCR. The gene expression was normalised to cellular RNA content using GAPDH expression as a reference. The

models from both hNM and hTM expressed high amounts of viral RNAs (Figure 23 A and C), but in RSV-infected samples high variations were observed (Figure 23 B). After infecting the hAM with all three viruses, followed by intracellular viral content analyses, we were able to measure viral gene copies in the intracellular cell lysate which indicates the successful penetration of each virus into the hAM. The infection pattern depended on the individual donor-derived models. To account for this, data are also represented regarding individual donor responses to infection (Figure 24).

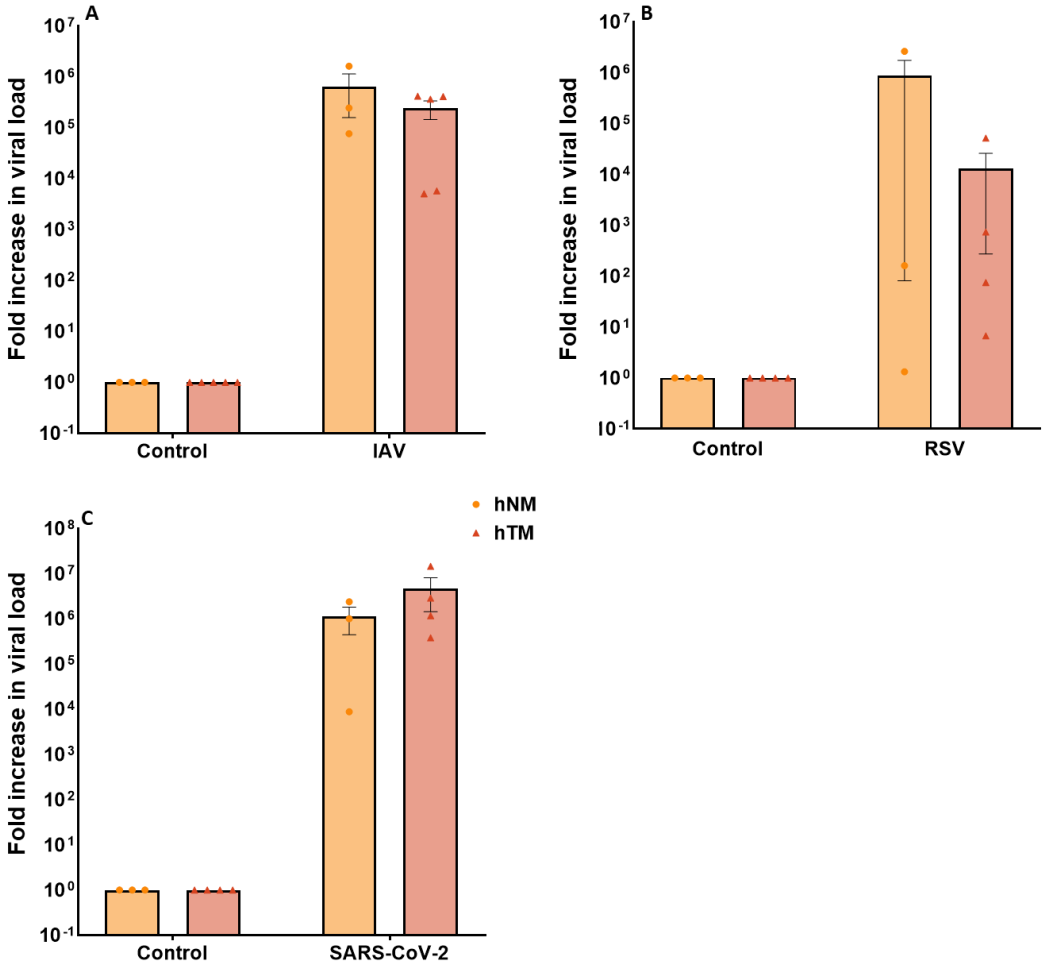

Figure 23. Intracellular viral content in the hAM after 24 h of virus infection: The models were infected with IAV (A), RSV (B), and SARS-CoV-2 (C) for 24 h, and the viral RNA loads were measured using RT-qPCR from infected samples after cell lysis and total RNA isolation. We observed that the cells had high copies of viral RNA content, suggesting the successful penetration of virus particles into the host cells. The data are presented as means ± SEM of independent experiments performed in duplicates. Sidak's multiple comparison tests were performed, and for IAV treatment, # p = 0.1010 (hNM control vs. IAV), and the other treatments were not statistically significant. N = 3, hNM and N = 5, hTM were used for the IAV infection. For RSV and SARS-CoV-2, N = 3, hNM and N = 4, hTM were used, respectively.

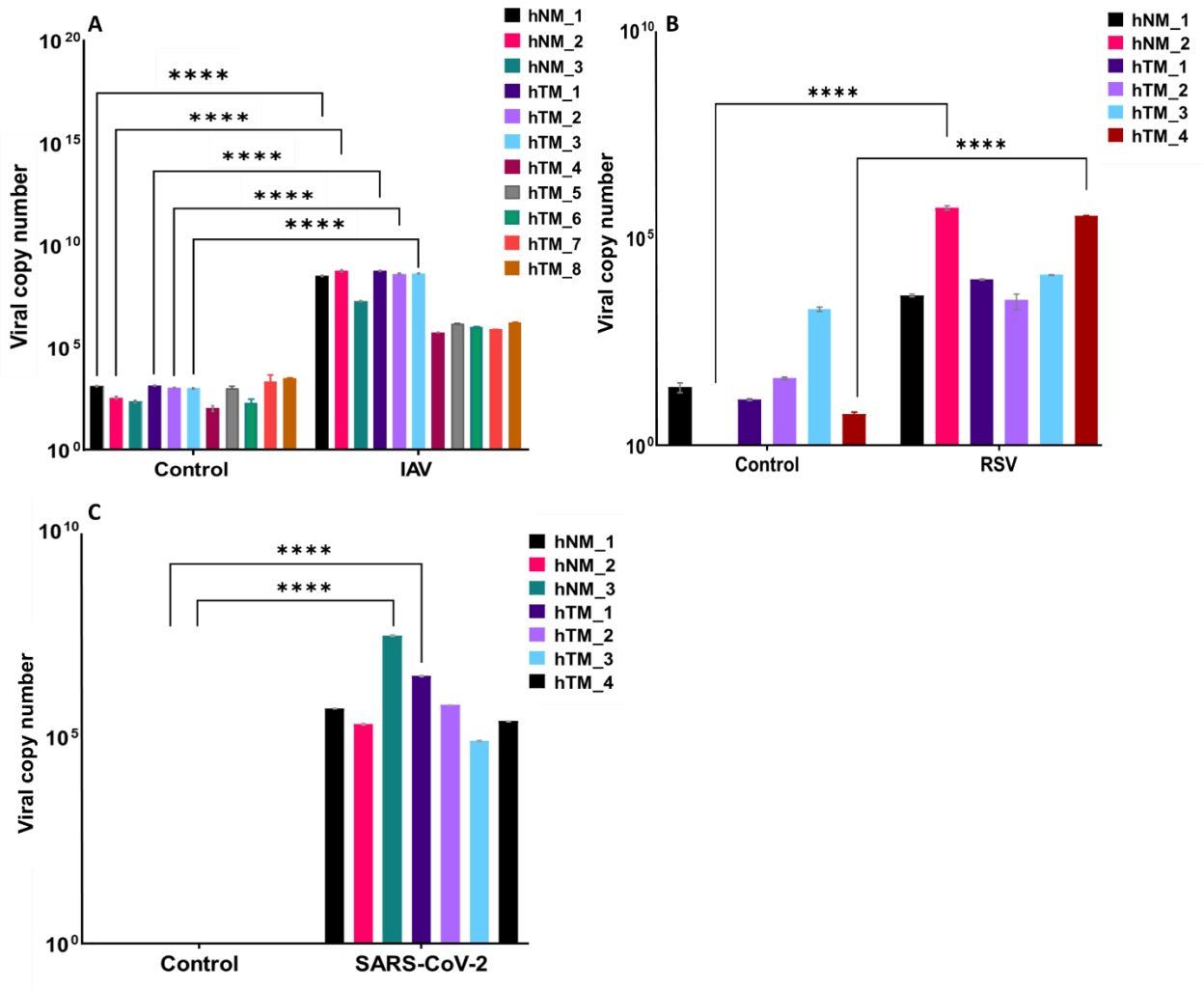

Figure 24. Individual representation of infected hAM: The susceptibility of different donors (A) towards IAV infection, hMN (N = 3) and hTM (N = 8); (B) RSV infection, hNM (N = 2) and hTM (N = 4); (C) SARS-CoV-2 infection, hNM (N = 3) and hTM (N = 4). The viral copies generated by different models were compared using Tukey's multiple comparison tests, and data are presented as means ± SEM of independent experiments performed in duplicates. (A) Two of three hNM (control vs infected) had ****p value ≤0.0001 and three of eight donors had **** p value ≤0.0001 for IAV infection. (B) One of two hNM donors had ****p value ≤0.0001, and one of four hTM donors had ****p value ≤0.0001 for RSV infection. (C) One of three hNM samples had ****p value ≤0.0001, and one of four hTM samples had ****p value ≤0.0001 for SARS-CoV-2 infection. This suggests a donor-dependent response to infection within 24 h of infection with respective viruses.

4.2.2.4. Immunofluorescence staining of infected hAM

Using RT-qPCR, we quantified the viral genome and a portion of the cells in the hAM or the entire epithelial layer may contribute to this signal so to identify the infected area, we used immunofluorescence staining. Optimising infection in models was challenging due to donor variability, the most common observance was infection hot spots (Figure 25) and not all donors had a uniformly infected epithelial layer (Figure 26). Increasing the virus concentration to increase the frequency of infected cells caused damage to the epithelial layer as previously mentioned (Figure 22 C).

The hNM derived from 5 donors were infected with RSV, on visualising these models using immunofluorescent staining, only one donor showed positive staining (Figure 27). We infected hTM derived from 6 donors and none of the models showed positive staining specific for RSV. The hAM infected with SARS-CoV-2 did not show detectable infection signals on 24 and 48 h post infection for immunofluorescence staining, and hence 72 h was used for SARS-CoV-2 infection (Figure 28). Out of the 5 hNM infected with SARS-CoV-2 and fixed for immunofluorescent staining, only one donor exhibited positive staining (Figure 28 B). Similarly, out of the 6 hTM infected, fixed, and stained, only one model displayed virus-specific positive staining (Figure 28 D). The hAM infected with the three respiratory viruses depicted donor-dependent infection patterns compared to uniformly infected monolayers in cell lines which underlines the significance of these models to represent a more reliable in vivo infection recapitulation.

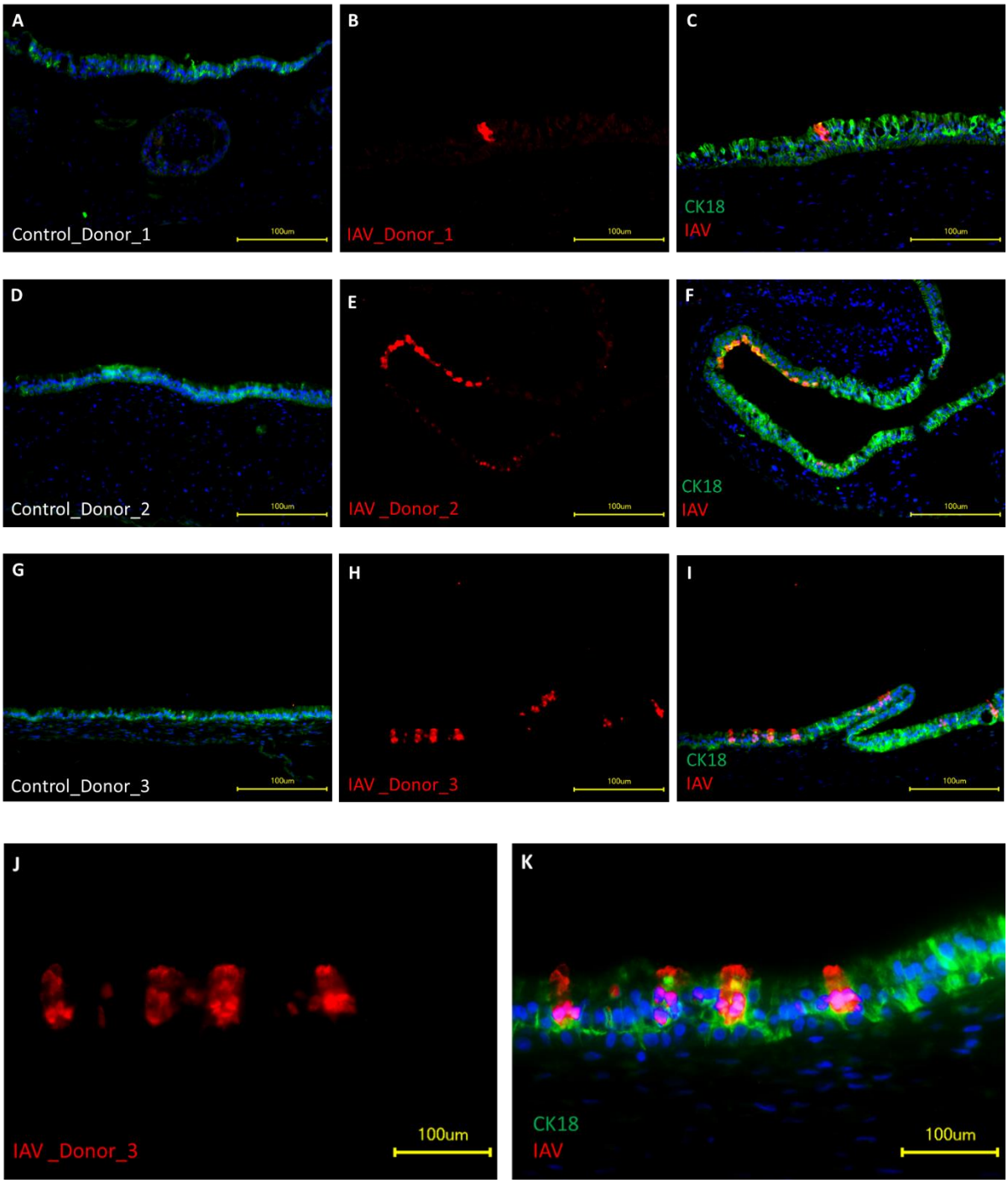

Figure 25. Hotspots of infection in hTM infected with IAV: Non-infected hTM controls (A, D, and G) and IAV-infected hTM tissue models after 24 h, showing infection hot spots (B, E, H, and J) and C, F, I and K represents the merged images from CK18 and IAV-specific staining. J and K represent the 20x magnified images from donor_3 (H and I) green, CK18; red, IAV nucleoprotein; blue, DAPI. Scale bar = 100 µm

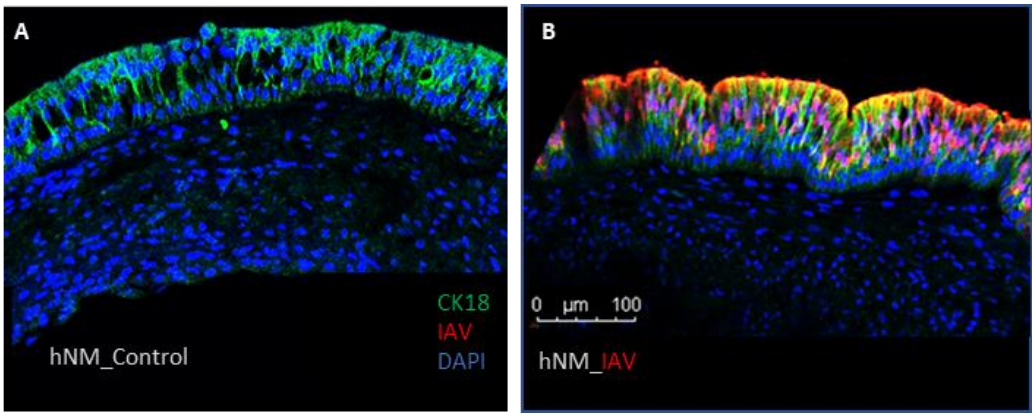

Figure 26. hNM infected with IAV: Non-infected hNM control (A) and IAV-infected tissue model for 24 h (B) with the entire epithelial layer infected with IAV. Green, CK18; red, IAV nucleoprotein; blue, DAPI. Scale bar = 100 µm

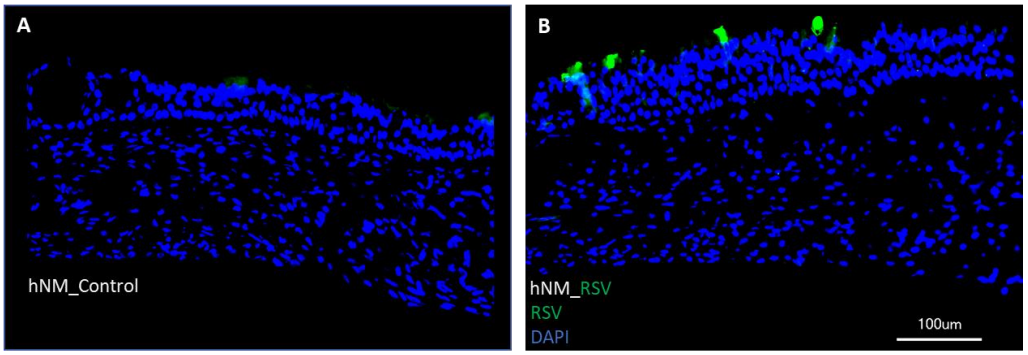

Figure 27. Hotspots of infection in hNM infected with RSV: The non-infected control (A) and the infected (B) with RSV for 24 h show localised areas of infection. Green, RSV phosphoprotein; blue, DAPI. Scale bar = 100 µm

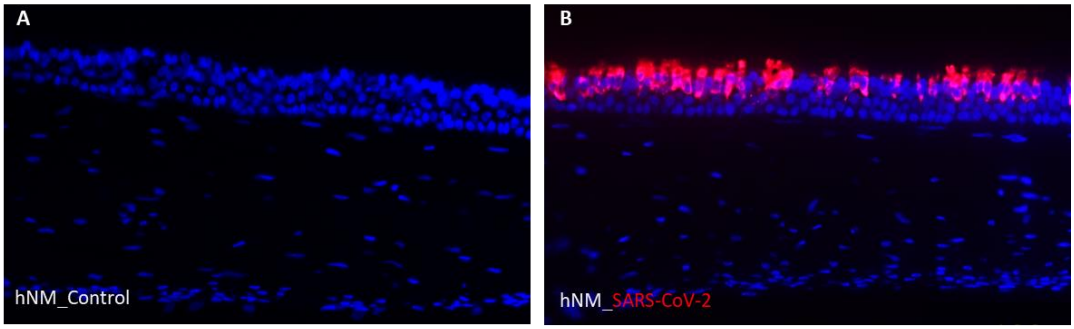

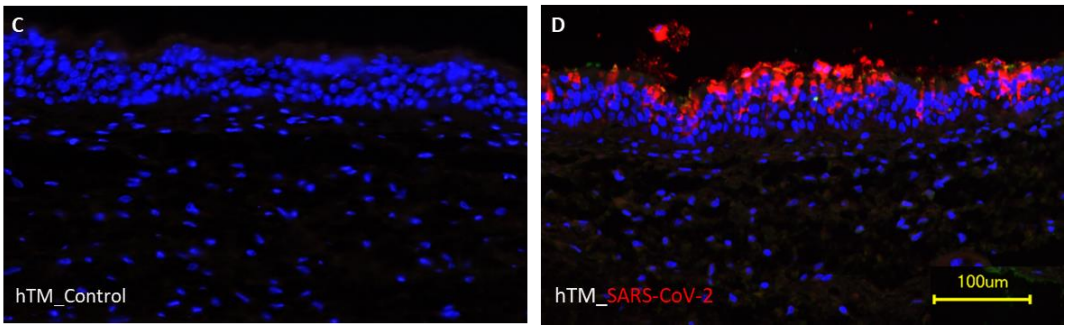

Figure 28. hAM infected with SARS-CoV-2: The hAM infected with SARS-CoV-2 for 72 h are shown in B and D (hNM and hTM) respectively; Red, SARS-CoV-2 N-protein; blue, DAPI. Scale bar = 100 µm

4.2.2.5. Ultrastructural analyses of infected hAM

We performed ultrastructural analyses to investigate infection associated morphological differences in the hAM induced by different viruses. Comparing the non-infected models to infected models (24 h, ~ MOI = 1), we could observe morphological changes associated with cellular stress and apoptosis in the infected group. Though the infection did not destroy the models entirely, specific areas showed disrupted tight junctions (Figure 29 J, K, L, S and T). There are signs of cell extrusions and damaged kinocilia (Figure 29 J, K, L and T). Arrows of different colours indicate different structures of the cell. White arrows indicate tight junctions (Figure 29 C, H, and Q), yellow arrows indicate desmosomes (Figure 29 C, H, and Q), green arrows indicate lamellar bodies (Figure 29 I), red arrows indicate cell extrusion (Figure 29 K, L and T), orange arrows indicate microvilli (Q and V), blue arrows indicate clathrin-coated pits (Figure 29 X), and purple arrows indicate endosomes (Figure 29 U, Y, and Z). Endosomes are small, membrane-bound structures within cells involved in endocytosis.

In the IAV-infected samples, there are increased mucus-filled vesicles compared to both control and RSV and SARS-CoV-2 infected models. The RSV-infected samples show areas of localised cell destruction (Figure 29 K and L; cell extrusions and necrosis) and a high number of lamellar bodies compared to the control (Figure 29 I). Similarly, the SARS-CoV-2 infected samples also show localised areas of cell destruction (Figure 29 S and T), like the RSV-infected samples and an increased number of endosomes compared to control samples (Figure 29 U, Y, and Z). Additionally, we observed double-membrane vesicles (DMV), which are sites of active

viral replication, in SARS-CoV-2 infected models (Figure 29 U). Identifying the viruses in the models was challenging due to the complex structure of the models and the close similarities of virus structure to cellular structures like microvilli (Figure 29 S), endosomes (Figure 29 U), and clathrin-coated pits (Figure 29 X). Overall, the ultrastructural analyses provided insights into the virus-associated early impacts on the human airway mucosa concerning localised areas of cell death and extrusion, disrupted tight junctions and general differences in the in cellular organisation and distribution of cell organelles compared to the non-infected samples.

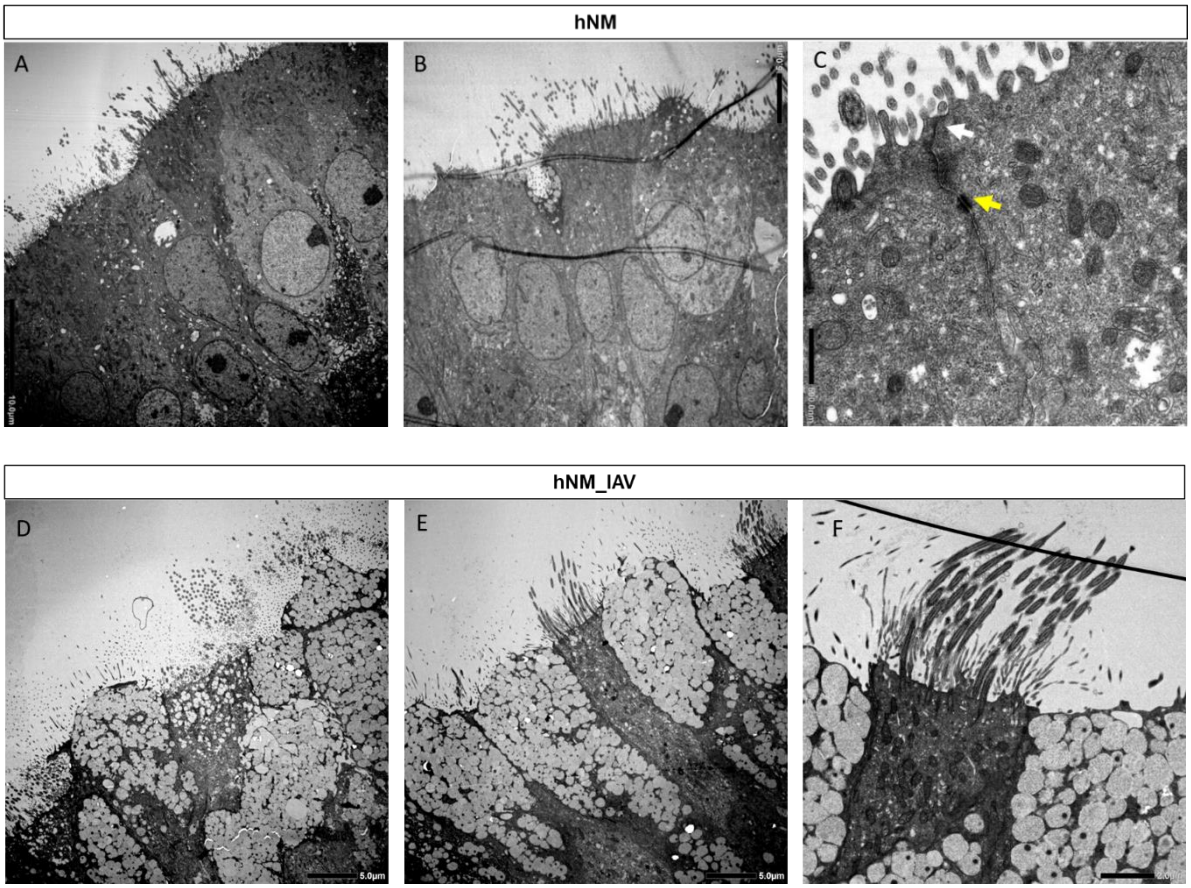

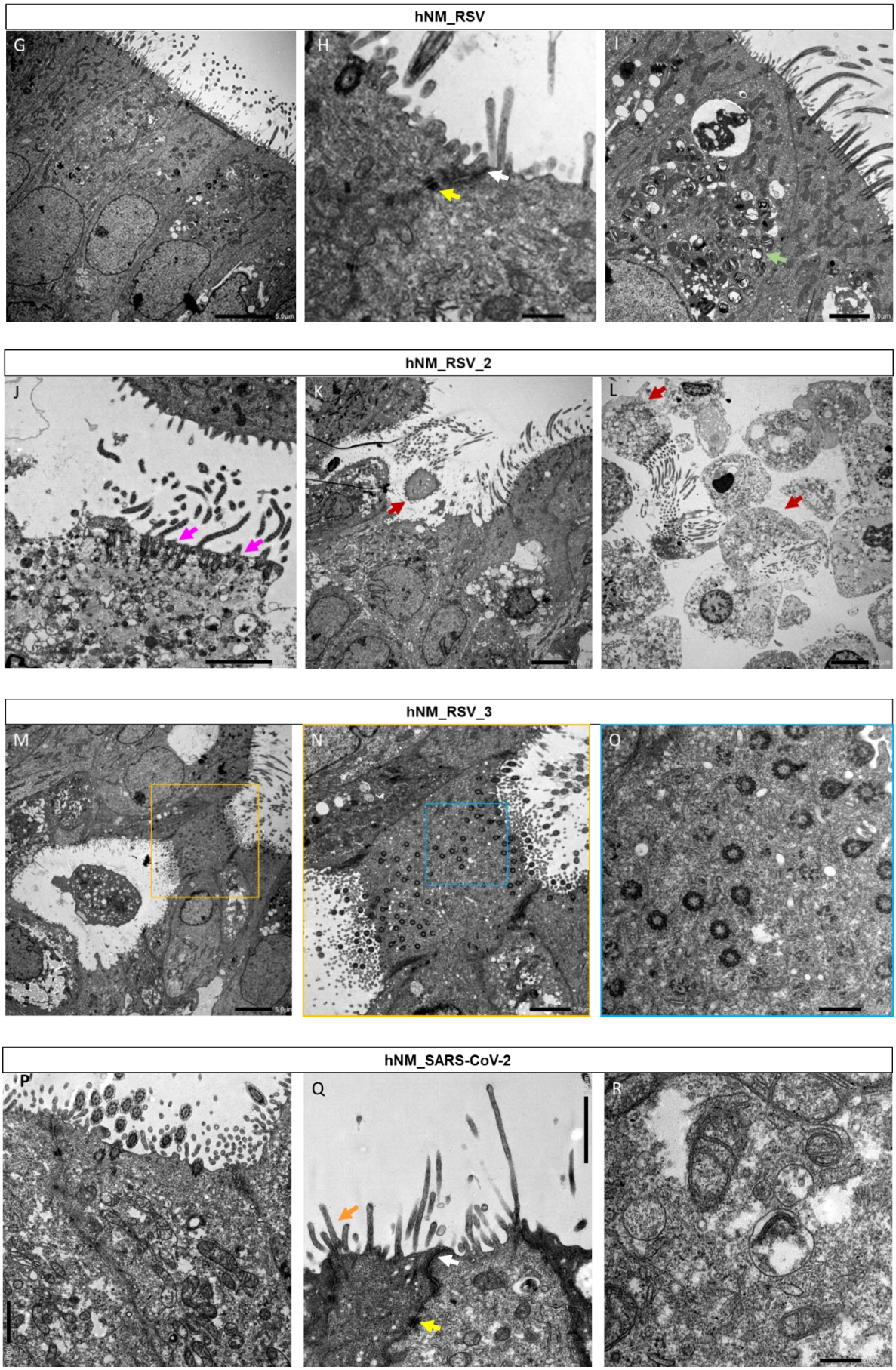
hNM_RSV
G
H
I
hNM_RSV_2
J
K
L
hNM_RSV_3
M
N
O
hNM_SARS-CoV-2
P
Q
R

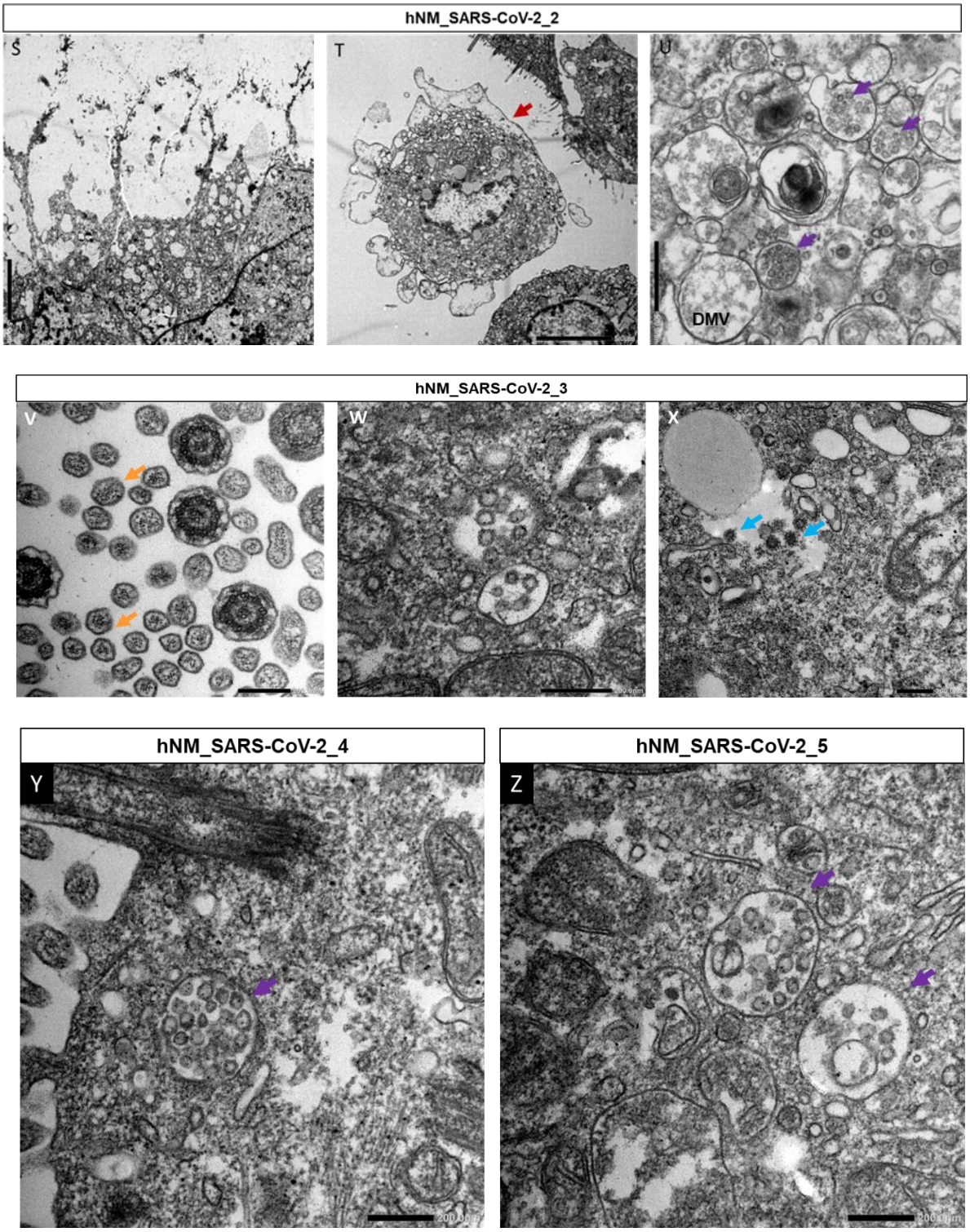

Figure 29. Summarises the different morphological features observed in infected hNM samples: The white arrows indicate tight junctions (C, H and Q), the yellow arrows indicate desmosomes (C, H and Q), the green arrow indicates lamellar bodies (I), the red arrow indicates cell extrusion (K, L and T), magenta arrow indicates damaged kinocilia (J), the orange arrow indicates microvilli (Q and V), the blue arrow indicates clathrin-coated pits (X), and the purple arrow indicates endosomes (U, Y, and Z). The IAV-infected samples show increased mucus-filled vesicles compared to both control and RSV and SARS-CoV-2 infected models (D-F). The RSV-infected samples showed areas of localised cell

destruction (cell extrusions and necrosis K and L) and a high number of lamellar bodies (I) compared to the control. The SARS-CoV-2 infected samples also showed localised areas of cell destruction (S and T) like the RSV-infected samples and a qualitatively increased number of endosomes compared to control samples (U, Y, and Z). We observed double-membrane vesicles (DMV), sites of active viral replication (U), in SARS-CoV-2 infected models. The identification of the viruses in the models was challenging due to the complex structure of models and the close similarities of cellular structures like microvilli (S), endosomes (U) and clathrin-coated pits (X). Scale bar: A = 10 µm; B, D, E, G, K, L, M, S, T = 5 µm; F, I, J, N = 2 µm; H, P, Q = 1 µm; C, O, U = 500 nm; R, V, W, X, Y and Z = 200 nm.

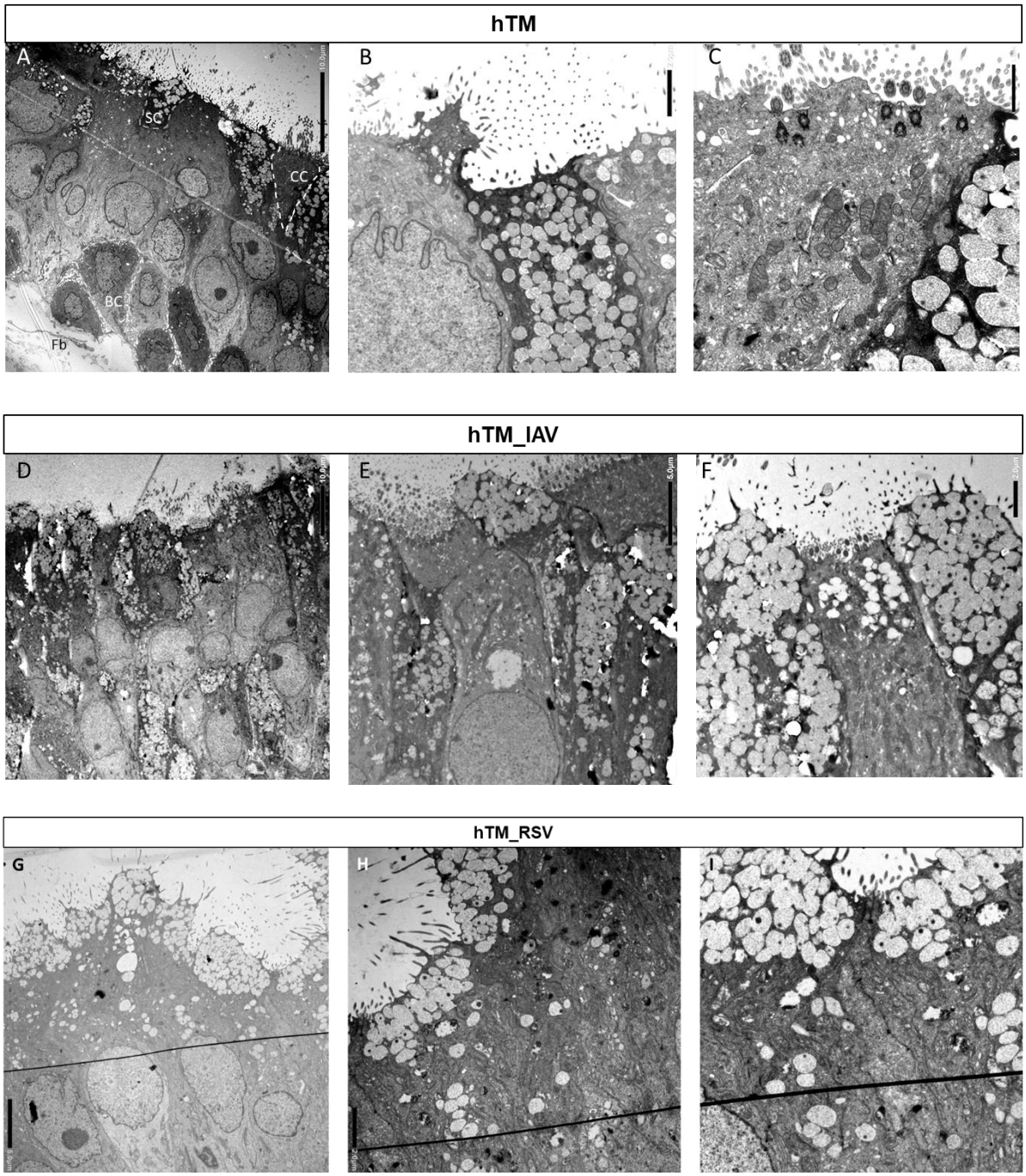

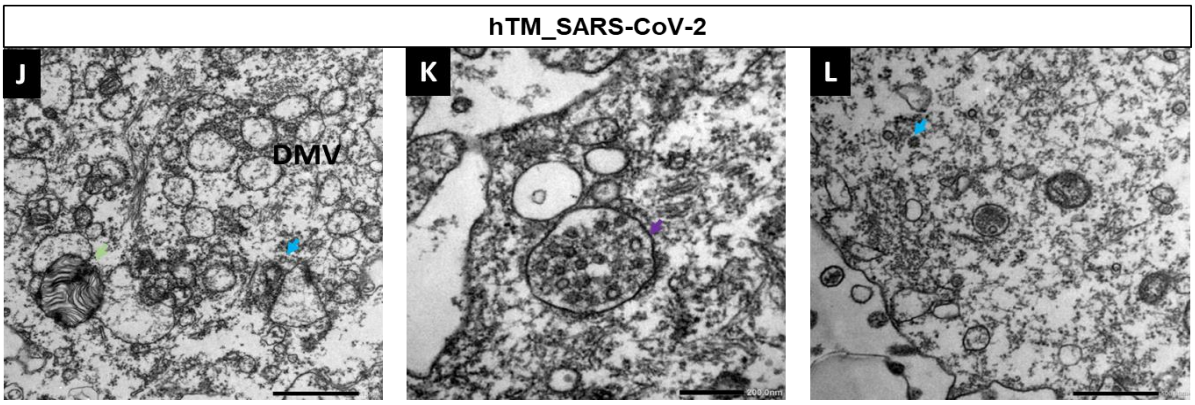

Figure 30. Summarises the different morphological features observed in infected hTM samples: (A, B, and C) Represents the non-infected control, showing the ciliated cells (CC), mucus-filled secretory cells, basal cells (BC) and fibroblast embedded in the extracellular matrix. Both the IAV (D, E and F) and RSV-infected (G, H and I) models show qualitatively increased mucus-filled vesicles compared to the control. The IAV-infected samples show increased mucus-filled vesicles compared to both control and RSV and SARS-CoV-2 infected models. The SARS-CoV-2 infected hTM samples also had an increased number of endosomes compared to control samples (K), and we observed double-membrane vesicles (DMV), which are sites of active viral replication (J), lamellar bodies indicated by the green arrow (J) and clathrin-coated pit indicated by blue arrow (L). Scale bar: A, and D = 10 µm; E, and G = 5 µm; B, F and H = 2 µm; C, I and J = 1 µm; L = 500 nm; K = 200 nm.

4.2.2.6. IAV infection induces mucin upregulation in hTM

As this research mainly focuses on IAV infection in the hTM, we also investigated the impact of infection on mucins found in the airway as this a clinical symptom associated with IAV infection. The major mucins found in the airways are MUC5B and MUC5AC; hence they were used for verifying the observation (Figure 31). The IAV infection induced hyper mucus secretion in hTM (N >8), which were visually observed and qualitatively confirmed using fluorescent microscopy and ultrastructural analyses (Figure 32).

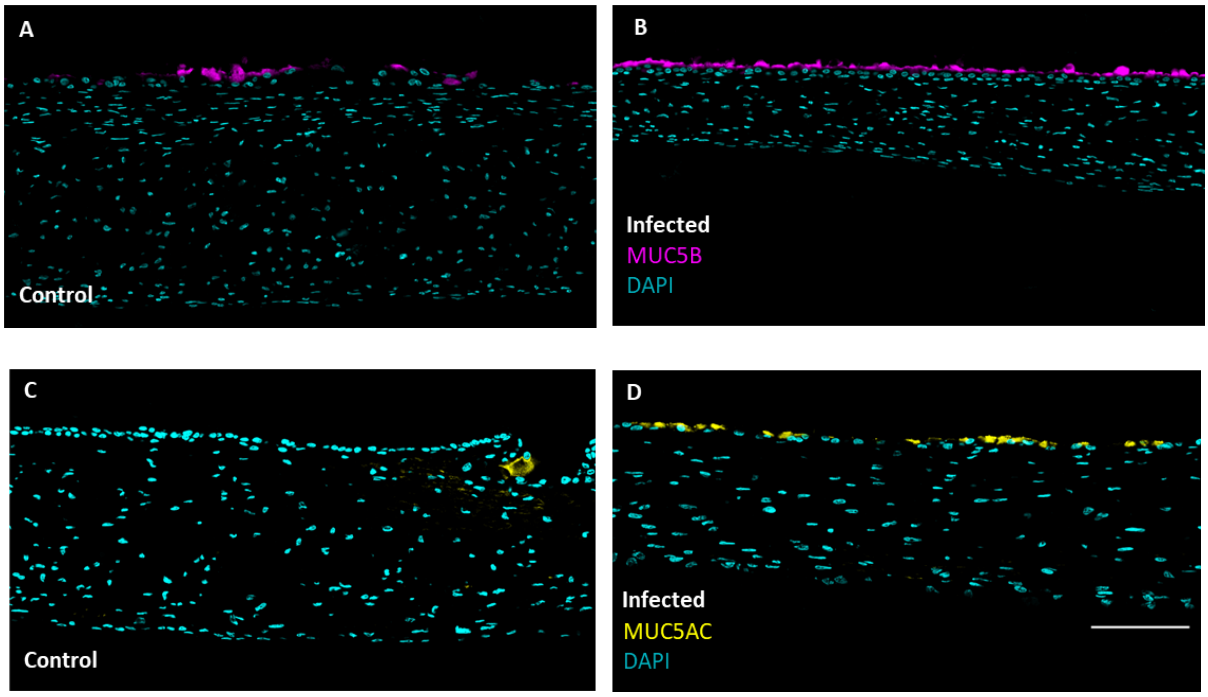

Figure 31. IAV-infected hTM after 24 h showed increased mucus production: The left panel (A and C) represents the non-infected control, and the right panel (B and D) shows the infected model. B and D shows an increase in MUC5B and MUC5AC secretion compared to the non-infected control (qualitative). MUC5B, magenta; MUC5AC, yellow and DAPI, cyan. Scale bar = 100 µm (A-D). N = 4

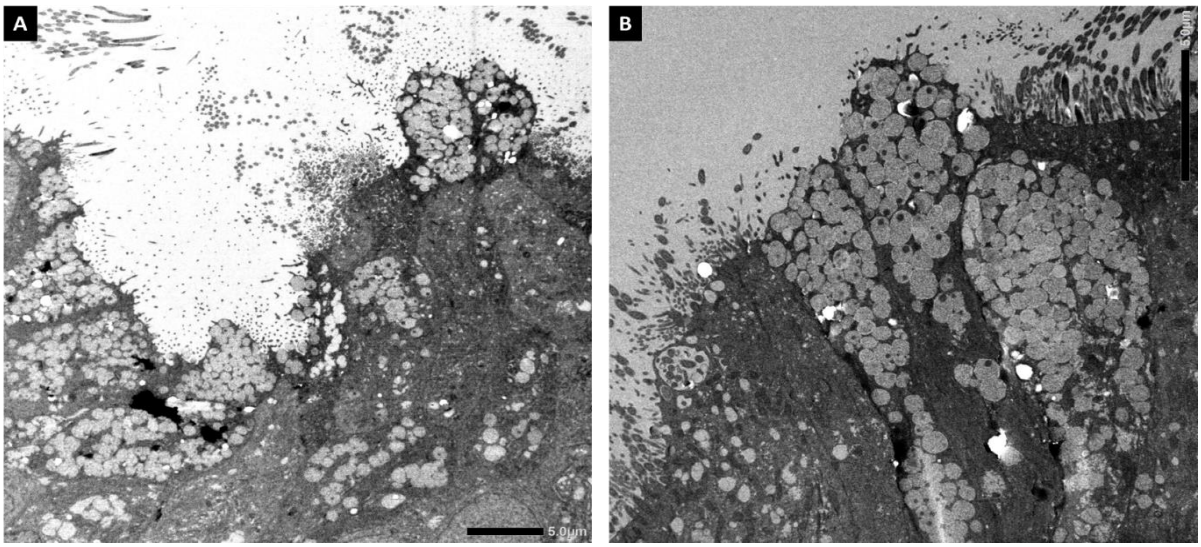

Figure 32. Ultrastructural images of hTM after 24 h of IAV infection showing mucus-filled vesicles: The infected models showed increased mucus production (A and B) compared to the non-infected control (qualitative) shown in Figure 30 (A, B and C). Models generated from three different donors (N = 3) were used for the TEM analyses. Scale bar = 5 µm.

4.2.2.7. Infection associated cytokine release in hAM

Viral infections are previously known to elicit inflammatory responses both in clinical and animal studies by activating both innate and adaptive immune system. Similarly, in hTM we assessed the early innate immune response against viruses by the non-immune cells of the airway mucosa. For this, the supernatant was collected from the apical compartment of the non-infected and infected samples to measure the IL-6, IL-8 and TNF-α secretion 24 h p.i (Figure 33 A, B and C). The hTM showed a significantly high IL-8 secretion in response to RSV infection (Figure 33 B). There was no detectable TNF-α release in the first 24 h of infection in both cell types and all three viruses.

The study results show that RSV infection significantly increased the secretion of IL-8 in hTM compared to hNM. Specifically, the relative IL-8 release by hTM was approximately 2.8 times higher than by hNM in response to RSV infection. Similar results were observed for IL-8 release in hTM infected with IAV and SARS-CoV-2, which showed approximately 2.6 and 2.7- times higher release compared to hNM, respectively. The data presented in the study are means ± SEM of independent experiments performed in duplicates for IL-6, IL-8, and TNF-α analyses. Sidak's multiple comparison tests were performed to compare the differences in IL-8, IL-6 and TNF-α release between hTM and hNM in response to viral infections. The result suggests that RSV, IAV, and SARS-CoV-2 infections may trigger higher levels of IL-8 release in the lower airways (hTM) compared to the upper airway mucosa (hNM).

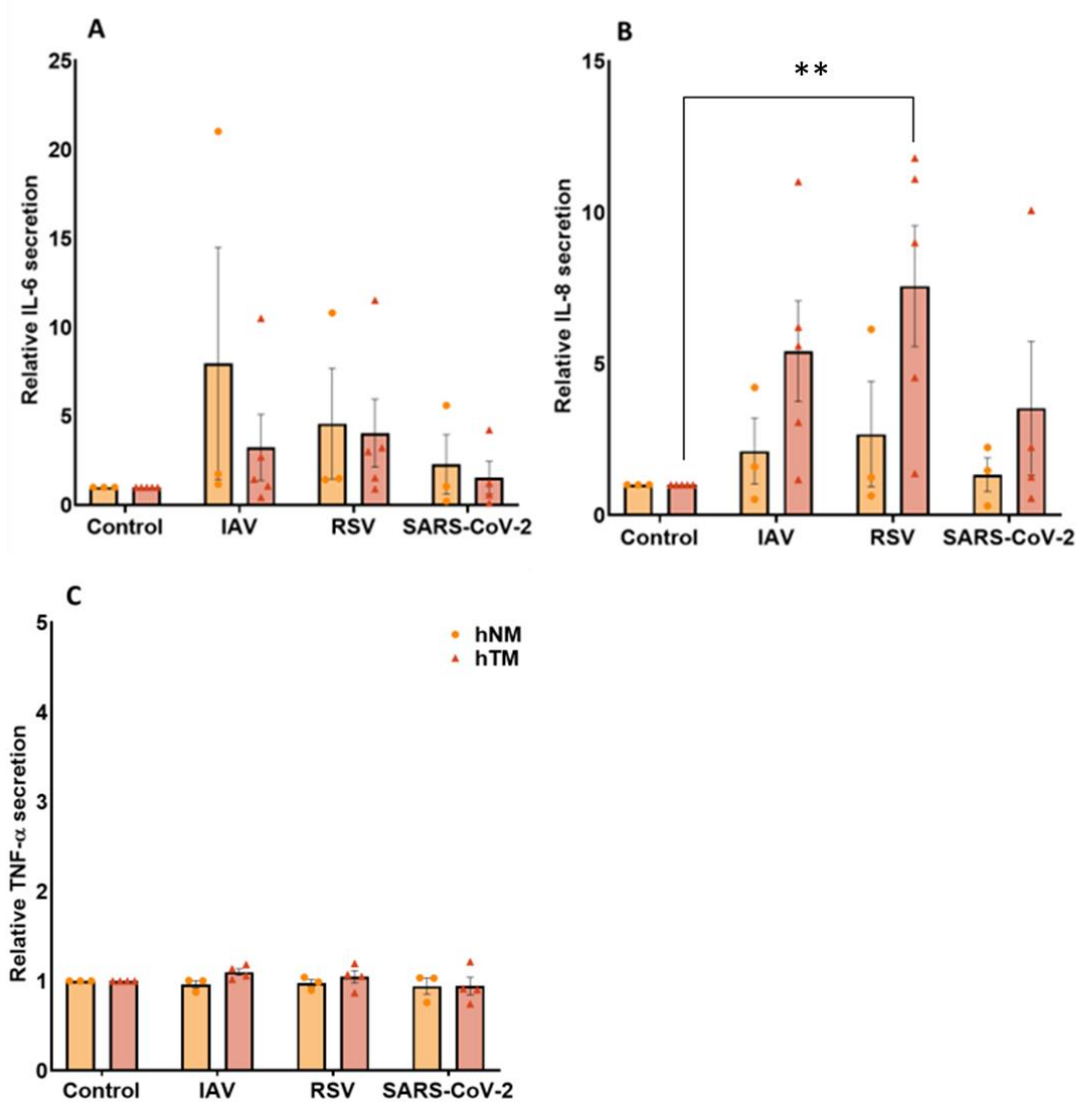

Figure 33. Relative IL-6, IL-8 and TNF-α secretion of hAM after viral infection: The release of IL-6 (A), IL-8 (B) and TNF-α (C) were investigated after 24 h infection with individual viruses. RSV significantly altered relative IL-8 (B) secretion in hTM. The relative IL-8 release by hTM was ~2.8 times higher than hNM against RSV, ~2.6 times higher against IAV and ~2.7 times higher against SARS-CoV-2 infection. The data are presented as means ± SEM of independent experiments performed in duplicates for both IL-6, IL-8 and TNF-α analyses. Sidak's multiple comparison tests were performed, **p value of (hTM - Control vs. RSV) was <0.008, and the other treatments were not statistically significant. N = 4, hNM were used for the IL-6 and IL-8 analyses (all three viruses), and N = 3 for TNF-α analyses (all three viruses). N = 4, hTM were used for TNF-α analyses and SARS-CoV-2 infection, and N = 5, hTM were used for (IL-6 and IL-8 analyses) IAV and RSV infection.

4.2.3. scRNA-seq for COPD vs. non-COPD

4.2.3.1. Timepoint analyses of IAV shedding from hTM

For the investigation of early events following IAV infection in non-COPD and COPD patient-derived models, we had to assess the replication time of virus in hTM. To achieve this, we monitored the spread of IAV infection at 0 h, 6 h, 12 h, and 24 h time points to estimate the replication time of the virus in hTM. To confirm the infectivity of the newly generated viruses, we collected the supernatant from the apical compartment of the models and serially diluted it. We used this diluted supernatant to infect MDCK cell lines and they were successfully infected, indicating that the newly produced viruses using the host machinery were fully infectious.

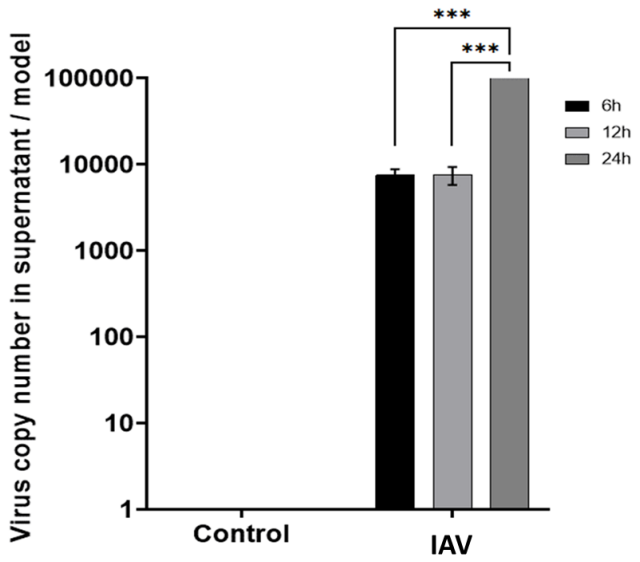

Figure 34. Viral content in the culture supernatants (apical) of hTM infected with the IAV after 6 h, 12 h, and 24 h time points: Shows the data from RT-qPCR of the RNA isolated from the supernatant collected from the apical side of the IAV-infected models vs. non-infected control. It shows a significant increase (10-fold increase) in the viral copy number at 24 h compared to the 12 h and 6 h time points, suggesting the shedding of new viruses. The data are presented as means ± SEM of independent experiments performed in duplicates (N = 3). Sidak's multiple comparison tests were performed, 6 h vs 24 h IAV and 12 h vs 24 h IAV infected group are indicated as***, $p < 0.0006$.

To confirm the results obtained from the RT-qPCR, we used immunofluorescent staining to visually track the progress of IAV infection. We observed that the signal

intensity of IAV gradually increased from 6 h and steeply increased at 24 h post-infection. Hence, we speculate that the shedding of small quantities of virions was insufficient to spread infection, while shedding large quantities of virions caused transmission via localised infection spots in tissue (Figure 35 D) at the 24 h time point. Our findings suggest that the spread of IAV infection in hTM depends on the quantity of virions shed and that the virus has a replication time that gradually increases before steeply increasing at 24 h. Immunofluorescent staining was used to confirm the results from the RT-qPCR and to track the progress of IAV infection visually. Our results also confirm the infectivity of the newly generated viruses within the models, which can be useful for further investigations into the pathogenesis of IAV infection in non-COPD and COPD patient-derived models.

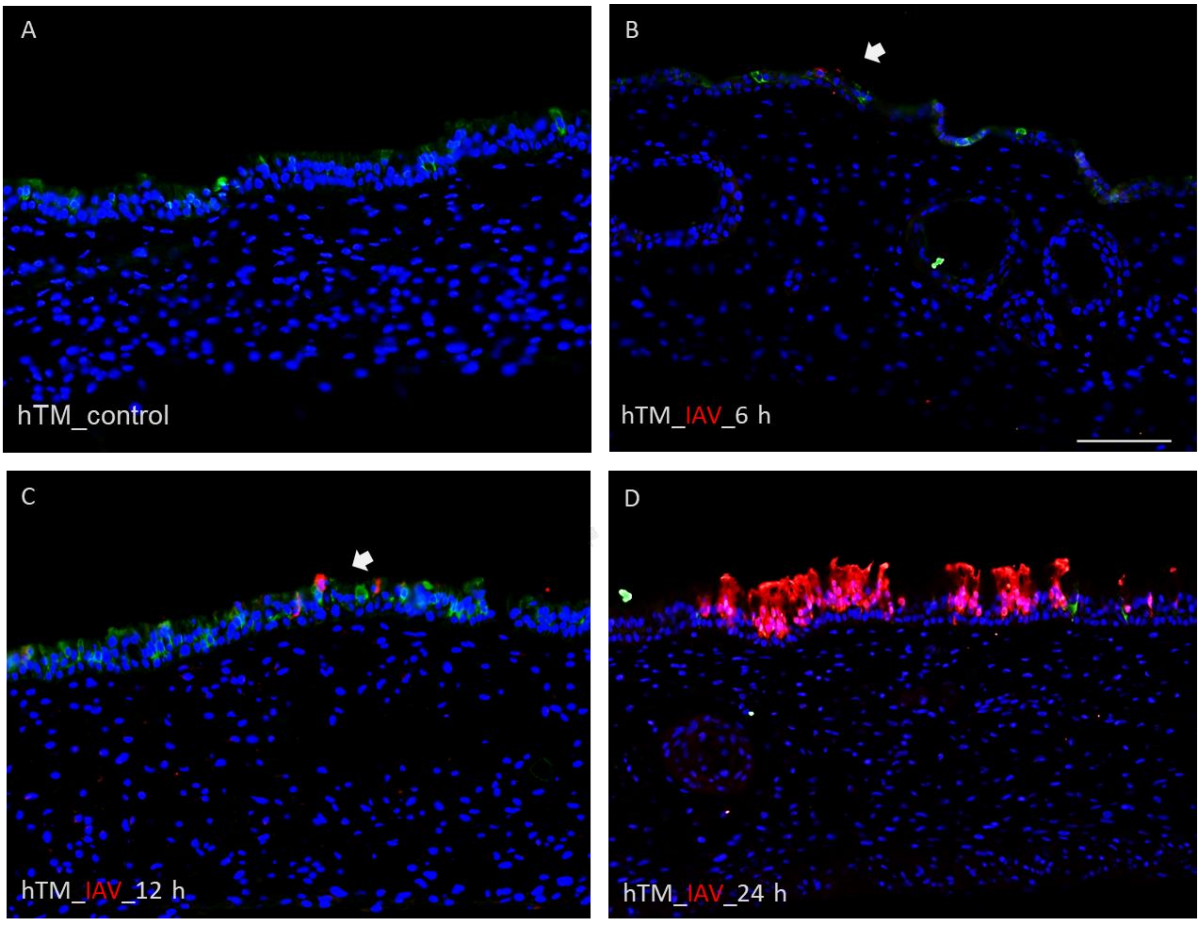

Figure 35. IAV-infected tissue models after 6 h, 12 h, and 24 h time points: We can observe an increase in IAV signal (indicated by white arrows- B and C) as time progressed, which suggests the cell-to-cell spread of infection. N = 4; Green = CK18, Red = IAV nucleoprotein, and blue = DAPI. Scale bar (applies for all figures) = 100 µm

4.2.3.2. Early tropism of IAV

From the scRNA-seq data, our first step was to investigate the tropism of IAV to specific cell types during infection to determine the early interaction targets of IAV. The preliminary analyses demonstrate the distribution of viral RNA in all the major cell types type (Figure 36 A – colour coded, and B – shows the percentage of IAV viral reads in the hTM, grey represents the cells with no viral RNA content), and we did not observe a specific affinity of IAV confined to a particular cell type during the first 6 h of infection based on the scRNA-seq data.

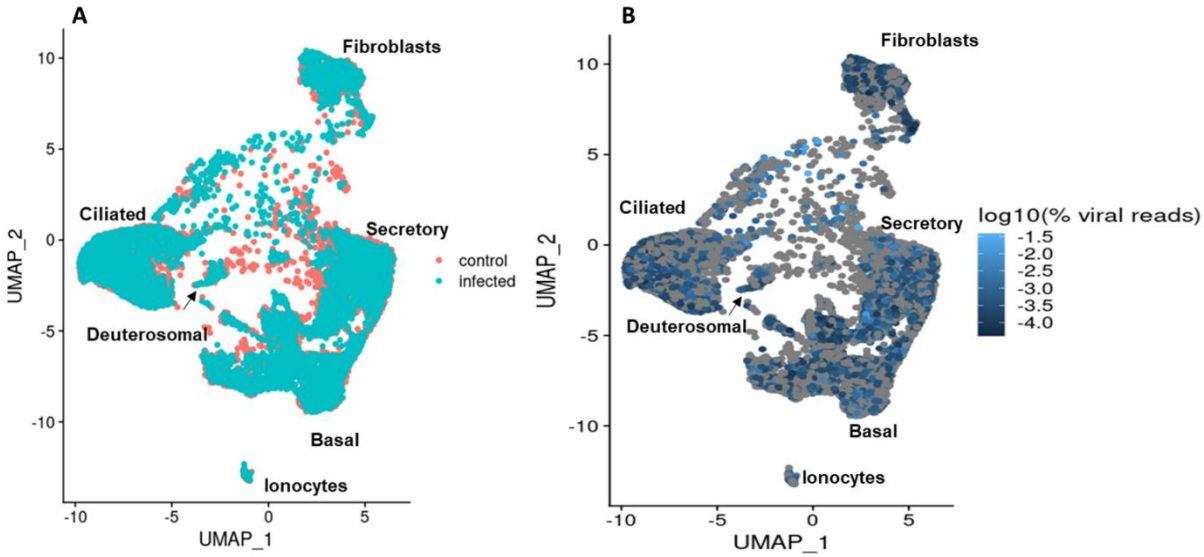

Figure 36. Represents the distribution of IAV RNA in the individual cell type: (A) The IAV RNA are present in all the major cell types and (B) Total viral reads in individual cells; grey, represents cells with no viral RNA content. The data represents the combined IAV RNA content in both COPD and non-COPD derived hTM models. N = 2, COPD patient derived hTM; N = 3, non-COPD patient derived hTM. Data extracted from the bioinformatic analyses performed by Prof. Florian Erhard and Kevin Berg (Institute of Virology and Immunobiology, Würzburg).

4.2.3.3. IAV infection induces MUC5AC gene upregulation as early as 6 h p.i in hTM

As we observed the upregulation of mucins followed by IAV infection (qualitatively) using immunofluorescence staining (Figure 31) and ultrastructural analyses (Figure 32) at 24 h p.i. we wanted to further investigate this effect during early infection time point. We could observe a qualitative increase in mucin secretion as early as 6 h p.i.

visible, from the apical washes of the infected models and the results from the scRNA-seq confirms the upregulation of MUC5AC gene in the basal, ciliated, deuterosomal and secretory cell types compared to the non-infected control during this time point (Figure 37).

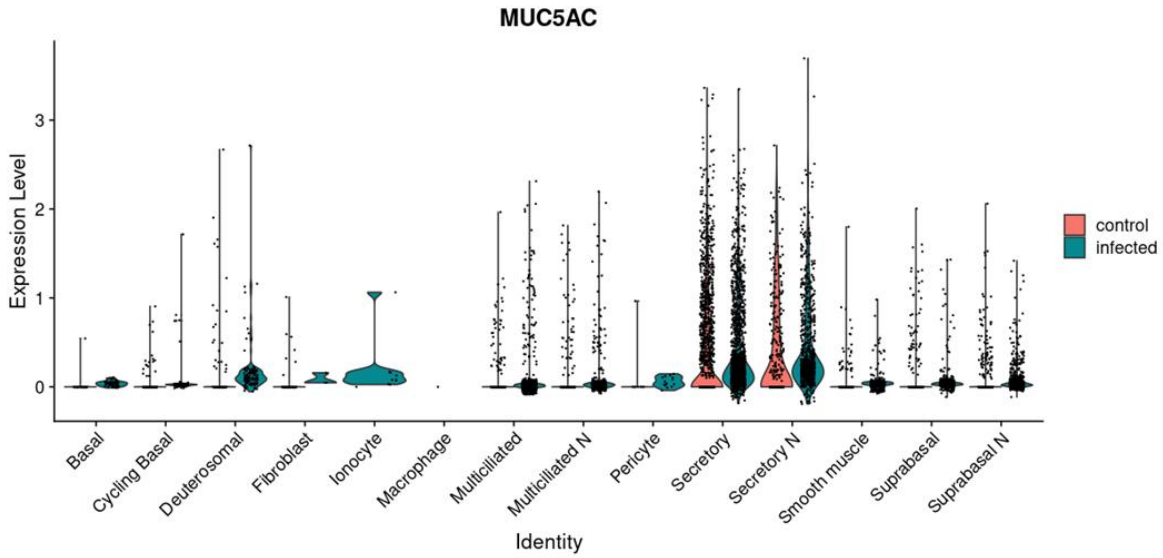

Figure 37. Represents the upregulation of MUC5AC gene in the individual cell type: The infected hTM (6 h p.i) show an increased MUC5AC expression especially the basal, ciliated, deuterosomal and secretory cell types compared to the non-infected control. The data represents the combined MUC5AC expression from both COPD and non-COPD derived hTM models. N = 2, COPD patient derived hTM; N = 3, non-COPD patient derived hTM. Data extracted from the bioinformatic analyses performed by Prof. Florian Erhard and Kevin Berg (Institute of Virology and Immunobiology, Würzburg).

4.2.3.4. IAV induces upregulation of SCGB1A1 gene in hTM

After analysing the differential gene expression from the scRNA-seq data, we explored further into early response targets specific to each cell type present in the airway mucosa of both COPD and non-COPD hTM. Our analysis revealed that among the top 10 differentially expressed gene targets, SCGB1A1, the club cell marker gene (secretoglobin family 1A member 1) showed significant expression patterns in both groups. At basal level, SCGB1A1 gene expression was lower in COPD control group than the non-COPD control group across major cell types including secretory cells. However, following IAV infection for 6 hours, the gene expression was upregulated in both groups (Figure 38 A). The secretory cells in the non-COPD-hTM group exhibited approximately 2.7 times higher expression of SCGB1A1 gene compared to the non-COPD group, while the secretory cells in the COPD infected group showed approximately 7.9 times SCGB1A1 upregulation compared to the COPD control.

These results from the scRNA-seq data indicate a significant impact of IAV, particularly on the COPD group, as demonstrated by the relative SCGB1A1 gene expression normalized to the respective control group (Figure 38 B).

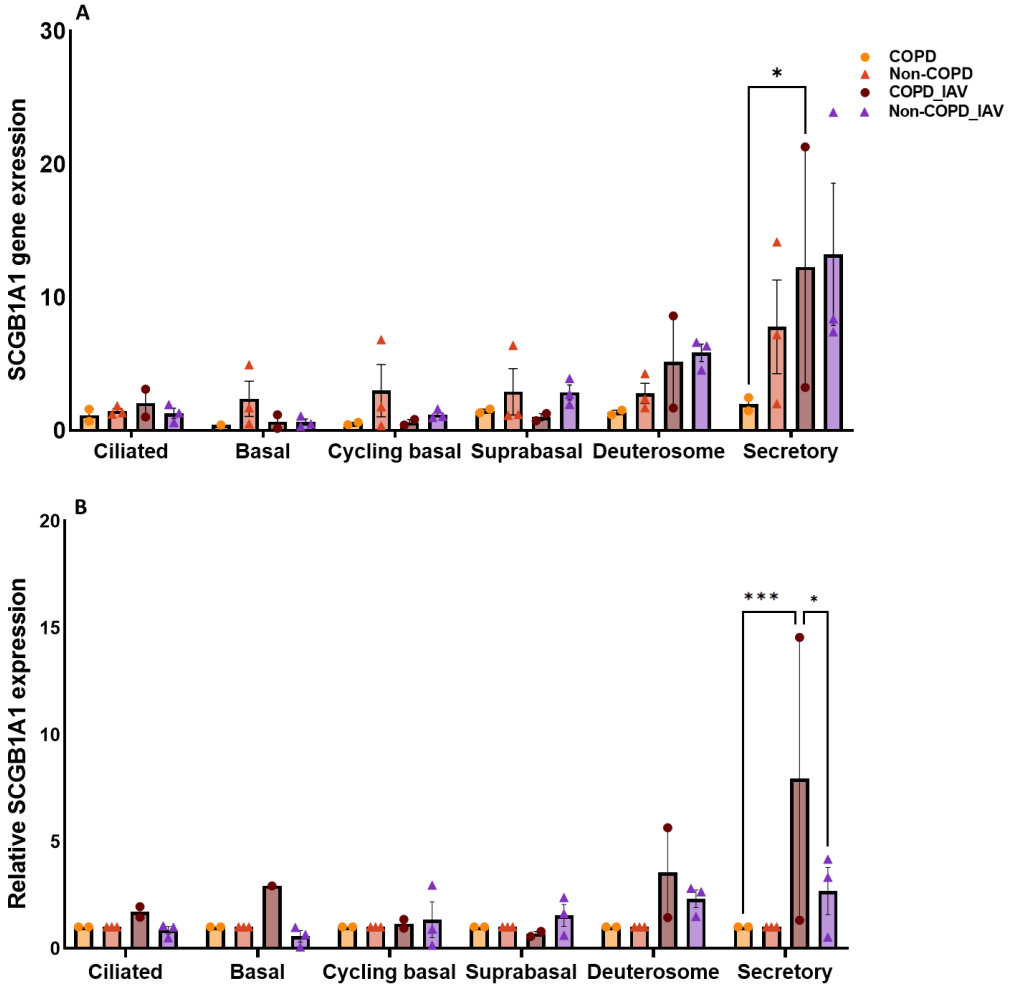

Figure 38. SCGB1A1 gene expression in COPD vs. IAV infection in hTM: (A) Basal level SCGB1A1 gene expression was lower in COPD hTM compared to non-COPD hTM. After 6 hours of IAV infection, the SCGB1A1 gene expression level increases in both groups, with a significant increase in COPD-infected hTM. The COPD and non-COPD hTM normalised to control group in each section (B) depicts the impact of IAV infection on both the groups. The IAV infection elevates SCGB1A1 gene expression in both COPD and non-COPD hTM and the COPD-infected group shows a significantly higher response to the infection and the effect is donor dependent. Data are presented as means ± SEM from 5 different donors; Tukey's multiple comparison tests within major cell types of COPD hTM (control vs. infected) was statistically significant (secretory) and * p value = 0.0464; *** p value = 0.0008 (relative gene expression). We further compared the response of both infected COPD vs. infected non-COPD group and * p value = 0.0138.

5. Discussion

This study generated hAM derived from primary human cells isolated from multiple unmatched donors' upper and lower respiratory tracts. The hAM was fully characterised at molecular and morphological level to validate their use for host-pathogen interaction studies to show the similarity with native human airways using scRNA-seq and histology. In addition to confirming the presence of major cell types such as basal, ciliated, and secretory cells we also found minor cell populations as ionocytes, and hillock cells and cell precursor populations such as deuterosomes and additional basal cell types such as suprabasal and cycling basal cells. This approach provided for the first time a comprehensive view of this engineered human airway mucosa. After the models were fully characterised, we used them for studying the interaction of human respiratory pathogens (clinical isolates).

We first used the models to study the effect of *B. pertussis* virulence factor CyaA which provided novel insights on the toxin's interaction with the hAM. We observed that the toxin induced significantly high cAMP production and innate immune response in hNM compared to hTM and there was no response by the bronchial cell line, HBEC3-KT that was used. It indicates the critical role of the upper airways in providing active immune response to external stimuli. This was also the first study that reported the differential susceptibility of the upper and lower respiratory mucosa towards CyaA. We further used the models to study respiratory viruses. We investigated the different events following infection addressing the individual response in terms of infection patterns, infection associated morphological characterisation and the innate immune response to IAV, RSV and SARS-CoV-2. The study highlights the critical role played by hAM in providing a dynamic defence response. In addition, we generated hTM from COPD patients (GOLD stages 2 and 4), we observed that the models recapitulated the donor characteristics morphologically (highly viscous mucus secretion, and high number of secretory cells compared to ciliated cells on the epithelium – qualitative). We then established and investigated the early infection events such as viral replication time, mucus upregulation, and suggests early response targets (club cells - observed by the upregulation of SCGB1A1) using scRNA-seq. The completed scRNA-seq data may reveal more information on potential targets that can be targeted for therapy in severe COPD patients.

A scRNA-seq provides new insights into the dynamics of airway differentiation, particularly regarding the relationship between goblet cells, ciliated cells, other specialised cell types and precursor cell population (Deprez et al., 2020; Ruiz García et al., 2019). We could identify the deuterosomal, ionocytes and hillock cell population in our hAM at the RNA level, with the extensive characterisation and aligning the information from scRNA-seq studies with the latest scientific findings (Deprez et al., 2020). We have gained an improved understanding of the model's complexity, which recommends its application in both infection biology and advance disease modelling. The scientific community is increasingly advocating for alternatives to animal testing and animal-derived materials. The European Medicines Agency (EMA) also supports implementing the 3Rs principles - replace, reduce, and refine - for the ethical use of animals in medicine testing across the European Union (EU). These principles encourage alternatives to animal studies while safeguarding scientific quality and improving animal welfare, where the use of animals cannot be avoided. Our study represents a significant step towards the long-term goal of entirely replacing animal studies in respiratory research.

In our study of the adenylate cyclase toxin, we gained novel insights into how *B. pertussis's* virulence factor CyaA interacts with primary cell-based human airway mucosa tissue models. Our finding that the innate immune response to the toxin was greater in nasal tissue models than in hTM suggests that the nasal airway mucosa plays a critical role as the first line of defence against airway pathogens. The nasal models exhibited more variation and response to treatment conditions than the tracheobronchial models. This result is predictable from a biological perspective, as the nasal mucosa is exposed to external factors and airborne pathogens and is constantly in a state of preparedness. Therefore, our findings contribute to a better understanding of the human airway mucosa - CyaA interaction.

We established an infection model using primary human epithelial cells to study the infection pattern of respiratory pathogens. These models could preserve the variance observed in the human population, including the severity of the infection, which was indicated by various morphological features such as infection hot spots, elevated mucus secretion associated with IAV infection and tracking the replication time of IAV within human tracheobronchial models. Furthermore, the models also exhibited morphological features like infection-induced cytotoxicity with RSV and the presence

of double-membrane vesicles (DMV), the sites of active viral replication (Knoops et al., 2008), and a high number of endosomes compared to non-infected samples (qualitative) during SARS-CoV-2 infection. Finally, we also observed an increased IL-6 and IL-8 response from models infected by all three viruses, suggesting that the condition caused inflammation in the airway mucosa as observed in the clinical study (Mori et al., 2022) and suggesting that these models can be used to study the immune response to respiratory pathogens. The IAV infection model provides a valuable tool for studying respiratory infections and may lead to in-vitro testing of new personalised therapeutic strategies.

When analysing respiratory tract diseases, various options exist for designing an appropriate model, depending on which part of the respiratory tract is being studied. Different factors govern pathogenesis followed by infection. Some include age, health, immunological history of the host, environment, and the tissues in which the infected cells reside. Specific readouts, such as cytokine release, will depend on the chosen airway epithelial cell type (primary cells from nasal or tracheobronchial regions or cell lines) and cell culture conditions (submerged or airlifted) (Bianchi et al., 2021; Sivarajan et al., 2021). Appropriate models that correlate with the in vivo situation are crucial to developing better treatments. Studies on the interaction between human airways and pathogens have been limited using models that do not accurately reflect the natural situation. As a result, our understanding of the host-pathogen interactions in human airways is still largely speculative. Hence, developing better disease models specific to human pathogens is essential.

Our earlier study observed that the nasal models displayed a higher degree of variation and response with or without CyaA treatment than the hTM regarding cAMP response and cytokine release (Sivarajan et al., 2021). Here, we additionally measured the basal levels of IL-6 and IL-8 in hNM and hTM and observed a difference. Though not statistically significant the difference could also suggest a previously preactivated inflammatory response that are stronger in the upper respiratory mucosa and lasts longer that are also specific to individual donors. Understanding the role of abnormal basal IL-6/IL-8 in the airways may be necessary for diagnosing and treating respiratory diseases. The porcine elements found in the SIS may also induce this increased cytokine secretion at the basal level. Berger et al. (2020) investigated the impact of organ-specific ECM composition on the functional differentiation of human

adipose-derived stem cells (hASCs), which provides essential insights into the role of organ-specific ECM properties in influencing cellular behaviour, highlighting the need for further consideration of these microenvironmental features in tissue engineering approaches (Berger et al., 2020). Hence replacing SIS with a synthetic fibrous scaffold, which is permeable and can facilitate the growth and support of fibroblasts, could be an alternative to an animal-based extracellular matrix, as discussed earlier. A comparison of basal cytokine levels in models developed using a SIS scaffold vs. synthetic scaffold could give direct information in this regard if the cytokine release at the basal level is induced by porcine-derived factors.

The nasal and tracheobronchial models, when treated with CyaA, had a differential susceptibility. This was also the first study showing the comparative analyses of CyaA treatment on human primary cell-derived airway mucosa models from two different anatomical sites (Sivarajan et al., 2021). The hNM had a higher response towards the treatment concerning cAMP production, IL-6, IL-8, and HBD-2 secretion than the hTM. A previous mice study showed that IL-6 is involved in leukocyte recruitment and is necessary to clear *B. pertussis* from the airways (Zhang et al., 2011). IL-6 also induces MUC5B secretion in human respiratory epithelial tissue models (Chen et al., 2003). Hence an increased IL-6 secretion plays a vital role in defending the host against *B. pertussis*.

The researchers in the study titled “Nasal and bronchial airway epithelial cell (AEC) mediator release in children” reported an increased IL-6, IL-8, and G-CSF release in nasal airway epithelial cultures compared to bronchial airway epithelial cultures on stimulation with IL-1β and TNF-α (Pringle et al., 2012). Studies show that nasal epithelial cells can be used as surrogates for studying lower respiratory tract diseases (Alves et al., 2016; Pringle et al., 2012; Roberts et al., 2018; Thavagnanam et al., 2014). However, based on the evidence from our experiments, we do not have evidence for using nasal cells to substitute bronchial cells, especially for bacterial toxin studies, as in agreement with other researchers (Comer et al., 2012). Thus, the experimental outcome might vary depending on the airway epithelial cell type and cell culture conditions.

The cell line HBEC3-KT used, however, did not respond to the toxin treatments with respect to cAMP production and cytokine release. A previous study in our group shows

HBEC3-KT lacks mucociliary phenotype (Lodes et al., 2020), which may contribute to its poor response. Some studies showed the differentiation potential of immortalised human bronchial epithelial cells (Vaughan et al., 2006). Still, in our study, their differentiation rate into mucociliary phenotype was poor, and the further use of HBEC3-KT was discontinued. Other studies with human airway cell lines VA10 (Hasan et al., 2018) showed that CyaA treatment caused an increase in the IL-6 secretion but had no impact on the IL-8 and HBD-2 levels.

A study on alveolar cell lines showed that CyaA treatment influenced cell morphology, adhesion, and cytoskeleton remodelling (Angely et al., 2020). Studies on VA10 cell line-based models showed that CyaA treatment for 24 h caused a significant drop in the transepithelial electrical resistance, suggesting that the membrane integrity was compromised (Hasan et al., 2018). In our previous publication (Sivarajan et al., 2021), Niklas Pallmann (Chair of Tissue Engineering and Regenerative Medicine, University Hospital Würzburg, Würzburg, Germany) assessed the CyaA-treated models using transmission electron microscopy. We found no significant disruptions in the cell-cell contact or the tight junctions with one-hour incubation with the treatment groups. So, here we investigated the influence of CyaA on the epithelial barrier integrity of the models for an extended time. It showed that 1 µg/mL of CyaA did not compromise the membrane integrity of the human airway mucosa models after 24 h of treatment. This was true for all cell types of nasal, tracheobronchial, and HBEC3-KT models. However, our experimental setup was not comparable to other studies as we used a biological scaffold which may provide relatively high stability to the models and resistance towards the toxin treatment. Also, the cell type and treatment conditions varied. For example, CyaA treatment on the basolateral side showed a higher impact on cytokine secretion and cAMP production than the apical treatment. In a recent study, human intestinal epithelial cell line-based tissue models were pre-incubated with IFNλ (Type III interferons), and this prevented bacteria-induced damage. The integrity of the epithelial barrier was intact, inhibiting the bacterial pathogens from crossing the epithelial layer (Odendall et al., 2017). Primary nasal epithelial cells can also express high levels of IFNλ following viral infections in vitro (Okabayashi et al., 2011), this might also provide epithelial protection followed by treatment with bacterial virulence factors, which needs further investigation.

Cell lines are well-suited for learning the basic biology of viral infections (Hoffmann et al., 2020; Schildgen et al., 2010; Youil et al., 2004). They are easy to maintain, genetically manipulate and are more widely used to study different aspects of the viral life cycle. In our study, unlike the hAM models, the cell lines used were infected in a virus concentration-dependent manner for each experimental replicate. Also, the viral concentration that infected most MDCK cells with minimum cell toxicity when used to infect the models, destroyed the entire epithelial layer within 24 h. Hence, we cannot always translate the information based on cell lines to in-vivo situations. In models, the infection pattern was dependent largely on the chosen donor hence with the same amount of virus used for infection, the percentage of cells infected varied. We could not identify the infected areas in the hTM for the RSV infection, using immunofluorescence though changes were observed at the gene expression level. The reason for the absence of signal after immunofluorescence staining in individual donors could be a longer replication cycle, the difference in the distribution of receptors specific to virus entry or the patient's age. This observation was also true for the SARS-CoV-2 infected models, not all the models were positively stained for the virus, and the percentage of infected cells varied among individual donors.

In the ultrastructural analyses of the infected models, we could observe the hot spots, the specific areas of the airway mucosa that are more prone to infection and inflammation. The factors contributing to the development of infection hot spots in the airway mucosa may include the presence of mucus or other secretions that provide a breeding ground for viruses and may increase the risk of infection in some regions of the airway mucosa. Another factor could be anatomical variations, such as having a different or increased number of specific cell types that make them more prone to infection and inflammation or unidentified random cues by the cell cluster, making them more susceptible to infection. The virus type and the individual's immune response could also contribute to developing infection hot spots in the airway mucosa. Increasing the virus concentration for infection increased cell damage. Hence, the exact mechanism or crosstalk behind specific areas more sensitised to infection is still unknown.

In RSV-infected models, we observed a higher number of lamellar bodies than in control, which may be seen in response to inflammation of the airway mucosa. Lamellar bodies are organelles found in the airway mucosa involved in the production

and secretion of surfactants in the lower airways (Schmitz & Müller, 1991). However, their presence in the nasal mucosa could suggest pathophysiology (Woodworth et al., 2005). There was also the presence of enlarged and damaged mitochondria, which could also suggest the cellular distress induced by the infection (observed in all the viral infections in both hNM and hTM). This study on RSV-infected hNM revealed that the infection strongly affected certain areas, characterised by cell extrusions, damaged kinocilia, and vacuolated cells. However, we could also observe areas suggestive of the dynamic airway repair and regeneration process for maintaining homeostasis after infection.

In the hAM infected with SARS-CoV-2, we observed an abnormal increase in endosomes compared to the non-infected control (qualitative). The S protein of SARS-CoV-2, on binding to ACE2, gets endocytosed in a vesicle which later fuses with the endosomal membrane and releases its genetic material into the cell (Khan et al., 2020; Poduri et al., 2020), so the increased number of endosomes in SARS-CoV-2-infected cells could be directly proportional to the active virus uptake by the host cells. The released viral RNA is then translated into two large polypeptide chains, pp1a and pp1ab, using the host cell machinery. These polypeptide chains undergo proteolytic cleavage to form non-structural proteins (nsps). The nsps 3, 4, and 6 are believed to play a crucial role in the replication of the virus by facilitating the remodelling of host cell membranes to form specialised organelles such as double-membrane vesicles (DMVs), convoluted membranes (CMs), and small open double-membrane spherules (DMSs). These organelles are thought to be the sites of active viral replication (Knoops et al., 2008; Neuman, 2016). The presence of these structures in the infected models confirms that the virus could infiltrate the hAM and induce viral replication.

Using ultrastructural analyses, identifying the virus-associated structures or viruses within hAM, or released viruses on the apical side of the model was challenging because of the similarity in structure and size of cell organelles in the tissue models to the virus-associated structures and virions. For example, the similarity of endosomes to intracellular non-coated SARS-CoV-2 viruses (Pinto et al., 2022; Zhao et al., 2020) made the identification of viruses inside the models challenging. The cross-sectional view of microtubules closely resembled in size and structure of all three viruses. In addition to the TEM reference from the above-mentioned work, we also compared images from Pizzarno et al., which showed SARS-CoV-2 infected airway epithelial

models (Figure 2 C2; Pizzorno et al., 2020). These reference images closely resemble the TEM images of microvilli. So, we could observe morphological features induced by the viral infection in all viruses. However, identifying individual viruses within the model was not completely successful with the TEM analyses due to the high complexity of the tissue models and the similarity in size and morphology to the cellular structures. Negative staining for actin filaments could specifically help differentiate the viruses from the microtubules in future studies.

We analysed interleukin levels in airway models generated from different donors to IAV, RSV, and SARS-CoV-2 infection and non-infected controls. IL-6 helps to regulate immune and inflammatory responses and is released in response to inflammation or tissue damage. However, excessive IL-6 production can have adverse effects on the body. For example, in the case of RSV infection in nasal models, we could observe high levels of IL-6 that may lead to excessive inflammation and tissue damage (McNamara et al., 2004; Vázquez et al., 2019). The tissue damage was evident in the ultrastructural analyses of RSV-infected samples (Villenave et al., 2012). Therefore, the body must maintain a balance of IL-6 production to effectively fight off infections without causing undesired outcomes.

IL-8 plays a role in the immune response by attracting and activating other immune cells to the site of infection or inflammation. The IL-6 and IL-8 can help stimulate the immune system to fight against diseases. Our observation shows that the exact pattern of IL-6/IL-8 secretion in the respiratory tract can vary depending on the specific stimulus (IAV, RSV or SARS-CoV2) and the individual's immune response. Wart et al. (2009) also reported considerable diversity in the innate immune response in primary bronchial epithelial cells in response to different Rhinovirus strains (Wark et al., 2009). Further research is needed to understand the factors contributing to differences in IL-6/IL-8 secretion between the upper and lower airways. High levels of IL-6 and other cytokines have been associated with an increased risk of complications such as pneumonia and bronchiolitis.

Viral infections can cause an increase in mucus production in the airway mucosa, also known as hyper mucus secretion leading to coughing, difficulty breathing, and excess phlegm production (Li & Tang, 2021). When the respiratory mucosa is infected with IAV, it stimulates mucus production as a protective response against the virus,

especially MUC5AC. Ehere et al. (2012) reported that the histopathological analyses from Muc5ac mRNA overexpressing mice revealed no airway mucus obstruction or inflammation in the lungs of transgenic mice, further challenging it with IAV showed a protective role of Muc5ac against influenza infection (Ehre et al., 2012). We could observe hyper mucus secretion and upregulation of MUC5AC in IAV-infected hTM using immunofluorescence. The TEM analyses of the infected models showed a more detailed morphology of the increased mucus-filled vesicles and mucus production compared to the non-infected controls. The preliminary scRNA seq data suggests the elevated MUC5AC gene expression which was also visually observed (increased mucus secretion from the apical washes of infected models) as early as 6 h p.i. Multiple pathways are reported to influence mucin production after IAV infection, including the MAPK pathway and NF-κB signalling (Barbier et al., 2012; Mata et al., 2011).

IAVs can escape the mucus barrier by using their surface proteins to bind to receptors on the surface of respiratory tract cells, allowing them to enter the cells and replicate. This enables IAVs to infect cells more profoundly in the respiratory tract (Gulati et al., 2013; Vahey & Fletcher, 2019). They can evade the mucus barrier by mutating or changing their surface proteins, such as the hemagglutinin (HA) and neuraminidase (NA) proteins, which can allow them to bind more efficiently to respiratory tract cells and evade recognition by the immune system (Vahey & Fletcher, 2019; Yang et al., 2016). IAVs use their NA enzyme to cleave sialylated glycans on the surface of mucus, which can thin the mucus and make it easier for the virus to reach the epithelial layer (Cohen et al., 2013).

Animal studies reported morphological evidence of transdifferentiating ciliated cells into mucus-secreting cells in asthma and viral (Sendai virus) infection models (Reader et al., 2003; Tyner et al., 2006). Further investigations are required to confirm whether the ciliated cells of human airway mucosa could also transdifferentiate into mucus-secreting cells followed by infection. Our observation on the increased number of mucus-secreting cells 24 h post-infection and elevated MUC5AC gene expression as early as 6 h p.i could indicate such a phenomenon in the human airway mucosa. Additionally, we recapitulated the clinical symptoms of IAV infection like altered mucus viscosity (highly viscous compared to non-infected control models-qualitative observance), yellow coloration of mucus secretion at high MOI infection (~ 10;

qualitative), and thick plugs composed of cell debris analysed using TEM (Deng et al., 2020; Ehre et al., 2012; Roy et al., 2014; Taubenberger & Morens, 2008).

Recent studies using lineage tracing with scRNA-seq have demonstrated that the stemness of basal cells differs during homeostasis and regeneration after acute injury. In homeostatic conditions, basal cells differentiate into secretory cell progeny, which then undergo trans-differentiation to give rise to the ciliated cells. However, after acute injury, basal cells can differentiate directly into either secretory or ciliated cells within 24 h (Mori et al., 2015; Pardo-Saganta et al., 2015). The increased gene expression of club cell marker (SCGB1A1) post-IAV infection could suggest the active proliferation of basal cells into secretory phenotype as a response to the infection stimuli or deuterosome trans-differentiation to secretory phenotype during stress response. It has been also previously reported that the club cells can proliferate or differentiate to maintain the ciliated cell population (Reynolds et al., 2009). These findings highlight the dynamic nature of stem cell differentiation and the critical role of Notch signalling in regulating their fate.

Lineage tracing studies in mice, show that Scgb1a1-expressing cells can differentiate into Alveolar Type I and II Cells to repair the lung damage caused by bleomycin treatment and Influenza (Zheng et al., 2012). So, our observation, could be an interesting finding demonstrating an active repair site during viral infection. Studies on transgenic mice have confirmed the protective role of SCGB1A1, as the SCGB1A1^{-} mice were associated with increased susceptibility to viral infections (Harrod et al., 1998). Studies on mice also report the role of SCGB1A1 in modulating the lung inflammatory and immune responses to RSV infection (Wang et al., 2003). Therefore, SCGB1A1 could also play a similar role during IAV infection and may be one of the early responders during IAV infection in the lower airways.

Patients diagnosed with COPD stages 3-4 (severe) demonstrated significantly lower levels of airway SCGB1A1 protein expression than those with stages 1-2 COPD, mild – moderate cases (Laucho-Contreras et al., 2016). A recent study on the SCGB1A1 gene, reported that polymorphism in SCGB1A1 is linked to airway diseases such as lung cancer, asthma, and COPD (Li et al., 2019). SCGB1A1 (protein) are also reported as biomarker for COPD patients (Chen et al., 2023; Kim et al., 2012). This may be due to the infiltration of SCGB1A1 into the blood and sputum due to the loss of epithelial

barrier integrity of diseased airways. Lower levels of SCGB1A1 in serum are also linked with impaired lung function, and moderate airflow limitation in adults (Guerra et al., 2015). Our scRNA-seq data of lower levels of SCGB1A1 gene expression in the control group also supports the clinical observation. But after IAV infection the COPD group had elevated SCGB1A1 gene expression especially for the model derived from stage 4 COPD patient sample. The hTM generated from diseased patients capability to recapitulate the patient's characteristics at molecular levels broaden the model's application to address more specific research questions and validate the potential of SCGB1A1 targeted therapy for severe COPD patients.

When using primary cells or primary cell-derived models for scientific research, most scientists report donor variability. This contrasts with cell lines, where outcomes are more comparable. The experimental outcomes of primary cells show a high degree of variance, and therefore we summarise and discuss potential reasons for the donor variability. This data obtained from the toxin studies with the hAM show an inter and intra-donor variance towards the toxin treatment. The individual variance of primary cells has been well-known and challenging while conducting experimental studies and have been reported previously.

Bovard et al. (2020) reported the difference in morphology and function of 3D lung epithelial cultures derived from different donors. Ilyushina et al. (2019) showed the IAV-induced interferon gene expression in human airway epithelial cells from two different donors. Rayner et al. (2019) showed the difference in the differentiation capacity of three donors from passages 1-8. Stewart et al. (2012) also reported a high degree of variability between donors, experiments, passage, and transepithelial electrical resistance. Veale et al. (1993) reported the variation in ciliary beat frequency (CBF) in nasal mucosal samples and in subjects with bronchiectasis. (Bovard et al., 2020; Ilyushina et al., 2019; Rayner et al., 2019; Stewart et al., 2012; Veale et al., 1993).

The inter-donor variation can be associated with several factors. The mucus can act as a selective pressure on transmissible viruses, influencing their ability to infect and transmit to new hosts by trapping and removing viruses before they can reach the epithelial layer. For example, the viscosity and pH of mucus can influence the ability of a virus to bind to and infect cells, as well as its ability to survive in the mucus

environment (Kaler et al., 2022). The respiratory tract's pH is slightly acidic, ranging from 6.5 to 7. The acidic pH might help to inhibit the growth of bacteria and other microorganisms and protect the respiratory tract from infections. In our lab, we checked the pH of hNM generated from two donors cultured under the same conditions and found that one donor had a pH of ~5.5 and the other ~7. Nasal pH can vary among individuals and can be influenced by factors such as smoking, environmental exposures, and genetics. Ethnic differences are also shown to contribute to the acidity of the nasal pH, which may be of direct relevance in the airways, as many of the functions of airway surface liquid depend on pH (Ireson et al., 2001).

Chen et al. (2014) reported that even low concentrations of nicotine (≤50 nM) significantly interfere with the normal function of mucins in the airway. Specifically, nicotine hindered the post-exocytotic swelling and hydration of released mucins, leading to a higher viscosity of the mucus. The close association of nicotine and mucins also allows the airway mucus to serve as a reservoir for prolonged nicotine release, which can lead to correlated pathogenic effects. Their findings also provided a new outlook on the poor hydration of mucus in smokers (Chen et al., 2014). This may increase the risk of IAV infection by making it easier for the virus to survive and replicate in the respiratory tract of a smoker. This may also be true for the models generated from donors who are smokers, which requires further investigation.

Low relative humidity can increase the transmission of IAV. When the air is dry, the mucus in the respiratory tract becomes dehydrated, making it easier for IAV to infect the respiratory tract cells. In addition, dry air can irritate the mucosa of the respiratory tract, making it more susceptible to infection. On the other hand, high relative humidity can help reduce the drying and irritation of the mucosa, making it less susceptible to infection (Ahlawat et al., 2022; Božič & Kanduč, 2021). Though the culture conditions in the incubator are with 95% humidity, when performing routine cell culture and ciliary beat analyses, there might be differences which have to be also considered in future experiments.

Huang et al. (2016) investigated the role of genetic variation (single nucleotide polymorphisms - SNP) of Toll-interacting protein (Tollip) in airway epithelial responses. The study's findings suggest that individuals with the Tollip SNP rs5743899 may

exhibit varying airway responses to Rhinovirus infection in asthma. This indicates that genetic factors may play a role in determining the severity of airway responses to viral infections in people with pre-existing health issues (Huang et al., 2016). According to the study by Lee et al. (2012), the bitter taste receptor T2R38 polymorphism is associated with susceptibility to upper respiratory infections caused by certain bacterial strains. This susceptibility may be partially attributed to impaired bacterial clearance in individuals who are homozygous for the functional allele of the T2R38 receptor. Together it suggests that the T2R38 receptor plays a crucial role in the innate defence system of the upper airway, and its genetic variation may influence the susceptibility of an individual to respiratory infections (Lee et al., 2012). Further analysing the expression of this gene in our nasal models could help us understand the increased susceptibility of some donors to treatment conditions.

Koehler et al. (2016) indicate the influence of the microenvironment on the individual's response. They reported that nitrogen dioxide exposure enhanced the IL-6 and IL-8 production in nasal epithelial cells in response to stimulation by major allergen of the house dust mite Der p1. The study suggests that nitrogen dioxide exposure can increase the pro-inflammatory potential of the house dust mite allergen Der p 1, which could exacerbate allergic responses in individuals exposed to nitrogen dioxide and Der p1 (Koehler et al., 2016). Benowitz et al. (2006) showed that women metabolise nicotine and cotinine faster than men, and this effect is amplified in women taking oral contraceptives due to the influence of estrogen (Benowitz et al., 2006). Bjerg et al. (2013) showed that female smokers have a higher risk of significant wheezing symptoms in younger ages compared to male smokers (Bjerg et al., 2013). Together these studies describe the gender-based variability to a stimulus which may influence their response to other factors (Bjerg et al., 2013). According to the study by Davies et al. (2011), the combination of budesonide and formoterol commonly used in asthma therapy inhibits early pro-inflammatory cytokines and key aspects of the type I IFN pathway in vitro. This suggests that these drugs can reduce excessive inflammation caused by Rhinovirus infections in asthma patients (Davies et al., 2011).

6. Conclusion and future perspectives

The use of hNM and hTM generated from primary human airway epithelial cells and fibroblasts provide a more physiologically relevant platform for investigating respiratory infections and related immune responses. We performed in-depth characterisation at the single cell RNA and protein levels. After confirming that these models recapitulate most of the in vivo features we used them to investigate the impact of *B. pertussis*, virulence factor CyaA on hAM. This was the first study to be reported that showed the differential susceptibility of human airway mucosa from two anatomical sites to the toxin. We determined that CyaA induced elevated innate immune response and intracellular cAMP production on the hNM compared to hTM.

We further used these complex models to study respiratory viruses. We successfully established physiologically relevant infection models of IAV, RSV and SARS-CoV-2. We observed that the infection patterns and the innate immune response of the airway mucosa captured various aspects of clinical findings like cell type-specific responses, mucus hypersecretion, cytokine release, and infection-associated epithelial cell damage which was also dependent on the donor and the type of viruses. The complex human airway mucosa models provide a more realistic representation of the human respiratory mucosa. They can reveal insights into host-pathogen interactions and immune responses, which we could demonstrate in our study.

We optimised the IAV titer to successfully establish an infection pattern with minimal cytotoxicity. Further we investigated the infection kinetics of IAV (clinical isolate) in the hTM and observed that the viruses are actively released ~ 24 h p.i. We successfully tracked the early IAV infection events of the hTM derived from the non-COPD and COPD patients infected using scRNA-seq. The lower levels of SCGB1A1 gene expression in the COPD-control group recapitulate the patient's characteristics reported in clinical studies. We also observed that the IAV infection elevated the SCGB1A1 gene expression specifically in the secretory cells in both COPD and non-COPD group. This will be the first reported research addressing the molecular diversity during early IAV infection (6h) in COPD and non-COPD disease models specific to individual cell types using scRNA-seq study. This also makes the model applicable for addressing more specific research questions and validating the potential targets such as SCGB1A1 targeted therapy for chronic lung diseases.

The models used here are more challenging to work with as they are derived from primary human cells which make them increasingly popular for animal replacement experiments. However, donor variation in primary human cells can be challenging in interpreting experimental outcomes due to their donor variation. We may overcome this by increasing the sample size and considering factors like health conditions of the donors, microenvironment, sex, age, previous exposure to disease, medication, and allergies which may contribute to lower individual variation when dealing with primary human cells or patients. Hence, these factors should be carefully considered and monitored when designing experiments and selecting donors or volunteers. A deeper understanding of genetic and epigenetic mosaicism may provide valuable insights into intra-donor and inter-donor variability in disease modelling and responses to infection and treatments. Further studies in this area could improve our ability to create advanced in vitro models and better understand the complexity of human biology.

7. Abbreviations

CyaA	Adenylate cyclase toxin
3D/2D	3 – dimensional / 2 – dimensional
TUC	50 mM Tris pH 8.0, 8 M Urea, and 2 mM $CaCl_2$ buffer
ALI	Air-liquid interface
ACE2	Angiotensin-converting enzyme 2
BSA	Bovine serum albumin
COPD	Chronic obstructive pulmonary disease
CM	convoluted membranes
cAMP	cyclic adenosine monophosphate
CF	cystic fibrosis
DMV	double-membrane vesicles
ECM	Extracellular matrix
FCS	Foetal calf serum
GOLD	Global Initiative for Chronic Obstructive Lung Disease
HA	Hemagglutinin
h	hour
Der p 1	House dust mite allergen
hAE	Human airway epithelium
hAM	human airway mucosa model
HBD	human beta-defensin
hNM	human nasal mucosa model
hTM	human tracheobronchial mucosa model
CyaA-AC $^-$	inactivated toxoid of CyaA
ifu	infectious units
IAV	Influenza A virus
IFN	Interferon
IL	Interleukin
min	minute
NA	Neuraminidase
PT	Pertussis toxin
PDMS	polydimethylsiloxane
PET	polyethylene terephthalate
p.i	post-infection
PCD	Primary ciliary dyskinesia
PNEC	Pulmonary neuroendocrine cell
RSV	Respiratory Syncytial Virus - subtype B
rpm	Revolutions per min
RNA	Ribonucleic acid
RNP	ribonucleoprotein
RdRp	RNA-dependent RNA polymerase
s	seconds
SARS-CoV-2	Severe Acute Respiratory Syndrome - Coronavirus - 2

SA	Sialic acid
SNP	single nucleotide polymorphisms
scRNA-seq	Single-cell RNA sequencing
SIS	small intestine submucosa
Tollip	Toll-interacting protein
TCT	Tracheal cytotoxin
TEER	trans-epithelial electrical resistance
TMPRSS2	transmembrane protease serine 2
TEM	Transmission Electron Microscopy
TNF	Tumour necrosis factor
WHO	World Health Organization

8. List of tables

9. List of figures

10. References

Agustí, A., & Vestbo, J. (2011). Current controversies and future perspectives in chronic obstructive pulmonary disease. Am J Respir Crit Care Med, 184(5), 507-513. https://doi.org/10.1164/rccm.201103-0405PP

Ahlawat, A., Mishra, S. K., Herrmann, H., Rajeev, P., Gupta, T., Goel, V., Sun, Y., & Wiedensohler, A. (2022). Impact of Chemical Properties of Human Respiratory Droplets and Aerosol Particles on Airborne Viruses' Viability and Indoor Transmission. Viruses, 14(7). https://doi.org/10.3390/v14071497

Akerley, B. J., Cotter, P. A., & Miller, J. F. (1995). Ectopic expression of the flagellar regulon alters development of the Bordetella-host interaction. Cell, 80(4), 611-620. https://doi.org/10.1016/0092-8674(95)90515-4

Alves, M. P., Schögler, A., Ebener, S., Vielle, N. J., Casaulta, C., Jung, A., Moeller, A., Geiser, T., & Regamey, N. (2016). Comparison of innate immune responses towards rhinovirus infection of primary nasal and bronchial epithelial cells. Respirology, 21(2), 304-312. https://doi.org/https://doi.org/10.1111/resp.12692

Andreasen, C., & Carbonetti, N. H. (2008). Pertussis toxin inhibits early chemokine production to delay neutrophil recruitment in response to Bordetella pertussis respiratory tract infection in mice. Infect Immun, 76(11), 5139-5148. https://doi.org/10.1128/iai.00895-08

Angely, C., Ladant, D., Planus, E., Louis, B., Filoche, M., Chenal, A., & Isabey, D. (2020). Functional and structural consequences of epithelial cell invasion by *Bordetella pertussis* adenylate cyclase toxin. PLOS ONE, 15(5), e0228606. https://doi.org/10.1371/journal.pone.0228606

Ariati, R., Sales, F., Souza, A., Lima, R. A., & Ribeiro, J. (2021). Polydimethylsiloxane Composites Characterization and Its Applications: A Review. Polymers (Basel), 13(23). https://doi.org/10.3390/polym13234258

Avota, E., Bodem, J., Chithelen, J., Mandasari, P., Beyersdorf, N., & Schneider-Schaulies, J. (2021). The Manifold Roles of Sphingolipids in Viral Infections [Review]. Frontiers in Physiology, 12. https://doi.org/10.3389/fphys.2021.715527

Baldassi, D., et al. (2021). "Air−Liquid Interface Cultures of the Healthy and Diseased Human Respiratory Tract: Promises, Challenges, and Future Directions." Advanced NanoBiomed Research 1(6): 2000111.

Barbier, D., Garcia-Verdugo, I., Pothlichet, J., Khazen, R., Descamps, D., Rousseau, K., Thornton, D., Si-Tahar, M., Touqui, L., Chignard, M., & Sallenave, J.-M. (2012). Influenza A Induces the Major Secreted Airway Mucin MUC5AC in a Protease–EGFR–Extracellular Regulated Kinase–Sp1–Dependent Pathway. American Journal of Respiratory Cell and Molecular Biology, 47(2), 149-157. https://doi.org/10.1165/rcmb.2011-0405oc

Barnes, P. J. (2014). Cellular and molecular mechanisms of chronic obstructive pulmonary disease. Clin Chest Med, 35(1), 71-86. https://doi.org/10.1016/j.ccm.2013.10.004

Bar-Shai, N., Sharabani-Yosef, O., Zollmann, M., Lesman, A., & Golberg, A. (2021). Seaweed cellulose scaffolds derived from green macroalgae for tissue engineering. Scientific Reports, 11(1), 11843. https://doi.org/10.1038/s41598-021-90903-2

Bassinet, L., Fitting, C., Housset, B., Cavaillon, J.-M., & Guiso, N. (2004). Bordetella pertussis Adenylate Cyclase-Hemolysin Induces Interleukin-6 Secretion by Human Tracheal Epithelial Cells. Infection and Immunity, 72(9), 5530-5533. https://doi.org/10.1128/iai.72.9.5530-5533.2004

Benowitz, N. L., Lessov-Schlaggar, C. N., Swan, G. E., & Jacob III, P. (2006). Female sex and oral contraceptive use accelerate nicotine metabolism. Clinical Pharmacology & Therapeutics, 79(5), 480-488. https://doi.org/https://doi.org/10.1016/j.clpt.2006.01.008

Berger, C., Bjørlykke, Y., Hahn, L., Mühlemann, M., Kress, S., Walles, H., Luxenhofer, R., Ræder, H., Metzger, M., & Zdzieblo, D. (2020). Matrix decoded - A pancreatic extracellular matrix with organ specific cues guiding human iPSC differentiation. Biomaterials, 244, 119766. https://doi.org/10.1016/j.biomaterials.2020.119766

Beyerstedt, S., Casaro, E. B., & Rangel É, B. (2021). COVID-19: angiotensin-converting enzyme 2 (ACE2) expression and tissue susceptibility to SARS-CoV-2 infection. Eur J Clin Microbiol Infect Dis, 40(5), 905-919. https://doi.org/10.1007/s10096-020-04138-6

Bianchi, M., Sivarajan, R., Walles, T., Hackenberg, S., & Steinke, M. (2021). Susceptibility of primary human airway epithelial cells to Bordetella pertussis adenylate cyclase toxin in two- and three-dimensional culture conditions. Innate Immunity, 27(1), 89-98. https://doi.org/10.1177/1753425920979354

Bjerg, A., Ekerljung, L., Eriksson, J., Ólafsdóttir, I. S., Middelveld, R., Franklin, K. A., Forsberg, B., Larsson, K., Lötvall, J., Torén, K., Dahlén, S.-E., Lundbäck, B., & Janson, C. (2013). Higher Risk of Wheeze in Female than Male Smokers. Results from the Swedish GA2LEN Study. PLOS ONE, 8(1), e54137. https://doi.org/10.1371/journal.pone.0054137

Bouchez, V., Hegerle, N., Strati, F., Njamkepo, E., & Guiso, N. (2015). New Data on Vaccine Antigen Deficient Bordetella pertussis Isolates. Vaccines, 3(3), 751-770. https://doi.org/10.3390/vaccines3030751

Bovard, D., Giralt, A., Trivedi, K., Neau, L., Kanellos, P., Iskandar, A., Kondylis, A., Luettich, K., Frentzel, S., Hoeng, J., & Peitsch, M. C. (2020). Comparison of the basic morphology and function of 3D lung epithelial cultures derived from several donors. Curr Res Toxicol, 1, 56-69. https://doi.org/10.1016/j.crtox.2020.08.002

Božič, A., & Kanduč, M. (2021). Relative humidity in droplet and airborne transmission of disease. Journal of Biological Physics, 47(1), 1-29. https://doi.org/10.1007/s10867-020-09562-5

Branchfield, K., Nantie, L., Verheyden, J. M., Sui, P., Wienhold, M. D., & Sun, X. (2016). Pulmonary neuroendocrine cells function as airway sensors to control lung immune response. Science, 351(6274), 707-710. https://doi.org/10.1126/science.aad7969

Breeze, R. G., & Wheeldon, E. B. (1977). The cells of the pulmonary airways. The American review of respiratory disease, 116(4), 705–777. https://doi.org/10.1164/arrd.1977.116.4.705

Bumba, L., Masin, J., Fiser, R., & Sebo, P. (2010). Bordetella Adenylate Cyclase Toxin Mobilizes Its β2 Integrin Receptor into Lipid Rafts to Accomplish Translocation across Target Cell Membrane in Two Steps. PLoS Pathogens, 6(5), e1000901. https://doi.org/10.1371/journal.ppat.1000901

Bumba, L., Masin, J., Macek, P., Wald, T., Motlova, L., Bibova, I., Klimova, N., Bednarova, L., Veverka, V., Kachala, M., Dmitri, Barinka, C., & Sebo, P. (2016). Calcium-Driven Folding of RTX Domain β-Rolls Ratchets Translocation of RTX Proteins through Type I Secretion Ducts. Molecular Cell, 62(1), 47-62. https://doi.org/10.1016/j.molcel.2016.03.018

Cai, Y., Zhang, J., Xiao, T., Peng, H., Sterling, S. M., Walsh, R. M., Jr., Rawson, S., Rits-Volloch, S., & Chen, B. (2020). Distinct conformational states of SARS-CoV-2 spike protein. Science, 369(6511), 1586-1592. https://doi.org/10.1126/science.abd4251

Carius, P., Jungmann, A., Bechtel, M., Grißmer, A., Boese, A., Gasparoni, G., Salhab, A., Seipelt, R., Urbschat, K., Richter, C., Meier, C., Bojkova, D., Cinatl, J., Walter, J., Schneider-Daum, N., & Lehr, C. M. (2023). A Monoclonal Human Alveolar Epithelial Cell Line ("Arlo") with Pronounced Barrier Function for Studying Drug Permeability and Viral Infections. Advanced Science, 10(8), 2207301. https://doi.org/10.1002/advs.202207301

Carraro, G., Mulay, A., Yao, C., Mizuno, T., Konda, B., Petrov, M., Lafkas, D., Arron, J. R., Hogaboam, C. M., Chen, P., Jiang, D., Noble, P. W., Randell, S. H., McQualter, J. L., & Stripp, B. R. (2020). Single-Cell Reconstruction of Human Basal Cell Diversity in Normal and Idiopathic Pulmonary Fibrosis Lungs. Am J Respir Crit Care Med, 202(11), 1540-1550. https://doi.org/10.1164/rccm.201904-0792OC

Cerny, O., Anderson, K. E., Stephens, L. R., Hawkins, P. T., & Sebo, P. (2017). cAMP Signaling of Adenylate Cyclase Toxin Blocks the Oxidative Burst of Neutrophils through Epac-Mediated Inhibition of Phospholipase C Activity. The Journal of Immunology, 198(3), 1285-1296. https://doi.org/10.4049/jimmunol.1601309

Cerny, O., Kamanova, J., Masin, J., Bibova, I., Skopova, K., & Sebo, P. (2015). Bordetella pertussisAdenylate Cyclase Toxin Blocks Induction of Bactericidal Nitric Oxide in Macrophages through cAMP-Dependent Activation of the SHP-1 Phosphatase. The Journal of Immunology, 194(10), 4901-4913. https://doi.org/10.4049/jimmunol.1402941

Chandra, D., Bogdanoff, R. F., Bowler, R. P., & Benam, K. H. (2023). Electronic cigarette menthol flavoring is associated with increased inhaled micro and sub-micron

particles and worse lung function in combustion cigarette smokers. Respiratory Research, 24(1), 108. https://doi.org/10.1186/s12931-023-02410-9

Chang, E. H., Pezzulo, A. A., & Zabner, J. (2011). Do cell junction protein mutations cause an airway phenotype in mice or humans? Am J Respir Cell Mol Biol, 45(2), 202-220. https://doi.org/10.1165/rcmb.2010-0498TR

Chen, E. Y., Sun, A., Chen, C. S., Mintz, A. J., & Chin, W. C. (2014). Nicotine alters mucin rheological properties. Am J Physiol Lung Cell Mol Physiol, 307(2), L149-157. https://doi.org/10.1152/ajplung.00396.2012

Chen, M., Xu, K., He, Y., Jin, J., Mao, R., Gao, L., Zhang, Y., Wang, G., Gao, P., Xie, M., Liu, C., & Chen, Z. (2023). CC16 as an Inflammatory Biomarker in Induced Sputum Reflects Chronic Obstructive Pulmonary Disease (COPD) Severity. International Journal of Chronic Obstructive Pulmonary Disease, 18, 705-717. https://doi.org/10.2147/COPD.S400999

Chen, N., Zhou, M., Dong, X., Qu, J., Gong, F., Han, Y., Qiu, Y., Wang, J., Liu, Y., Wei, Y., Xia, J. A., Yu, T., Zhang, X., & Zhang, L. (2020). Epidemiological and clinical characteristics of 99 cases of 2019 novel coronavirus pneumonia in Wuhan, China: a descriptive study. The Lancet, 395(10223), 507-513. https://doi.org/10.1016/s0140-6736(20)30211-7

Chen, R. E., Zhang, X., Case, J. B., Winkler, E. S., Liu, Y., Vanblargan, L. A., Liu, J., Errico, J. M., Xie, X., Suryadevara, N., Gilchuk, P., Zost, S. J., Tahan, S., Droit, L., Turner, J. S., Kim, W., Schmitz, A. J., Thapa, M., Wang, D., . . . Diamond, M. S. (2021). Resistance of SARS-CoV-2 variants to neutralization by monoclonal and serum-derived polyclonal antibodies. Nature Medicine, 27(4), 717-726. https://doi.org/10.1038/s41591-021-01294-w

Chen, Y., Thai, P., Zhao, Y.-H., Ho, Y.-S., DeSouza, M. M., & Wu, R. (2003). Stimulation of Airway Mucin Gene Expression by Interleukin (IL)-17 through IL-6 Paracrine/Autocrine Loop*. Journal of Biological Chemistry, 278(19), 17036-17043. https://doi.org/https://doi.org/10.1074/jbc.M210429200

Cherry, J. D. (1984). The epidemiology of pertussis and pertussis immunization in the United Kingdom and the United States: a comparative study. Curr Probl Pediatr, 14(2), 1-78. https://doi.org/10.1016/0045-9380(84)90016-1

Cherry, J. D. (1996). Historical review of pertussis and the classical vaccine. J Infect Dis, 174 Suppl 3, S259-263. https://doi.org/10.1093/infdis/174.supplement_3.s259

Cohen, M., Zhang, X. Q., Senaati, H. P., Chen, H. W., Varki, N. M., Schooley, R. T., & Gagneux, P. (2013). Influenza A penetrates host mucus by cleaving sialic acids with neuraminidase. Virol J, 10, 321. https://doi.org/10.1186/1743-422x-10-321

Collins, P., Chanock, R., Murphy, B., Knipe, D., Howley, P., Griffin, D., Lamb, R., Martin, M., Roizman, B., & Straus, S. (1996). Respiratory syncytial virus. Fields virology. Fields BN, Knipe DM.

Comer, D. M., Elborn, J. S., & Ennis, M. (2012). Comparison of Nasal and Bronchial Epithelial Cells Obtained from Patients with COPD. PLOS ONE, 7(3), e32924. https://doi.org/10.1371/journal.pone.0032924

Confer, D. L., & Eaton, J. W. (1982). Phagocyte impotence caused by an invasive bacterial adenylate cyclase. Science, 217(4563), 948-950. https://doi.org/10.1126/science.6287574

Connor, R. J., Kawaoka, Y., Webster, R. G., & Paulson, J. C. (1994). Receptor Specificity in Human, Avian, and Equine H2 and H3 Influenza Virus Isolates. Virology, 205(1), 17-23. https://doi.org/https://doi.org/10.1006/viro.1994.1615

Costa, A., de Souza Carvalho-Wodarz, C., Seabra, V., Sarmento, B., & Lehr, C.-M. (2019). Triple co-culture of human alveolar epithelium, endothelium and macrophages for studying the interaction of nanocarriers with the air-blood barrier. Acta Biomaterialia, 91, 235-247. https://doi.org/https://doi.org/10.1016/j.actbio.2019.04.037

Cotter, P. A., & Miller, J. F. (1994). BvgAS-mediated signal transduction: analysis of phase-locked regulatory mutants of Bordetella bronchiseptica in a rabbit model. Infect Immun, 62(8), 3381-3390. https://doi.org/10.1128/iai.62.8.3381-3390.1994

Currier, M. G., Lee, S., Stobart, C. C., Hotard, A. L., Villenave, R., Meng, J., Pretto, C. D., Shields, M. D., Nguyen, M. T., Todd, S. O., Chi, M. H., Hammonds, J., Krumm, S. A., Spearman, P., Plemper, R. K., Sakamoto, K., Peebles, R. S., Jr., Power, U. F., & Moore, M. L. (2016). EGFR Interacts with the Fusion Protein of Respiratory Syncytial Virus Strain 2-20 and Mediates Infection and Mucin Expression. PLoS Pathog, 12(5), e1005622. https://doi.org/10.1371/journal.ppat.1005622

Davies, J. M., Carroll, M. L., Li, H., Poh, A. M., Kirkegard, D., Towers, M., & Upham, J. W. (2011). Budesonide and Formoterol Reduce Early Innate Anti-Viral Immune Responses In Vitro. PLOS ONE, 6(11), e27898. https://doi.org/10.1371/journal.pone.0027898

Delmas, B., & Laude, H. (1990). Assembly of coronavirus spike protein into trimers and its role in epitope expression. J Virol, 64(11), 5367-5375. https://doi.org/10.1128/jvi.64.11.5367-5375.1990

Deng, L. S., Yuan, J., Ding, L., Chen, Y. L., Zhao, C. H., Chen, G. Q., Li, X. H., Li, X. H., Luo, W. T., Lan, J. F., Tan, G. Y., Tang, S. H., Xia, J. Y., & Liu, X. (2020). Comparison of patients hospitalized with COVID-19, H7N9 and H1N1. Infect Dis Poverty, 9(1), 163. https://doi.org/10.1186/s40249-020-00781-5

Deprez, M., Zaragosi, L. E., Truchi, M., Becavin, C., Ruiz García, S., Arguel, M. J., Plaisant, M., Magnone, V., Lebrigand, K., Abelanet, S., Brau, F., Paquet, A., Pe'er, D., Marquette, C. H., Leroy, S., & Barbry, P. (2020). A Single-Cell Atlas of the Human Healthy Airways. Am J Respir Crit Care Med, 202(12), 1636-1645. https://doi.org/10.1164/rccm.201911-2199OC

Dou, D., Hernández-Neuta, I., Wang, H., Östbye, H., Qian, X., Thiele, S., Resa-Infante, P., Kouassi, N. M., Sender, V., Hentrich, K., Mellroth, P., Henriques-Normark, B., Gabriel, G., Nilsson, M., & Daniels, R. (2017). Analysis of IAV Replication and Co-infection Dynamics by a Versatile RNA Viral Genome Labeling Method. Cell Reports, 20(1), 251-263. https://doi.org/10.1016/j.celrep.2017.06.021

Eby, J. C., Ciesla, W. P., Hamman, W., Donato, G. M., Pickles, R. J., Hewlett, E. L., & Lencer, W. I. (2010). Selective Translocation of the Bordetella pertussis Adenylate Cyclase Toxin across the Basolateral Membranes of Polarized Epithelial Cells. Journal of Biological Chemistry, 285(14), 10662-10670. https://doi.org/10.1074/jbc.m109.089219

ECDC, & Stockholm. (2020). Pertussis - Annual epidemiological report.

Edinger, T. O., Pohl, M. O., & Stertz, S. (2014). Entry of influenza A virus: host factors and antiviral targets. Journal of General Virology, 95(2), 263-277. https://doi.org/10.1099/vir.0.059477-0

Ehre, C., Worthington, E. N., Liesman, R. M., Grubb, B. R., Barbier, D., O'Neal, W. K., Sallenave, J. M., Pickles, R. J., & Boucher, R. C. (2012). Overexpressing mouse model demonstrates the protective role of Muc5ac in the lungs. Proc Natl Acad Sci U S A, 109(41), 16528-16533. https://doi.org/10.1073/pnas.1206552109

Ekanger, C. T., Zhou, F., Bohan, D., Lotsberg, M. L., Ramnefjell, M., Hoareau, L., Røsland, G. V., Lu, N., Aanerud, M., Gärtner, F., Salminen, P. R., Bentsen, M., Halvorsen, T., Ræder, H., Akslen, L. A., Langeland, N., Cox, R., Maury, W., Stuhr, L. E. B., . . . Engelsen, A. S. T. (2022). Human Organotypic Airway and Lung Organoid Cells of Bronchiolar and Alveolar Differentiation Are Permissive to Infection by Influenza and SARS-CoV-2 Respiratory Virus [Original Research]. Frontiers in Cellular and Infection Microbiology, 12. https://doi.org/10.3389/fcimb.2022.841447

Elbert, K. J., Schäfer, U. F., Schäfers, H. J., Kim, K. J., Lee, V. H., & Lehr, C. M. (1999). Monolayers of human alveolar epithelial cells in primary culture for pulmonary absorption and transport studies. Pharm Res, 16(5), 601-608. https://doi.org/10.1023/a:1018887501927

El Najjar, F., Schmitt, A. P., & Dutch, R. E. (2014). Paramyxovirus glycoprotein incorporation, assembly and budding: a three way dance for infectious particle production. Viruses, 6(8), 3019-3054. https://doi.org/10.3390/v6083019

El-Azami-El-Idrissi, M., Bauche, C., Loucka, J., Osicka, R., Sebo, P., Ladant, D., & Leclerc, C. (2003). Interaction of Bordetella pertussis Adenylate Cyclase with CD11b/CD18. Journal of Biological Chemistry, 278(40), 38514-38521. https://doi.org/10.1074/jbc.m304387200

Essaidi-Laziosi, M., Brito, F., Benaoudia, S., Royston, L., Cagno, V., Fernandes-Rocha, M., Piuz, I., Zdobnov, E., Huang, S., Constant, S., Boldi, M. O., Kaiser, L., & Tapparel, C. (2018). Propagation of respiratory viruses in human airway epithelia reveals persistent virus-specific signatures. J Allergy Clin Immunol, 141(6), 2074-2084. https://doi.org/10.1016/j.jaci.2017.07.018

Falsey, A. R., Treanor, J. J., Betts, R. F., & Walsh, E. E. (1992). Viral respiratory infections in the institutionalized elderly: clinical and epidemiologic findings. J Am Geriatr Soc, 40(2), 115-119. https://doi.org/10.1111/j.1532-5415.1992.tb01929.x

Feng, Z., Xu, L., & Xie, Z. (2022). Receptors for Respiratory Syncytial Virus Infection and Host Factors Regulating the Life Cycle of Respiratory Syncytial Virus [Review]. Frontiers in Cellular and Infection Microbiology, 12. https://doi.org/10.3389/fcimb.2022.858629

Flak, T. A., & Goldman, W. E. (1999). Signalling and cellular specificity of airway nitric oxide production in pertussis. Cellular Microbiology, 1(1), 51-60. https://doi.org/10.1046/j.1462-5822.1999.00004.x

Galloway, S. E., Reed, M. L., Russell, C. J., & Steinhauer, D. A. (2013). Influenza HA Subtypes Demonstrate Divergent Phenotypes for Cleavage Activation and pH of Fusion: Implications for Host Range and Adaptation. PLoS Pathogens, 9(2), e1003151. https://doi.org/10.1371/journal.ppat.1003151

Gambhir, M., Clark, T. A., Cauchemez, S., Tartof, S. Y., Swerdlow, D. L., & Ferguson, N. M. (2015). A Change in Vaccine Efficacy and Duration of Protection Explains Recent Rises in Pertussis Incidence in the United States. PLOS Computational Biology, 11(4), e1004138. https://doi.org/10.1371/journal.pcbi.1004138

Georgiou, P., Zanos, P., Mou, T.-C. M., An, X., Gerhard, D. M., Dryanovski, D. I., Potter, L. E., Highland, J. N., Jenne, C. E., Stewart, B. W., Pultorak, K. J., Yuan, P., Powels, C. F., Lovett, J., Pereira, E. F. R., Clark, S. M., Tonelli, L. H., Moaddel, R., Zarate, C. A., . . . Gould, T. D. (2022). Experimenters' sex modulates mouse behaviors and neural responses to ketamine via corticotropin releasing factor. Nature Neuroscience, 25(9), 1191-1200. https://doi.org/10.1038/s41593-022-01146-x

Gierer, S., Bertram, S., Kaup, F., Wrensch, F., Heurich, A., Krämer-Kühl, A., Welsch, K., Winkler, M., Meyer, B., Drosten, C., Dittmer, U., von Hahn, T., Simmons, G., Hofmann, H., & Pöhlmann, S. (2013). The spike protein of the emerging betacoronavirus EMC uses a novel coronavirus receptor for entry, can be activated by TMPRSS2, and is targeted by neutralizing antibodies. J Virol, 87(10), 5502-5511. https://doi.org/10.1128/jvi.00128-13

Glaser, L., Coulter, P. J., Shields, M., Touzelet, O., Power, U. F., & Broadbent, L. (2019). Airway Epithelial Derived Cytokines and Chemokines and Their Role in the Immune Response to Respiratory Syncytial Virus Infection. Pathogens, 8(3), 106. https://www.mdpi.com/2076-0817/8/3/106

Glaser, P., Ladant, D., Sezer, O., Pichot, F., Ullmann, A., & Danchin, A. (1988). The calmodulin-sensitive adenylate cyclase of Bordetella pertussis: cloning and expression in Escherichia coli. Mol Microbiol, 2(1), 19-30.

Global Initiative for Chronic Obstructive Lung Disease, https://goldcopd.org/wp-content/uploads/2018/02/WMS-GOLD-2018-Feb-Final-to-print-v2.pdf; accessed in May 2023

Goldfarbmuren, K. C., Jackson, N. D., Sajuthi, S. P., Dyjack, N., Li, K. S., Rios, C. L., Plender, E. G., Montgomery, M. T., Everman, J. L., Bratcher, P. E., Vladar, E. K., & Seibold, M. A. (2020). Dissecting the cellular specificity of smoking effects and reconstructing lineages in the human airway epithelium. Nature Communications, 11(1). https://doi.org/10.1038/s41467-020-16239-z

Goldman, W. E., Klapper, D. G., & Baseman, J. B. (1982). Detection, isolation, and analysis of a released Bordetella pertussis product toxic to cultured tracheal cells. Infection and Immunity, 36(2), 782-794. https://doi.org/10.1128/iai.36.2.782-794.1982

Gomi, K., Arbelaez, V., Crystal, R. G., & Walters, M. S. (2015). Activation of NOTCH1 or NOTCH3 Signaling Skews Human Airway Basal Cell Differentiation toward a Secretory Pathway. PLOS ONE, 10(2), e0116507. https://doi.org/10.1371/journal.pone.0116507

Grainger, C. I., Greenwell, L. L., Lockley, D. J., Martin, G. P., & Forbes, B. (2006). Culture of Calu-3 cells at the air interface provides a representative model of the airway epithelial barrier. Pharm Res, 23(7), 1482-1490. https://doi.org/10.1007/s11095-006-0255-0

Gray, M., Szabo, G., Otero, A. S., Gray, L., & Hewlett, E. (1998). Distinct Mechanisms for K+ Efflux, Intoxication, and Hemolysis by Bordetella pertussis AC Toxin. Journal of Biological Chemistry, 273(29), 18260-18267. https://doi.org/10.1074/jbc.273.29.18260

Green, K. J., & Jones, J. C. (1996). Desmosomes and hemidesmosomes: structure and function of molecular components. Faseb j, 10(8), 871-881. https://doi.org/10.1096/fasebj.10.8.8666164

Griffiths, C. D., Bilawchuk, L. M., McDonough, J. E., Jamieson, K. C., Elawar, F., Cen, Y., Duan, W., Lin, C., Song, H., Casanova, J.-L., Ogg, S., Jensen, L. D., Thienpont, B., Kumar, A., Hobman, T. C., Proud, D., Moraes, T. J., & Marchant, D. J. (2020). IGF1R is an entry receptor for respiratory syncytial virus. Nature, 583(7817), 615-619. https://doi.org/10.1038/s41586-020-2369-7

Guermonprez, P., Khelef, N., Blouin, E., Rieu, P., Ricciardi-Castagnoli, P., Guiso, N., Ladant, D., & Leclerc, C. (2001). The Adenylate Cyclase Toxin of Bordetella pertussis Binds to Target Cells via the αMβ2 Integrin (Cd11b/Cd18). Journal of Experimental Medicine, 193(9), 1035-1044. https://doi.org/10.1084/jem.193.9.1035

Guerra, S., Halonen, M., Vasquez, M. M., Spangenberg, A., Stern, D. A., Morgan, W. J., Wright, A. L., Lavi, I., Tarès, L., Carsin, A. E., Dobaño, C., Barreiro, E., Zock, J. P., Martínez-Moratalla, J., Urrutia, I., Sunyer, J., Keidel, D., Imboden, M., Probst-Hensch, N., . . . Martinez, F. D. (2015). Relation between circulating CC16 concentrations, lung function, and development of chronic obstructive pulmonary disease across the lifespan: a prospective study. Lancet Respir Med, 3(8), 613-620. https://doi.org/10.1016/s2213-2600(15)00196-4

Gulati, S., Smith, D. F., Cummings, R. D., Couch, R. B., Griesemer, S. B., St. George, K., Webster, R. G., & Air, G. M. (2013). Human H3N2 Influenza Viruses Isolated from 1968 To 2012 Show Varying Preference for Receptor Substructures with No Apparent Consequences for Disease or Spread. PLOS ONE, 8(6), e66325. https://doi.org/10.1371/journal.pone.0066325

Hamada, A., Torre, C., Drancourt, M., & Ghigo, E. (2019). Trained Immunity Carried by Non-immune Cells [Review]. Frontiers in Microbiology, 9. https://doi.org/10.3389/fmicb.2018.03225

Hamming, I., Timens, W., Bulthuis, M., Lely, A., Navis, G., & Van Goor, H. (2004). Tissue distribution of ACE2 protein, the functional receptor for SARS coronavirus. A first step in understanding SARS pathogenesis. The Journal of Pathology, 203(2), 631-637. https://doi.org/10.1002/path.1570

Hanski, E. (1989). Invasive adenylate cyclase toxin of Bordetella pertussis. Trends Biochem Sci, 14(11), 459-463. https://doi.org/10.1016/0968-0004(89)90106-0

Harrod, K. S., Mounday, A. D., Stripp, B. R., & Whitsett, J. A. (1998). Clara cell secretory protein decreases lung inflammation after acute virus infection. Am J Physiol, 275(5), L924-930. https://doi.org/10.1152/ajplung.1998.275.5.L924

Hasan, S., Kulkarni, N. N., Asbjarnarson, A., Linhartova, I., Osicka, R., Sebo, P., & Gudmundsson, G. H. (2018). Bordetella pertussis Adenylate Cyclase Toxin Disrupts Functional Integrity of Bronchial Epithelial Layers. Infection and Immunity, 86(3), e00445-00417. https://doi.org/doi:10.1128/IAI.00445-17

Hasan, S., Osickova, A., Bumba, L., Novák, P., Sebo, P., & Osicka, R. (2015). Interaction of Bordetella adenylate cyclase toxin with complement receptor 3 involves multivalent glycan binding. FEBS Letters, 589(3), 374-379. https://doi.org/https://doi.org/10.1016/j.febslet.2014.12.023

Heiss, L. N., Lancaster, J. R., Corbett, J. A., & Goldman, W. E. (1994). Epithelial autotoxicity of nitric oxide: role in the respiratory cytopathology of pertussis. Proceedings of the National Academy of Sciences, 91(1), 267-270. https://doi.org/10.1073/pnas.91.1.267

Hewitt, R.J., Lloyd, C.M. Regulation of immune responses by the airway epithelial cell landscape. Nat Rev Immunol 21, 347–362 (2021). https://doi.org/10.1038/s41577-020-00477-9

Hillyer, P., Shepard, R., Uehling, M., Krenz, M., Sheikh, F., Thayer, K. R., Huang, L., Yan, L., Panda, D., Luongo, C., Buchholz, U. J., Collins, P. L., Donnelly, R. P., & Rabin, R. L. (2018). Differential Responses by Human Respiratory Epithelial Cell Lines to Respiratory Syncytial Virus Reflect Distinct Patterns of Infection Control. J Virol, 92(15). https://doi.org/10.1128/jvi.02202-17

Hoffmann, M., Kleine-Weber, H., Schroeder, S., Krüger, N., Herrler, T., Erichsen, S., Schiergens, T. S., Herrler, G., Wu, N.-H., & Nitsche, A. (2020). SARS-CoV-2 cell entry depends on ACE2 and TMPRSS2 and is blocked by a clinically proven protease inhibitor. Cell, 181(2), 271-280. e278.

Hong, K. U., Reynolds, S. D., Watkins, S., Fuchs, E., & Stripp, B. R. (2004). Basal cells are a multipotent progenitor capable of renewing the bronchial epithelium. Am J Pathol, 164(2), 577-588. https://doi.org/10.1016/s0002-9440(10)63147-1

Howley P. M. (2021). Fields virology : emerging viruses (Seventh). Lippincott Williams & Wilkins.

Huang, C., Jiang, D., Francisco, D., Berman, R., Wu, Q., Ledford, J. G., Moore, C. M., Ito, Y., Stevenson, C., Munson, D., Li, L., Kraft, M., & Chu, H. W. (2016). Tollip SNP rs5743899 modulates human airway epithelial responses to rhinovirus infection. Clin Exp Allergy, 46(12), 1549-1563. https://doi.org/10.1111/cea.12793

Hui, K. P. Y., Cheung, M. C., Perera, R., Ng, K. C., Bui, C. H. T., Ho, J. C. W., Ng, M. M. T., Kuok, D. I. T., Shih, K. C., Tsao, S. W., Poon, L. L. M., Peiris, M., Nicholls, J. M., & Chan, M. C. W. (2020). Tropism, replication competence, and innate immune responses of the coronavirus SARS-CoV-2 in human respiratory tract and conjunctiva: an analysis in ex-vivo and in-vitro cultures. Lancet Respir Med, 8(7), 687-695. https://doi.org/10.1016/s2213-2600(20)30193-4

Ioannidis, I., McNally, B., Willette, M., Peeples, M. E., Chaussabel, D., Durbin, J. E., Ramilo, O., Mejias, A., & Flaño, E. (2012). Plasticity and Virus Specificity of the Airway Epithelial Cell Immune Response during Respiratory Virus Infection. Journal of Virology, 86(10), 5422-5436. https://doi.org/doi:10.1128/JVI.06757-11

Ilyushina, N. A., Dickensheets, H., & Donnelly, R. P. (2019). A comparison of interferon gene expression induced by influenza A virus infection of human airway epithelial cells from two different donors. Virus Res, 264, 1-7. https://doi.org/10.1016/j.virusres.2019.02.002

Ireson, N. J., Tait, J. S., MacGregor, G. A., & Baker, E. H. (2001). Comparison of nasal pH values in black and white individuals with normal and high blood pressure. Clin Sci (Lond), 100(3), 327-333.

Jason, Gao, X., Xue, Y., Scott, Kong, Y.-Y., & Brigid. (2011). Notch-Dependent Differentiation of Adult Airway Basal Stem Cells. Cell Stem Cell, 8(6), 639-648. https://doi.org/10.1016/j.stem.2011.04.003

Johnson, P. R., Spriggs, M. K., Olmsted, R. A., & Collins, P. L. (1987). The G glycoprotein of human respiratory syncytial viruses of subgroups A and B: extensive sequence divergence between antigenically related proteins. Proc Natl Acad Sci U S A, 84(16), 5625-5629. https://doi.org/10.1073/pnas.84.16.5625

Johnson, S. M., McNally, B. A., Ioannidis, I., Flano, E., Teng, M. N., Oomens, A. G., Walsh, E. E., & Peeples, M. E. (2015). Respiratory Syncytial Virus Uses CX3CR1 as a Receptor on Primary Human Airway Epithelial Cultures. PLoS Pathog, 11(12), e1005318. https://doi.org/10.1371/journal.ppat.1005318

Johnston, S. L., Goldblatt, D. L., Evans, S. E., Tuvim, M. J., & Dickey, B. F. (2021). Airway Epithelial Innate Immunity [Perspective]. Frontiers in Physiology, 12. https://doi.org/10.3389/fphys.2021.749077

Kaler, L., Iverson, E., Bader, S., Song, D., Scull, M. A., & Duncan, G. A. (2022). Influenza A virus diffusion through mucus gel networks. Communications Biology, 5(1), 249. https://doi.org/10.1038/s42003-022-03204-3

Kessie, D. K., Lodes, N., Oberwinkler, H., Goldman, W. E., Walles, T., Steinke, M., & Gross, R. (2021). Activity of Tracheal Cytotoxin of Bordetella pertussis in a Human Tracheobronchial 3D Tissue Model [Original Research]. Frontiers in Cellular and Infection Microbiology, 10. https://doi.org/10.3389/fcimb.2020.614994

Khan, N., Chen, X., & Geiger, J. D. (2020). Role of Endolysosomes in Severe Acute Respiratory Syndrome Coronavirus-2 Infection and Coronavirus Disease 2019 Pathogenesis: Implications for Potential Treatments [Hypothesis and Theory]. Frontiers in Pharmacology, 11. https://doi.org/10.3389/fphar.2020.595888

Kim, D. K., Cho, M. H., Hersh, C. P., Lomas, D. A., Miller, B. E., Kong, X., Bakke, P., Gulsvik, A., Agustí, A., Wouters, E., Celli, B., Coxson, H., Vestbo, J., MacNee, W., Yates, J. C., Rennard, S., Litonjua, A., Qiu, W., Beaty, T. H., . . . Silverman, E. K. (2012). Genome-wide association analysis of blood biomarkers in chronic obstructive pulmonary disease. Am J Respir Crit Care Med, 186(12), 1238-1247. https://doi.org/10.1164/rccm.201206-1013OC

Kirimanjeswara, G. S. (2005). Pertussis toxin inhibits neutrophil recruitment to delay antibody-mediated clearance of Bordetella pertussis. Journal of Clinical Investigation, 115(12), 3594-3601. https://doi.org/10.1172/jci24609

Kirkham, S., Sheehan, J. K., Knight, D., Richardson, P. S., & Thornton, D. J. (2002). Heterogeneity of airways mucus: variations in the amounts and glycoforms of the major oligomeric mucins MUC5AC and MUC5B. Biochem J, 361(Pt 3), 537-546. https://doi.org/10.1042/0264-6021:3610537

Knoops, K., Kikkert, M., Worm, S. H. E. V. D., Zevenhoven-Dobbe, J. C., Van Der Meer, Y., Koster, A. J., Mommaas, A. M., & Snijder, E. J. (2008). SARS-Coronavirus Replication Is Supported by a Reticulovesicular Network of Modified Endoplasmic Reticulum. PLoS Biology, 6(9), e226. https://doi.org/10.1371/journal.pbio.0060226

Koehler, C., Paulus, M., Ginzkey, C., Hackenberg, S., Scherzad, A., Ickrath, P., Hagen, R., & Kleinsasser, N. (2016). The Proinflammatory Potential of Nitrogen Dioxide and Its Influence on the House Dust Mite Allergen Der p 1. Int Arch Allergy Immunol, 171(1), 27-35. https://doi.org/10.1159/000450751

Kotob, S. I., Hausman, S. Z., & Burns, D. L. (1995). Localization of the promoter for the ptl genes of Bordetella pertussis, which encode proteins essential for secretion of pertussis toxin. Infect Immun, 63(8), 3227-3230. https://doi.org/10.1128/iai.63.8.3227-3230.1995

Krammer, F., Smith, G. J. D., Fouchier, R. A. M., Peiris, M., Kedzierska, K., Doherty, P. C., Palese, P., Shaw, M. L., Treanor, J., Webster, R. G., & García-Sastre, A. (2018). Influenza. Nature Reviews Disease Primers, 4(1), 3. https://doi.org/10.1038/s41572-018-0002-y

Krusat, T., & Streckert, H. J. (1997). Heparin-dependent attachment of respiratory syncytial virus (RSV) to host cells. Arch Virol, 142(6), 1247-1254. https://doi.org/10.1007/s007050050156

Krzyzaniak, M. A., Zumstein, M. T., Gerez, J. A., Picotti, P., & Helenius, A. (2013). Host cell entry of respiratory syncytial virus involves macropinocytosis followed by proteolytic activation of the F protein. PLoS Pathog, 9(4), e1003309. https://doi.org/10.1371/journal.ppat.1003309

Kuchipudi, S. V., Nelli, R. K., Gontu, A., Satyakumar, R., Surendran Nair, M., & Subbiah, M. (2021). Sialic Acid Receptors: The Key to Solving the Enigma of Zoonotic Virus Spillover. Viruses, 13(2), 262. https://doi.org/10.3390/v13020262

Kwong, J. C., Schwartz, K. L., Campitelli, M. A., Chung, H., Crowcroft, N. S., Karnauchow, T., Katz, K., Ko, D. T., McGeer, A. J., McNally, D., Richardson, D. C., Rosella, L. C., Simor, A., Smieja, M., Zahariadis, G., & Gubbay, J. B. (2018). Acute Myocardial Infarction after Laboratory-Confirmed Influenza Infection. N Engl J Med, 378(4), 345-353. https://doi.org/10.1056/NEJMoa1702090

Larrañaga, C. L., Ampuero, S. L., Luchsinger, V. F., Carrión, F. A., Aguilar, N. V., Morales, P. R., Palomino, M. A., Tapia, L. F., & Avendaño, L. F. (2009). Impaired immune response in severe human lower tract respiratory infection by respiratory syncytial virus. Pediatr Infect Dis J, 28(10), 867-873. https://doi.org/10.1097/INF.0b013e3181a3ea71

Laucho-Contreras, M. E., Polverino, F., Tesfaigzi, Y., Pilon, A., Celli, B. R., & Owen, C. A. (2016). Club Cell Protein 16 (CC16) Augmentation: A Potential Disease-modifying Approach for Chronic Obstructive Pulmonary Disease (COPD). Expert Opinion on Therapeutic Targets, 20(7), 869-883. https://doi.org/10.1517/14728222.2016.1139084

Lauenstein, L., Switalla, S., Prenzler, F., Seehase, S., Pfennig, O., Förster, C., Fieguth, H., Braun, A., & Sewald, K. (2014). Assessment of immunotoxicity induced by chemicals in human precision-cut lung slices (PCLS). Toxicology in Vitro, 28(4), 588-599. https://doi.org/https://doi.org/10.1016/j.tiv.2013.12.016

Le Sage, V., Nanni, A., Bhagwat, A., Snyder, D., Cooper, V., Lakdawala, S., & Lee, N. (2018). Non-Uniform and Non-Random Binding of Nucleoprotein to Influenza A and B Viral RNA. Viruses, 10(10), 522. https://doi.org/10.3390/v10100522

Lee, R. J., Xiong, G., Kofonow, J. M., Chen, B., Lysenko, A., Jiang, P., Abraham, V., Doghramji, L., Adappa, N. D., Palmer, J. N., Kennedy, D. W., Beauchamp, G. K., Doulias, P. T., Ischiropoulos, H., Kreindler, J. L., Reed, D. R., & Cohen, N. A. (2012). T2R38 taste receptor polymorphisms underlie susceptibility to upper respiratory infection. J Clin Invest, 122(11), 4145-4159. https://doi.org/10.1172/jci64240

Li, F. (2016). Structure, Function, and Evolution of Coronavirus Spike Proteins. Annual Review of Virology, 3(1), 237-261. https://doi.org/10.1146/annurev-virology-110615-042301

Li, W., Moore, M. J., Vasilieva, N., Sui, J., Wong, S. K., Berne, M. A., Somasundaran, M., Sullivan, J. L., Luzuriaga, K., Greenough, T. C., Choe, H., & Farzan, M. (2003). Angiotensin-converting enzyme 2 is a functional receptor for the SARS coronavirus. Nature, 426(6965), 450-454. https://doi.org/10.1038/nature02145

Li, W., Zhang, C., Sui, J., Kuhn, J. H., Moore, M. J., Luo, S., Wong, S. K., Huang, I. C., Xu, K., Vasilieva, N., Murakami, A., He, Y., Marasco, W. A., Guan, Y., Choe, H., &

Farzan, M. (2005). Receptor and viral determinants of SARS-coronavirus adaptation to human ACE2. Embo j, 24(8), 1634-1643. https://doi.org/10.1038/sj.emboj.7600640

Li, X. X., Peng, T., Gao, J., Feng, J. G., Wu, D. D., Yang, T., Zhong, L., Fu, W. P., & Sun, C. (2019). Allele-specific expression identified rs2509956 as a novel long-distance cis-regulatory SNP for SCGB1A1, an important gene for multiple pulmonary diseases. Am J Physiol Lung Cell Mol Physiol, 317(4), L456-l463. https://doi.org/10.1152/ajplung.00275.2018

Li, Y., & Tang, X. X. (2021). Abnormal Airway Mucus Secretion Induced by Virus Infection [Review]. Frontiers in Immunology, 12. https://doi.org/10.3389/fimmu.2021.701443

Liesman, R. M., Buchholz, U. J., Luongo, C. L., Yang, L., Proia, A. D., DeVincenzo, J. P., Collins, P. L., & Pickles, R. J. (2014). RSV-encoded NS2 promotes epithelial cell shedding and distal airway obstruction. The Journal of Clinical Investigation, 124(5), 2219-2233. https://doi.org/10.1172/JCI72948

Lillehoj, E. P., Kato, K., Lu, W., & Kim, K. C. (2013). Chapter Four - Cellular and Molecular Biology of Airway Mucins. In K. W. Jeon (Ed.), International Review of Cell and Molecular Biology (Vol. 303, pp. 139-202). Academic Press. https://doi.org/https://doi.org/10.1016/B978-0-12-407697-6.00004-0

Liu, G., Betts, C., Cunoosamy, D. M., Åberg, P. M., Hornberg, J. J., Sivars, K. B., & Cohen, T. S. (2019). Use of precision cut lung slices as a translational model for the study of lung biology. Respiratory Research, 20(1), 162. https://doi.org/10.1186/s12931-019-1131-x

Lodes, N., Seidensticker, K., Perniss, A., Nietzer, S., Oberwinkler, H., May, T., Walles, T., Hebestreit, H., Hackenberg, S., & Steinke, M. (2020). Investigation on Ciliary Functionality of Different Airway Epithelial Cell Lines in Three-Dimensional Cell Culture. Tissue Eng Part A, 26(7-8), 432-440. https://doi.org/10.1089/ten.TEA.2019.0188

Luengen, A. E., Cheremkhina, M., Gonzalez-Rubio, J., Weckauf, J., Kniebs, C., Uebner, H., Buhl, E. M., Taube, C., Cornelissen, C. G., Schmitz-Rode, T., Jockenhoevel, S., & Thiebes, A. L. (2022). Bone Marrow Derived Mesenchymal Stromal Cells Promote Vascularization and Ciliation in Airway Mucosa Tri-Culture

Models in Vitro [Original Research]. Frontiers in Bioengineering and Biotechnology, 10. https://doi.org/10.3389/fbioe.2022.872275

Mariano, G., Farthing, R. J., Lale-Farjat, S. L. M., & Bergeron, J. R. C. (2020). Structural Characterization of SARS-CoV-2: Where We Are, and Where We Need to Be [Review]. Frontiers in Molecular Biosciences, 7. https://doi.org/10.3389/fmolb.2020.605236

Maisonnasse, P., Guedj, J., Contreras, V., Behillil, S., Solas, C., Marlin, R., Naninck, T., Pizzorno, A., Lemaitre, J., Gonçalves, A., Kahlaoui, N., Terrier, O., Fang, R. H. T., Enouf, V., Dereuddre-Bosquet, N., Brisebarre, A., Touret, F., Chapon, C., Hoen, B., . . . Le Grand, R. (2020). Hydroxychloroquine use against SARS-CoV-2 infection in non-human primates. Nature, 585(7826), 584-587. https://doi.org/10.1038/s41586-020-2558-4

Mastrangelo, P., Chin, A. A., Tan, S., Jeon, A. H., Ackerley, C. A., Siu, K. K., Lee, J. E., & Hegele, R. G. (2021). Identification of RSV Fusion Protein Interaction Domains on the Virus Receptor, Nucleolin. Viruses, 13(2), 261. https://www.mdpi.com/1999-4915/13/2/261

Mata, M., Morcillo, E., Gimeno, C., & Cortijo, J. (2011). N-acetyl-L-cysteine (NAC) inhibit mucin synthesis and pro-inflammatory mediators in alveolar type II epithelial cells infected with influenza virus A and B and with respiratory syncytial virus (RSV). Biochem Pharmacol, 82(5), 548-555. https://doi.org/10.1016/j.bcp.2011.05.014

McConnochie, K. M., Hall, C. B., Walsh, E. E., & Roghmann, K. J. (1990). Variation in severity of respiratory syncytial virus infections with subtype. J Pediatr, 117(1 Pt 1), 52-62. https://doi.org/10.1016/s0022-3476(05)82443-6

McNamara, P. S., Flanagan, B. F., Selby, A. M., Hart, C. A., & Smyth, R. L. (2004). Pro- and anti-inflammatory responses in respiratory syncytial virus bronchiolitis. European Respiratory Journal, 23(1), 106-112. https://doi.org/10.1183/09031936.03.00048103

Min, K. A., Rosania, G. R., & Shin, M. C. (2016). Human Airway Primary Epithelial Cells Show Distinct Architectures on Membrane Supports Under Different Culture Conditions. Cell Biochem Biophys, 74(2), 191-203. https://doi.org/10.1007/s12013-016-0719-8

Miranda, I., Souza, A., Sousa, P., Ribeiro, J., Castanheira, E. M. S., Lima, R., & Minas, G. (2021). Properties and Applications of PDMS for Biomedical Engineering: A Review. Journal of Functional Biomaterials, 13(1), 2. https://doi.org/10.3390/jfb13010002

Mohammadi Farsani, T., Motevaseli, E., Neyazi, N., Khorramizadeh, M. R., Zafarvahedian, E., & Ghahremani, M. H. (2018). Effect of Passage Number and Culture Time on the Expression and Activity of Insulin-Degrading Enzyme in Caco-2 Cells. Iran Biomed J, 22(1), 70-75. https://doi.org/10.22034/ibj.22.1.70

Montoro, D. T., Haber, A. L., Biton, M., Vinarsky, V., Lin, B., Birket, S. E., Yuan, F., Chen, S., Leung, H. M., Villoria, J., Rogel, N., Burgin, G., Tsankov, A. M., Waghray, A., Slyper, M., Waldman, J., Nguyen, L., Dionne, D., Rozenblatt-Rosen, O., . . . Rajagopal, J. (2018). A revised airway epithelial hierarchy includes CFTR-expressing ionocytes. Nature, 560(7718), 319-324. https://doi.org/10.1038/s41586-018-0393-7

Mori, K., Sasamoto, T., Nakayama, T., Morichi, S., Kashiwagi, Y., Sawada, A., & Kawashima, H. (2022). Chemokine/Interleukin Imbalance Aggravates the Pathology of Respiratory Syncytial Virus Infection. Journal of Clinical Medicine, 11(20), 6042. https://doi.org/10.3390/jcm11206042

Mori, M., Mahoney, J. E., Stupnikov, M. R., Paez-Cortez, J. R., Szymaniak, A. D., Varelas, X., Herrick, D. B., Schwob, J., Zhang, H., & Cardoso, W. V. (2015). Notch3-Jagged signaling controls the pool of undifferentiated airway progenitors. Development, 142(2), 258-267. https://doi.org/10.1242/dev.116855

Morova, J., Osicka, R., Masin, J., & Sebo, P. (2008). RTX cytotoxins recognize β ₂ integrin receptors through N-linked oligosaccharides. Proceedings of the National Academy of Sciences, 105(14), 5355-5360. https://doi.org/10.1073/pnas.0711400105

Morse, S. I., & Morse, J. H. (1976). Isolation and properties of the leukocytosis- and lymphocytosis-promoting factor of Bordetella pertussis. Journal of Experimental Medicine, 143(6), 1483-1502. https://doi.org/10.1084/jem.143.6.1483

Naik, S., Larsen, S. B., Gomez, N. C., Alaverdyan, K., Sendoel, A., Yuan, S., Polak, L., Kulukian, A., Chai, S., & Fuchs, E. (2017). Inflammatory memory sensitizes skin

epithelial stem cells to tissue damage. Nature, 550(7677), 475-480. https://doi.org/10.1038/nature24271

Neuman, B. W. (2016). Bioinformatics and functional analyses of coronavirus nonstructural proteins involved in the formation of replicative organelles. Antiviral Res, 135, 97-107. https://doi.org/10.1016/j.antiviral.2016.10.005

Niessen, C. M. (2007). Tight Junctions/Adherens Junctions: Basic Structure and Function. Journal of Investigative Dermatology, 127(11), 2525-2532. https://doi.org/10.1038/sj.jid.5700865

Nicolas de Lamballerie, C., Pizzorno, A., Dubois, J., Julien, T., Padey, B., Bouveret, M., Traversier, A., Legras-Lachuer, C., Lina, B., Boivin, G., Terrier, O., & Rosa-Calatrava, M. (2019). Characterization of cellular transcriptomic signatures induced by different respiratory viruses in human reconstituted airway epithelia. Scientific Reports, 9(1), 11493. https://doi.org/10.1038/s41598-019-48013-7

Novakovic, B., & Stunnenberg, H. G. (2017). I Remember You: Epigenetic Priming in Epithelial Stem Cells. Immunity, 47(6), 1019-1021. https://doi.org/10.1016/j.immuni.2017.12.005

Odendall, C., Voak, A. A., & Kagan, J. C. (2017). Type III IFNs Are Commonly Induced by Bacteria-Sensing TLRs and Reinforce Epithelial Barriers during Infection. J Immunol, 199(9), 3270-3279. https://doi.org/10.4049/jimmunol.1700250

Okabayashi, T., Kojima, T., Masaki, T., Yokota, S., Imaizumi, T., Tsutsumi, H., Himi, T., Fujii, N., & Sawada, N. (2011). Type-III interferon, not type-I, is the predominant interferon induced by respiratory viruses in nasal epithelial cells. Virus Res, 160(1-2), 360-366. https://doi.org/10.1016/j.virusres.2011.07.011

O'Leary, C. E., Schneider, C., & Locksley, R. M. (2019). Tuft Cells-Systemically Dispersed Sensory Epithelia Integrating Immune and Neural Circuitry. Annu Rev Immunol, 37, 47-72. https://doi.org/10.1146/annurev-immunol-042718-041505

Pardo-Saganta, A., Brandon, Purushothama, Villoria, J., Saez, B., Mou, H., Zhao, R., & Rajagopal, J. (2015). Injury Induces Direct Lineage Segregation of Functionally Distinct Airway Basal Stem/Progenitor Cell Subpopulations. Cell Stem Cell, 16(2), 184-197. https://doi.org/10.1016/j.stem.2015.01.002

Pearson, R. D., Symes, P., Conboy, M., Weiss, A. A., & Hewlett, E. L. (1987). Inhibition of monocyte oxidative responses by Bordetella pertussis adenylate cyclase toxin. J Immunol, 139(8), 2749-2754.

Persson, B. D., Jaffe, A. B., Fearns, R., & Danahay, H. (2014). Respiratory syncytial virus can infect basal cells and alter human airway epithelial differentiation. PLOS ONE, 9(7), e102368. https://doi.org/10.1371/journal.pone.0102368

Pesci, A., Balbi, B., Majori, M., Cacciani, G., Bertacco, S., Alciato, P., & Donner, C. (1998). Inflammatory cells and mediators in bronchial lavage of patients with chronic obstructive pulmonary disease. European Respiratory Journal, 12(2), 380-386. https://doi.org/10.1183/09031936.98.12020380

Pinto, A. L., Rai, R. K., Brown, J. C., Griffin, P., Edgar, J. R., Shah, A., Singanayagam, A., Hogg, C., Barclay, W. S., Futter, C. E., & Burgoyne, T. (2022). Ultrastructural insight into SARS-CoV-2 entry and budding in human airway epithelium. Nat Commun, 13(1), 1609. https://doi.org/10.1038/s41467-022-29255-y

Pizzato, M., Baraldi, C., Boscato Sopetto, G., Finozzi, D., Gentile, C., Gentile, M. D., Marconi, R., Paladino, D., Raoss, A., Riedmiller, I., Ur Rehman, H., Santini, A., Succetti, V., & Volpini, L. (2022). SARS-CoV-2 and the Host Cell: A Tale of Interactions [Review]. Frontiers in Virology, 1. https://doi.org/10.3389/fviro.2021.815388

Pizzorno, A., Padey, B., Julien, T., Trouillet-Assant, S., Traversier, A., Errazuriz-Cerda, E., Fouret, J., Dubois, J., Gaymard, A., Lescure, F. X., Dulière, V., Brun, P., Constant, S., Poissy, J., Lina, B., Yazdanpanah, Y., Terrier, O., & Rosa-Calatrava, M. (2020). Characterization and Treatment of SARS-CoV-2 in Nasal and Bronchial Human Airway Epithelia. Cell Rep Med, 1(4), 100059. https://doi.org/10.1016/j.xcrm.2020.100059

Planas, D., Veyer, D., Baidaliuk, A., Staropoli, I., Guivel-Benhassine, F., Rajah, M. M., Planchais, C., Porrot, F., Robillard, N., Puech, J., Prot, M., Gallais, F., Gantner, P., Velay, A., Le Guen, J., Kassis-Chikhani, N., Edriss, D., Belec, L., Seve, A., . . . Schwartz, O. (2021). Reduced sensitivity of SARS-CoV-2 variant Delta to antibody neutralization. Nature, 596(7871), 276-280. https://doi.org/10.1038/s41586-021-03777-9

Poduri, R., Joshi, G., & Jagadeesh, G. (2020). Drugs targeting various stages of the SARS-CoV-2 life cycle: Exploring promising drugs for the treatment of Covid-19. Cellular Signalling, 74, 109721. https://doi.org/https://doi.org/10.1016/j.cellsig.2020.109721

Porotto, M., Ferren, M., Chen, Y.-W., Siu, Y., Makhsous, N., Rima, B., Briese, T., Greninger, A. L., Snoeck, H.-W., & Moscona, A. (2019). Authentic Modeling of Human Respiratory Virus Infection in Human Pluripotent Stem Cell-Derived Lung Organoids. mBio, 10(3), e00723-00719. https://doi.org/doi:10.1128/mBio.00723-19

Pringle, E. J., Richardson, H. B., Miller, D., Cornish, D. S., Devereux, G. S., Walsh, G. M., & Turner, S. W. (2012). Nasal and bronchial airway epithelial cell mediator release in children. Pediatric Pulmonology, 47(12), 1215-1225. https://doi.org/https://doi.org/10.1002/ppul.22672

Proença de Oliveira-Maul, J., Barbosa de Carvalho, H., Goto, D. M., Maia, R. M., Fló, C., Barnabé, V., Franco, D. R., Benabou, S., Perracini, M. R., Jacob-Filho, W., Saldiva, P. H. N., Lorenzi-Filho, G., Rubin, B. K., & Nakagawa, N. K. (2013). Aging, diabetes, and hypertension are associated with decreased nasal mucociliary clearance. Chest, 143(4), 1091-1097. https://doi.org/10.1378/chest.12-1183

Qian, Z., Travanty, E. A., Oko, L., Edeen, K., Berglund, A., Wang, J., Ito, Y., Holmes, K. V., & Mason, R. J. (2013). Innate immune response of human alveolar type II cells infected with severe acute respiratory syndrome-coronavirus. Am J Respir Cell Mol Biol, 48(6), 742-748. https://doi.org/10.1165/rcmb.2012-0339OC

Ravindra, N. G., Alfajaro, M. M., Gasque, V., Huston, N. C., Wan, H., Szigeti-Buck, K., Yasumoto, Y., Greaney, A. M., Habet, V., Chow, R. D., Chen, J. S., Wei, J., Filler, R. B., Wang, B., Wang, G., Niklason, L. E., Montgomery, R. R., Eisenbarth, S. C., Chen, S., . . . Wilen, C. B. (2021). Single-cell longitudinal analysis of SARS-CoV-2 infection in human airway epithelium identifies target cells, alterations in gene expression, and cell state changes. PLoS Biology, 19(3), e3001143. https://doi.org/10.1371/journal.pbio.3001143

Rayner, R. E., Makena, P., Prasad, G. L., & Cormet-Boyaka, E. (2019). Optimization of Normal Human Bronchial Epithelial (NHBE) Cell 3D Cultures for in vitro Lung Model Studies. Scientific Reports, 9(1), 500. https://doi.org/10.1038/s41598-018-36735-z

Reader, J. R., Tepper, J. S., Schelegle, E. S., Aldrich, M. C., Putney, L. F., Pfeiffer, J. W., & Hyde, D. M. (2003). Pathogenesis of mucous cell metaplasia in a murine asthma model. Am J Pathol, 162(6), 2069-2078. https://doi.org/10.1016/s0002-9440(10)64338-6

Reynolds, S. D., & Malkinson, A. M. (2010). Clara cell: progenitor for the bronchiolar epithelium. Int J Biochem Cell Biol, 42(1), 1-4. https://doi.org/10.1016/j.biocel.2009.09.002

Roberts, N., Al Mubarak, R., Francisco, D., Kraft, M., & Chu, H. W. (2018). Comparison of paired human nasal and bronchial airway epithelial cell responses to rhinovirus infection and IL-13 treatment. Clinical and Translational Medicine, 7(1), e13. https://doi.org/https://doi.org/10.1186/s40169-018-0189-2

Rock, J. R., Onaitis, M. W., Rawlins, E. L., Lu, Y., Clark, C. P., Xue, Y., Randell, S. H., & Hogan, B. L. (2009). Basal cells as stem cells of the mouse trachea and human airway epithelium. Proc Natl Acad Sci U S A, 106(31), 12771-12775. https://doi.org/10.1073/pnas.0906850106

Roy, M. G., Livraghi-Butrico, A., Fletcher, A. A., McElwee, M. M., Evans, S. E., Boerner, R. M., Alexander, S. N., Bellinghausen, L. K., Song, A. S., Petrova, Y. M., Tuvim, M. J., Adachi, R., Romo, I., Bordt, A. S., Bowden, M. G., Sisson, J. H., Woodruff, P. G., Thornton, D. J., Rousseau, K., . . . Evans, C. M. (2014). Muc5b is required for airway defence. Nature, 505(7483), 412-416. https://doi.org/10.1038/nature12807

Runft, S., Färber, I., Krüger, J., Krüger, N., Armando, F., Rocha, C., Pöhlmann, S., Burigk, L., Leitzen, E., Ciurkiewicz, M., Braun, A., Schneider, D., Baumgärtner, L., Freisleben, B., & Baumgärtner, W. (2022). Alternatives to animal models and their application in the discovery of species susceptibility to SARS-CoV-2 and other respiratory infectious pathogens: A review. Vet Pathol, 59(4), 565-577. https://doi.org/10.1177/03009858211073678

Ruiz García, S., Deprez, M., Lebrigand, K., Cavard, A., Paquet, A., Arguel, M.-J., Magnone, V., Truchi, M., Caballero, I., Leroy, S., Marquette, C.-H., Marcet, B., Barbry, P., & Zaragosi, L.-E. (2019). Novel dynamics of human mucociliary differentiation

revealed by single-cell RNA sequencing of nasal epithelial cultures. Development, 146(20), dev.177428. https://doi.org/10.1242/dev.177428

Ruysseveldt, E., Martens, K., & Steelant, B. (2021). Airway Basal Cells, Protectors of Epithelial Walls in Health and Respiratory Diseases [Review]. Frontiers in Allergy, 2. https://doi.org/10.3389/falgy.2021.787128

Rydell-Törmänen, K., & Johnson, J. R. (2019). The Applicability of Mouse Models to the Study of Human Disease. Methods Mol Biol, 1940, 3-22. https://doi.org/10.1007/978-1-4939-9086-3_1

Sakamoto, H., Bellalou, J., Sebo, P., & Ladant, D. (1992). Bordetella pertussis adenylate cyclase toxin. Structural and functional independence of the catalytic and hemolytic activities. J Biol Chem, 267(19), 13598-13602.

San-Juan-Vergara, H., Sampayo-Escobar, V., Reyes, N., Cha, B., Pacheco-Lugo, L., Wong, T., Peeples, M. E., Collins, P. L., Castaño, M. E., & Mohapatra, S. S. (2012). Cholesterol-rich microdomains as docking platforms for respiratory syncytial virus in normal human bronchial epithelial cells. J Virol, 86(3), 1832-1843. https://doi.org/10.1128/jvi.06274-11

Satir, P., & Christensen, S. T. (2007). Overview of structure and function of mammalian cilia. Annual review of physiology, 69, 377–400. https://doi.org/10.1146/annurev.physiol.69.040705.141236

Schanz, J., Pusch, J., Hansmann, J., & Walles, H. (2010). RETRACTED: Vascularised human tissue models: A new approach for the refinement of biomedical research. Journal of Biotechnology, 148(1), 56-63. https://doi.org/https://doi.org/10.1016/j.jbiotec.2010.03.015

Schildgen, V., Lüsebrink, J., Ditt, V., Tillmann, R., Simon, A., Müller, A., & Schildgen, O. (2010). Human cells support respiratory syncytial virus and human metapneumovirus replication. J Virol Methods, 163(1), 74-81. https://doi.org/10.1016/j.jviromet.2009.08.024

Schmitz, G., & Müller, G. (1991). Structure and function of lamellar bodies, lipid-protein complexes involved in storage and secretion of cellular lipids. J Lipid Res, 32(10), 1539-1570.

Schürch, S., Gehr, P., Im Hof, V., Geiser, M., & Green, F. (1990). Surfactant displaces particles toward the epithelium in airways and alveoli. Respiration physiology, 80(1), 17–32. https://doi.org/10.1016/0034-5687(90)90003-h

Schweitzer, K. S., Crue, T., Nall, J. M., Foster, D., Sajuthi, S., Correll, K. A., Nakamura, M., Everman, J. L., Downey, G. P., Seibold, M. A., Bridges, J. P., Serban, K. A., Chu, H. W., & Petrache, I. (2021). Influenza virus infection increases ACE2 expression and shedding in human small airway epithelial cells. Eur Respir J, 58(1). https://doi.org/10.1183/13993003.03988-2020

Sellers, S. A., Hagan, R. S., Hayden, F. G., & Fischer, W. A., 2nd. (2017). The hidden burden of influenza: A review of the extra-pulmonary complications of influenza infection. Influenza Other Respir Viruses, 11(5), 372-393. https://doi.org/10.1111/irv.12470

Sengupta, A., Roldan, N., Kiener, M., Froment, L., Raggi, G., Imler, T., de Maddalena, L., Rapet, A., May, T., Carius, P., Schneider-Daum, N., Lehr, C. M., Kruithof-de Julio, M., Geiser, T., Marti, T. M., Stucki, J. D., Hobi, N., & Guenat, O. T. (2022). A New Immortalized Human Alveolar Epithelial Cell Model to Study Lung Injury and Toxicity on a Breathing Lung-On-Chip System. Front Toxicol, 4, 840606. https://doi.org/10.3389/ftox.2022.840606

Sheridan, S. L., Ware, R. S., Grimwood, K., & Lambert, S. B. (2012). Number and order of whole cell pertussis vaccines in infancy and disease protection. Jama, 308(5), 454-456. https://doi.org/10.1001/jama.2012.6364

Shi, T., McAllister, D. A., O'Brien, K. L., Simoes, E. A. F., Madhi, S. A., Gessner, B. D., Polack, F. P., Balsells, E., Acacio, S., Aguayo, C., Alassani, I., Ali, A., Antonio, M., Awasthi, S., Awori, J. O., Azziz-Baumgartner, E., Baggett, H. C., Baillie, V. L., Balmaseda, A., . . . Nair, H. (2017). Global, regional, and national disease burden estimates of acute lower respiratory infections due to respiratory syncytial virus in young children in 2015: a systematic review and modelling study. The Lancet, 390(10098), 946-958. https://doi.org/10.1016/s0140-6736(17)30938-8

Sivarajan, R., Kessie, D. K., Oberwinkler, H., Pallmann, N., Walles, T., Scherzad, A., Hackenberg, S., & Steinke, M. (2021). Susceptibility of Human Airway Tissue Models Derived From Different Anatomical Sites to Bordetella pertussis and Its Virulence

Factor Adenylate Cyclase Toxin [Original Research]. Frontiers in Cellular and Infection Microbiology, 11. https://doi.org/10.3389/fcimb.2021.797491

Slepushkin, V. A., Staber, P. D., Wang, G., McCray, P. B., & Davidson, B. L. (2001). Infection of Human Airway Epithelia with H1N1, H2N2, and H3N2 Influenza A Virus Strains. Molecular Therapy, 3(3), 395-402. https://doi.org/10.1006/mthe.2001.0277

Smith, C. M., Do Hyang Lee, D., Kulkarni, H., Radhakrishnan, P., Hirst, R., Easton, A., & O'Callaghan, C. (2019). Influenza virus infection of well-differentiated human airway epithelial cells by infectious aerosols: insights into the earliest stages of infection. F1000Research, 8, 337. https://doi.org/10.12688/f1000research.18513.1

Stein, P. E., Boodhoo, A., Armstrong, G. D., Cockle, S. A., Klein, M. H., & Read, R. J. (1994). The crystal structure of pertussis toxin. Structure, 2(1), 45-57. https://doi.org/10.1016/s0969-2126(00)00007-1

Steinke, M., Gross, R., Walles, H., Gangnus, R., Schütze, K., & Walles, T. (2014). An engineered 3D human airway mucosa model based on an SIS scaffold. Biomaterials, 35(26), 7355-7362. https://doi.org/https://doi.org/10.1016/j.biomaterials.2014.05.031

Stewart, C. E., Torr, E. E., Mohd Jamili, N. H., Bosquillon, C., & Sayers, I. (2012). Evaluation of differentiated human bronchial epithelial cell culture systems for asthma research. J Allergy (Cairo), 2012, 943982. https://doi.org/10.1155/2012/943982

Stibitz, S., & Yang, M. S. (1991). Subcellular localization and immunological detection of proteins encoded by the vir locus of Bordetella pertussis. J Bacteriol, 173(14), 4288-4296. https://doi.org/10.1128/jb.173.14.4288-4296.1991

Tamerius, J., Nelson, M. I., Zhou, S. Z., Viboud, C., Miller, M. A., & Alonso, W. J. (2011). Global influenza seasonality: reconciling patterns across temperate and tropical regions. Environ Health Perspect, 119(4), 439-445. https://doi.org/10.1289/ehp.1002383

Tan, J., Guo, Q., Tian, L., Pei, Z., Li, D., Wu, M., Zhang, J., & Gao, X. (2023). Biomimetic lung-on-a-chip to model virus infection and drug evaluation. European Journal of Pharmaceutical Sciences, 180, 106329. https://doi.org/https://doi.org/10.1016/j.ejps.2022.106329

Tan, K. S., Yan, Y., Koh, W. L. H., Li, L., Choi, H., Tran, T., Sugrue, R., Wang, D. Y., & Chow, V. T. (2018). Comparative Transcriptomic and Metagenomic Analyses of Influenza Virus-Infected Nasal Epithelial Cells From Multiple Individuals Reveal Specific Nasal-Initiated Signatures [Original Research]. Frontiers in Microbiology, 9. https://doi.org/10.3389/fmicb.2018.02685

Taubenberger, J. K., & Morens, D. M. (2008). The pathology of influenza virus infections. Annu Rev Pathol, 3, 499-522. https://doi.org/10.1146/annurev.pathmechdis.3.121806.154316

Taylor, C. E., Morrow, S., Scott, M., Young, B., & Toms, G. L. (1989). Comparative virulence of respiratory syncytial virus subgroups A and B. Lancet, 1(8641), 777-778. https://doi.org/10.1016/s0140-6736(89)92592-0

Tayyari, F., Marchant, D., Moraes, T. J., Duan, W., Mastrangelo, P., & Hegele, R. G. (2011). Identification of nucleolin as a cellular receptor for human respiratory syncytial virus. Nat Med, 17(9), 1132-1135. https://doi.org/10.1038/nm.2444

Thavagnanam, S., Parker, J. C., McBrien, M. E., Skibinski, G., Shields, M. D., & Heaney, L. G. (2014). Nasal Epithelial Cells Can Act as a Physiological Surrogate for Paediatric Asthma Studies. PLOS ONE, 9(1), e85802. https://doi.org/10.1371/journal.pone.0085802

Thompson, C. I., Barclay, W. S., Zambon, M. C., & Pickles, R. J. (2006). Infection of human airway epithelium by human and avian strains of influenza a virus. J Virol, 80(16), 8060-8068. https://doi.org/10.1128/jvi.00384-06

Thornton, D. J., Gray, T., Nettesheim, P., Howard, M., Koo, J. S., & Sheehan, J. K. (2000). Characterization of mucins from cultured normal human tracheobronchial epithelial cells. Am J Physiol Lung Cell Mol Physiol, 278(6), L1118-1128. https://doi.org/10.1152/ajplung.2000.278.6.L1118

Tran, E., Shi, T., Li, X., Chowdhury, A. Y., Jiang, D., Liu, Y., Wang, H., Yan, C., Wallace, W. D., Lu, R., Ryan, A. L., Marconett, C. N., Zhou, B., Borok, Z., & Offringa, I. A. (2022). Development of human alveolar epithelial cell models to study distal lung biology and disease. iScience, 25(2), 103780. https://doi.org/https://doi.org/10.1016/j.isci.2022.103780

Travaglini, K. J., Nabhan, A. N., Penland, L., Sinha, R., Gillich, A., Sit, R. V., Chang, S., Conley, S. D., Mori, Y., Seita, J., Berry, G. J., Shrager, J. B., Metzger, R. J., Kuo, C. S., Neff, N., Weissman, I. L., Quake, S. R., & Krasnow, M. A. (2020). A molecular cell atlas of the human lung from single-cell RNA sequencing. Nature, 587(7835), 619-625. https://doi.org/10.1038/s41586-020-2922-4

Tyner, J. W., Kim, E. Y., Ide, K., Pelletier, M. R., Roswit, W. T., Morton, J. D., Battaile, J. T., Patel, A. C., Patterson, G. A., Castro, M., Spoor, M. S., You, Y., Brody, S. L., & Holtzman, M. J. (2006). Blocking airway mucous cell metaplasia by inhibiting EGFR antiapoptosis and IL-13 transdifferentiation signals. J Clin Invest, 116(2), 309-321. https://doi.org/10.1172/jci25167

Utley, T. J., Ducharme, N. A., Varthakavi, V., Shepherd, B. E., Santangelo, P. J., Lindquist, M. E., Goldenring, J. R., & Crowe, J. E., Jr. (2008). Respiratory syncytial virus uses a Vps4-independent budding mechanism controlled by Rab11-FIP2. Proc Natl Acad Sci U S A, 105(29), 10209-10214. https://doi.org/10.1073/pnas.0712144105

Villenave, R., Thavagnanam, S., Sarlang, S., Parker, J., Douglas, I., Skibinski, G., Heaney, L. G., McKaigue, J. P., Coyle, P. V., Shields, M. D., & Power, U. F. (2012). In vitro modeling of respiratory syncytial virus infection of pediatric bronchial epithelium, the primary target of infection in vivo. Proc Natl Acad Sci U S A, 109(13), 5040-5045. https://doi.org/10.1073/pnas.1110203109

V'kovski, P., Kratzel, A., Steiner, S., Stalder, H., & Thiel, V. (2021). Coronavirus biology and replication: implications for SARS-CoV-2. Nature Reviews Microbiology, 19(3), 155-170. https://doi.org/10.1038/s41579-020-00468-6

Vahey, M. D., & Fletcher, D. A. (2019). Influenza A virus surface proteins are organized to help penetrate host mucus. Elife, 8. https://doi.org/10.7554/eLife.43764

Van Itallie, C. M., & Anderson, J. M. (2006). Claudins and epithelial paracellular transport. Annu Rev Physiol, 68, 403-429. https://doi.org/10.1146/annurev.physiol.68.040104.131404

Varki, A. (2008). Sialic acids in human health and disease. Trends in Molecular Medicine, 14(8), 351-360. https://doi.org/10.1016/j.molmed.2008.06.002

Vaughan, M. B., Ramirez, R. D., Wright, W. E., Minna, J. D., & Shay, J. W. (2006). A three-dimensional model of differentiation of immortalized human bronchial epithelial cells. Differentiation, 74(4), 141-148. https://doi.org/10.1111/j.1432-0436.2006.00069.x

Vázquez, Y., González, L., Noguera, L., González, P. A., Riedel, C. A., Bertrand, P., & Bueno, S. M. (2019). Cytokines in the Respiratory Airway as Biomarkers of Severity and Prognosis for Respiratory Syncytial Virus Infection: An Update [Review]. Frontiers in Immunology, 10. https://doi.org/10.3389/fimmu.2019.01154

Veale, D., Rodgers, A. D., Griffiths, C. J., Ashcroft, T., & Gibson, G. J. (1993). Variability in ciliary beat frequency in normal subjects and in patients with bronchiectasis. Thorax, 48(10), 1018-1020. https://doi.org/10.1136/thx.48.10.1018

Villenave, R., Thavagnanam, S., Sarlang, S., Parker, J., Douglas, I., Skibinski, G., Heaney, L. G., McKaigue, J. P., Coyle, P. V., Shields, M. D., & Power, U. F. (2012). In vitro modeling of respiratory syncytial virus infection of pediatric bronchial epithelium, the primary target of infection in vivo. Proc Natl Acad Sci U S A, 109(13), 5040-5045. https://doi.org/10.1073/pnas.1110203109

Wallace, L. E., Liu, M., van Kuppeveld, F. J. M., de Vries, E., & de Haan, C. A. M. (2021). Respiratory mucus as a virus-host range determinant. Trends Microbiol, 29(11), 983-992. https://doi.org/10.1016/j.tim.2021.03.014

Walther, T., Karamanska, R., Chan, R. W. Y., Chan, M. C. W., Jia, N., Air, G., Hopton, C., Wong, M. P., Dell, A., Malik Peiris, J. S., Haslam, S. M., & Nicholls, J. M. (2013). Glycomic Analysis of Human Respiratory Tract Tissues and Correlation with Influenza Virus Infection. PLoS Pathogens, 9(3), e1003223. https://doi.org/10.1371/journal.ppat.1003223

Wang, D., Hu, B., Hu, C., Zhu, F., Liu, X., Zhang, J., Wang, B., Xiang, H., Cheng, Z., Xiong, Y., Zhao, Y., Li, Y., Wang, X., & Peng, Z. (2020). Clinical Characteristics of 138 Hospitalized Patients With 2019 Novel Coronavirus–Infected Pneumonia in Wuhan, China. Jama, 323(11), 1061. https://doi.org/10.1001/jama.2020.1585

Wang, S. Z., Rosenberger, C. L., Bao, Y. X., Stark, J. M., & Harrod, K. S. (2003). Clara cell secretory protein modulates lung inflammatory and immune responses to

respiratory syncytial virus infection. Journal of immunology (Baltimore, Md. : 1950), 171(2), 1051–1060. https://doi.org/10.4049/jimmunol.171.2.1051

Wark, P. A., Grissell, T., Davies, B., See, H., & Gibson, P. G. (2009). Diversity in the bronchial epithelial cell response to infection with different rhinovirus strains. Respirology, 14(2), 180-186. https://doi.org/10.1111/j.1440-1843.2009.01480.x

Weigel, T., Malkmus, C., Weigel, V., Wußmann, M., Berger, C., Brennecke, J., Groeber-Becker, F., & Hansmann, J. (2022). Fully Synthetic 3D Fibrous Scaffolds for Stromal Tissues—Replacement of Animal-Derived Scaffold Materials Demonstrated by Multilayered Skin. Advanced Materials, 34(10), 2106780. https://doi.org/https://doi.org/10.1002/adma.202106780

Weiss, A. A., & Hewlett, E. L. (1986). Virulence factors of Bordetella pertussis. Annu Rev Microbiol, 40, 661-686. https://doi.org/10.1146/annurev.mi.40.100186.003305

Wibmer, C. K., Ayres, F., Hermanus, T., Madzivhandila, M., Kgagudi, P., Oosthuysen, B., Lambson, B. E., De Oliveira, T., Vermeulen, M., Van Der Berg, K., Rossouw, T., Boswell, M., Ueckermann, V., Meiring, S., Von Gottberg, A., Cohen, C., Morris, L., Bhiman, J. N., & Moore, P. L. (2021). SARS-CoV-2 501Y.V2 escapes neutralization by South African COVID-19 donor plasma. Nature Medicine, 27(4), 622-625. https://doi.org/10.1038/s41591-021-01285-x

Widdicombe J. H. (2019). Early studies on the surface epithelium of mammalian airways. American journal of physiology. Lung cellular and molecular physiology, 317(4), L486–L495. https://doi.org/10.1152/ajplung.00240.2019

Wolff, J., Cook, G. H., Goldhammer, A. R., & Berkowitz, S. A. (1980). Calmodulin activates prokaryotic adenylate cyclase. Proceedings of the National Academy of Sciences, 77(7), 3841-3844. https://doi.org/10.1073/pnas.77.7.3841

Woodworth, B. A., Smythe, N., Spicer, S. S., Schulte, B. A., & Schlosser, R. J. (2005). Presence of surfactant lamellar bodies in normal and diseased sinus mucosa. ORL J Otorhinolaryngol Relat Spec, 67(4), 199-202. https://doi.org/10.1159/000087093

Wright, P. F., Ikizler, M. R., Gonzales, R. A., Carroll, K. N., Johnson, J. E., & Werkhaven, J. A. (2005). Growth of respiratory syncytial virus in primary epithelial cells

from the human respiratory tract. Journal of virology, 79(13), 8651–8654. https://doi.org/10.1128/JVI.79.13.8651-8654.2005

Wu, A., Mihaylova, V. T., Landry, M. L., & Foxman, E. F. (2020). Interference between rhinovirus and influenza A virus: a clinical data analysis and experimental infection study. The Lancet Microbe, 1(6), e254-e262. https://doi.org/10.1016/s2666-5247(20)30114-2

Wu, W., Booth, J. L., Duggan, E. S., Wu, S., Patel, K. B., Coggeshall, K. M., & Metcalf, J. P. (2010). Innate immune response to H3N2 and H1N1 influenza virus infection in a human lung organ culture model. Virology, 396(2), 178-188. https://doi.org/10.1016/j.virol.2009.10.016

Yang, J., Liu, S., Du, L., & Jiang, S. (2016). A new role of neuraminidase (NA) in the influenza virus life cycle: implication for developing NA inhibitors with novel mechanism of action. Rev Med Virol, 26(4), 242-250. https://doi.org/10.1002/rmv.1879

Yang, J.-W., Shen, Y.-C., Lin, K.-C., Cheng, S.-J., Chen, S.-L., Chen, C.-Y., Kumar, P. V., Lin, S.-F., Lu, H.-E., & Chen, G.-Y. (2020). Organ-on-a-Chip: Opportunities for Assessing the Toxicity of Particulate Matter [Review]. Frontiers in Bioengineering and Biotechnology, 8. https://doi.org/10.3389/fbioe.2020.00519

Yao, L., Korteweg, C., Hsueh, W., & Gu, J. (2008). Avian influenza receptor expression in H5N1-infected and noninfected human tissues. Faseb j, 22(3), 733-740. https://doi.org/10.1096/fj.06-7880com

Youil, R., Su, Q., Toner, T. J., Szymkowiak, C., Kwan, W. S., Rubin, B., Petrukhin, L., Kiseleva, I., Shaw, A. R., & DiStefano, D. (2004). Comparative study of influenza virus replication in Vero and MDCK cell lines. Journal of Virological Methods, 120(1), 23-31. https://doi.org/https://doi.org/10.1016/j.jviromet.2004.03.011

Zarkoob, H., Allué-Guardia, A., Chen, Y. C., Garcia-Vilanova, A., Jung, O., Coon, S., Song, M. J., Park, J. G., Oladunni, F., Miller, J., Tung, Y. T., Kosik, I., Schultz, D., Iben, J., Li, T., Fu, J., Porter, F. D., Yewdell, J., Martinez-Sobrido, L., . . . Lee, E. M. (2022). Modeling SARS-CoV-2 and influenza infections and antiviral treatments in human lung epithelial tissue equivalents. Commun Biol, 5(1), 810. https://doi.org/10.1038/s42003-022-03753-7

Zhang, L., Peeples, M. E., Boucher, R. C., Collins, P. L., & Pickles, R. J. (2002). Respiratory syncytial virus infection of human airway epithelial cells is polarized, specific to ciliated cells, and without obvious cytopathology. J Virol, 76(11), 5654-5666. https://doi.org/10.1128/jvi.76.11.5654-5666.2002

Zhang, X., Goel, T., Goodfield, L. L., Muse, S. J., & Harvill, E. T. (2011). Decreased leukocyte accumulation and delayed Bordetella pertussis clearance in IL-6-/- mice. J Immunol, 186(8), 4895-4904. https://doi.org/10.4049/jimmunol.1000594

Zhao, J., Zhou, H., Huang, W., Zhou, J., Qiu, M., Deng, Z., Chen, L., Weng, Y., Cai, L., Gu, Y., Zheng, Q., Chen, Q., Hou, X., Wang, L., Shen, L., & Yang, Z. (2020). Cell morphological analysis of SARS-CoV-2 infection by transmission electron microscopy. J Thorac Dis, 12(8), 4368-4373. https://doi.org/10.21037/jtd-20-1368

Zhou, J., Li, C., Sachs, N., Chiu, M. C., Wong, B. H.-Y., Chu, H., Poon, V. K.-M., Wang, D., Zhao, X., Wen, L., Song, W., Yuan, S., Wong, K. K.-Y., Chan, J. F.-W., To, K. K.-W., Chen, H., Clevers, H., & Yuen, K.-Y. (2018). Differentiated human airway organoids to assess infectivity of emerging influenza virus. Proceedings of the National Academy of Sciences, 115(26), 6822-6827. https://doi.org/10.1073/pnas.1806308115

Zimniak, M., Kirschner, L., Hilpert, H., Geiger, N., Danov, O., Oberwinkler, H., Steinke, M., Sewald, K., Seibel, J., & Bodem, J. (2021). The serotonin reuptake inhibitor Fluoxetine inhibits SARS-CoV-2 in human lung tissue. Scientific Reports, 11(1), 5890. https://doi.org/10.1038/s41598-021-85049-0

Zheng, D., Limmon, G. V., Yin, L., Leung, N. H. N., Yu, H., Chow, V. T. K., & Chen, J. (2012). Regeneration of Alveolar Type I and II Cells from Scgb1a1-Expressing Cells following Severe Pulmonary Damage Induced by Bleomycin and Influenza. PLOS ONE, 7(10), e48451. https://doi.org/10.1371/journal.pone.0048451

Zhu, N., Wang, W., Liu, Z., Liang, C., Wang, W., Ye, F., Huang, B., Zhao, L., Wang, H., Zhou, W., Deng, Y., Mao, L., Su, C., Qiang, G., Jiang, T., Zhao, J., Wu, G., Song, J., & Tan, W. (2020). Morphogenesis and cytopathic effect of SARS-CoV-2 infection in human airway epithelial cells. Nature Communications, 11(1). https://doi.org/10.1038/s41467-020-17796-z

11. Acknowledgement

I would like to express my gratitude to all the dear people who have supported me, or simply been there and believed in me, for without you, this wouldn't be possible.

I would like to start with my PhD supervisor Dr. Maria Steinke: Thank you for your support and mentoring during the past years, patience in explaining concepts, helping with the writing, quick feedback, for the days spent doing TEM analyses, help with official documents, and for all those days you took us out!

I would like to thank Prof. Dr. Jochen Bodem: For accepting me as your PhD student and letting me join your team during corona regulations, for the active discussions, explanations, all times you took us out and the fun-filled canoeing.

Thanks to Prof. Dr. Roy Gross for the motivation and kind words!

Thank you, Prof. Dr. Sibylle Schneider-Schaulies for the support and for sharing relevant research articles.

I thank Prof. Dr. David Stegner for agreeing to be the Chairperson for my thesis.

I would like to thank Dr. Joachim Nickel: for being so welcoming since we first met, for all the insights during team meetings and fun conversations.

Many thanks to Prof. Dr. Thomas Rudel with the guidance in the GRK-2157 3D infect program. I also thank Meike Scheuring for her consistent support during this time.

I would like to thank Prof. Dr. Christian Stigloher for helping me analyse the TEM results effectively. Special thanks to Daniela Bunsen and Claudia Gehrig-Höhn for their great smiling attitude and support.

I would like to thank all my collaborators Prof. Dr. Stephan Hackenberg, Dr. Totta Ehret Kasemo, Dr. Agmal Scherzad, Dr. Danjouma Cheufou, Prof. Dr. Thorsten Walles, Dr. Ali Akil, Prof. Dr. Stephan Fischer, Prof. Dr. Florian Erhard, Kevin Berg, Dr. Emmanuel Saliba, Dr. Fabian Imdahl, Oliver Dietrich, Dr. Tom Gräfenhan, and the members of the Single-Cell Center, Würzburg.

I would like to thank the members of the Chair of Tissue Engineering and Regenerative Medicine, especially Renate, Tom, Consti, Jesús, Ives and Dr. Gudrun Dandekar for

the active discussions. I would also like to specially thank Anna Kristina. I also thank the entire GSLS team, Würzburg for your patience, and constant support.

I would also like to thank my teachers, Dr. Geetha Nagaraja, Dr. H. S. Aparna, Dr. K. Ramachandra Kini, Mrs. Asha Anto, Mr. Jayan Alexander and Dr. Sanjay Pal. I would like to also thank Dr. Balaji Sinhadri for your support!

I want to thank my friends, who have become my family in the past three years. Thank you, Roksaneh, for offering me a place to stay during my initial days, and the love you have shown me. David and Jihyoung, you made my life less miserable away from home, thank you! Heike, your warm hugs, support, and care have meant so much to me. Sooraj, thank you for the excellent photographs, for being my travel buddy, and for your technical and emotional support. Thank you, Jeanne, your smile gave me the power I needed some days. Christina, thank you for the support, kindness, and motivation. Philipp, I will always cherish the memories of our fun-filled moments, sports activities, and translating important information for us. Thank you, Niklas, for the help and support and with proofreading my abstract! Eva, Valeria, Nina, Viktoria, Helena, Fizzah and Uddhav, thank you for everything!

I would like to thank my dear friends Norin, Devika, Anjaly, Aswathy, Parvathy, Noureen, Febin, Sajin, Vineeth, and Prem. I want you to know that I am here for you just as you have always been there for me.

Thank you, Dominik, your encouragement, help, and love, have been invaluable, and I couldn't have made it through these last steps without you by my side!

Lastly, I extend my heartfelt gratitude to my family who have been a constant source of love, patience, support, and belief in me. My mother Suseela Devi, for being the guiding light in my life and for shaping me into the person I am today along with my father Sivarajan, I deeply appreciate your tireless efforts to provide me with the best education possible. Every sacrifice you've both made will always be cherished; my dear sister, Sinu, you have stood by my side, offering solace and reassurance. You bring warmth to my soul and a sense of belonging, thank you for being my saviour! My brother-in-law, Rahulan, for being a great brother and being my main support through these years; my nephew, Dhyan, and niece, Dhyanvi, your love inspires me to be the best aunt and find joy in the simplest of things; my uncle, Sunil, for a colourful childhood; Subin, Saran, and Sandra, for being the best cousins!

12. Contributions

Virology: Heike Oberwinkler generated the RSV and IAV stocks used for the experiments and immunofluorescence stainings for SARS-CoV-2. SARS-CoV-2 stocks were maintained, and titer checked by Dr. Eva Maria Koening, Nina Geiger and Valeria Roll (AG Bodem, Institute of Virology and Immunobiology, Würzburg).

Transmission electron microscopy: The fixed samples were processed at the Imaging Core Facility of the Biocenter - Prof. Dr. Christian Stigloher's lab, University of Würzburg, by Daniela Bunsen and Claudia Gehrig-Höhn where they dehydrated and embedded the samples in Epon812 and made semi and ultrathin sections.

scRNA-seq for hNM: Dr. Fabian Imdahl (working group of Dr. Antoine-Emmanuel Saliba, Helmholtz Institute for RNA-based Infection, Würzburg, Germany) did the sample processing and sequencing.

scRNA-seq for hTM (Single-cell seed grant): sample processing and sequencing Mélanie Villard and Dr. Fabian Imdahl and the initial data processing by Dr. Panagiota Arampatzi, and Dr. Mugdha Srivastava (AG Gräfenhan, Single-cell center, Würzburg).

Bioinformatics: Prof. Dr. Florian Erhard and Kevin Berg, MSc (AG Erhard, Institute of Virology and Immunobiology, Würzburg) performed the final bioinformatical data clustering and processing.

13. List of publications

Sivarajan, R., Oberwinkler, H., Roll, V., Maria-König, E., Steinke, M., Bodem, J. (2022) A defined mixture with 30% anthocyanins sourced from bilberry and black currant inhibits the Measles virus and various Herpes viruses. BMC Complement Med Ther 22, 181., doi.org/10.1186/s12906-022-03661-7.

Sivarajan, R., Kessie, D. K., Oberwinkler, H., Pallmann, N., Walles, T., Scherzad, A., Hackenberg, S., and Steinke, M. (2021). Susceptibility of Human Airway Tissue Models Derived from Different Anatomical Sites to *Bordetella pertussis* and Its Virulence Factor Adenylate Cyclase Toxin. Front. Cell. Infect. Microbiol., doi.org/10.3389/fcimb.2021.79749.

Bianchi, M., **Sivarajan, R.**, Walles, T., Hackenberg, S., and Steinke, M. (2021). Susceptibility of Primary Human Airway Epithelial Cells to *Bordetella pertussis* Adenylate Cyclase Toxin in Two- and Three-Dimensional Culture Conditions. Innate Immun. 27, 89–98. doi: 10.1177/1753425920979354.

14. Affidavit

I hereby confirm that my thesis entitled Engineered Human Airway Mucosa for Modelling Respiratory Infections: Characterisation and Applications is the result of my own work. I did not receive any help or support from commercial consultants. All sources and / or materials applied are listed and specified in the thesis.

Furthermore, I confirm that this thesis has not yet been submitted as part of another examination process neither in identical nor in similar form.

Wuerzburg, 24.05.2023

Place, Date Signature

Eidesstattliche Erklärung

Hiermit erkläre ich an Eides statt, die Dissertation Gewebemodelle der humanen Atemwegsschleimhaut für Infektionsstudien der Atemwege: Charakterisierung und Anwendungen eigenständig, d.h. insbesondere selbständig und ohne Hilfe eines kommerziellen Promotionsberaters, angefertigt und keine anderen als die von mir angegebenen Quellen und Hilfsmittel verwendet zu haben.

Ich erkläre außerdem, dass die Dissertation weder in gleicher noch in ähnlicher Form bereits in einem anderen Prüfungsverfahren vorgelegen hat.

Wuerzburg, 24.05.2023

Ort, Datum Unterschrift